materials

Volume 1

Sustainable Designed Pavement Materials

Edited by
Sandra Erkens, Yue Xiao, Mingliang Li, Tao Ma and Xueyan Liu

Printed Edition of the Special Issue Published in *Materials*

www.mdpi.com/journal/materials

MDPI

Sustainable Designed Pavement Materials

Sustainable Designed Pavement Materials

Volume 1

Special Issue Editors

Sandra Erkens
Yue Xiao
Mingliang Li
Tao Ma
Xueyan Liu

MDPI • Basel • Beijing • Wuhan • Barcelona • Belgrade • Manchester • Tokyo • Cluj • Tianjin

Special Issue Editors
Sandra Erkens
Delft University of Technology (TUDelft)
The Netherlands

Mingliang Li
Research Institute of Highway Ministry of Transport (RIOH)
China

Xueyan Liu
Delft University of Technology (TUDelft)
The Netherlands

Yue Xiao
Wuhan University of Technology (WUT)
China

Tao Ma
Southeast University (SEU)
China

Editorial Office
MDPI
St. Alban-Anlage 66
4052 Basel, Switzerland

This is a reprint of articles from the Special Issue published online in the open access journal *Materials* (ISSN 1996-1944) (available at: https://www.mdpi.com/journal/materials/special_issues/sdpm).

For citation purposes, cite each article independently as indicated on the article page online and as indicated below:

LastName, A.A.; LastName, B.B.; LastName, C.C. Article Title. *Journal Name* **Year**, *Article Number*, Page Range.

Volume 1
ISBN 978-3-03928-985-1 (Hbk)
ISBN 978-3-03928-986-8 (PDF)

Volume 1-2
ISBN 978-3-03936-004-8 (Hbk)
ISBN 978-3-03936-005-5 (PDF)

Contents

About the Special Issue Editors

Sandra Erkens is the principal specialist in pavement materials and structures at Rijkswaterstaat, the Dutch highway authority. She is a full professor, holding the Chair of Pavement Engineering Practice, at Delft University of Technology. She is an internationally acknowledged expert in pavement materials and structures in general and asphalt concrete in particular. Prof. Erkens was a member of national and international groups involved in developing technical requirements for pavement materials and several (inter)national organizations for the dissemination of research. These include the ISAP technical committee on the Constitutive Modelling of Asphalt Concrete, the organization committee of the two-yearly Dutch conference on Infrastructure (CROW-infradagen) and the organizing committee of the 4th International Chinese European Workshop on Functional Pavement Design. She has been involved in road engineering research since 1997, has published over a hundred papers on her work and is a regular reviewer for conferences and journals.

Yue Xiao is a full-time research professor of the State Key Lab of Silicate Materials for Architectures in the Wuhan University of Technology. He was awarded the Fok Ying Tung Outstanding Young Teacher award by the Ministry of Education of China in 2018. He received the title of CHUTIAN Scholar in material science and engineering from the Hubei provincial department of education in 2014. Prof. Xiao received his Ph.D. degree in Road and Railway Engineering from Delft University of Technology, The Netherlands. He then joined Wuhan University of Technology in 2013. His research interests are in asphalt pavement surfacing, road and pavement materials, asphalt pavement design. Dr. Xiao is now conducting three innovative projects funded by the National Natural Science Foundation of China (NSFC), and projects supported by provincial departments as well. Since 2011, Dr. Xiao has published 62 SCI peer-reviewed journal papers.

Mingliang Li is a full-time associate researcher at the Road Research Center, Research Institute of Highway Ministry of Transport (RIOH) in China. Dr. Li received his Ph.D. degree in Road and Railway Engineering from Delft University of Technology, The Netherlands. His research interests are in functional pavement material and technology, pavement maintenance, asphalt materials, and recycling technology. He has participated in and completed more than 10 national and provincial scientific research projects, such as the National Key R & D plan of the Ministry of Science and Technology, research projects from the Ministry of Transport, etc. He was in charge of more than 20 design and consultant projects, including porous asphalt pavement, Sponge City permeable pavement and in-place recycling, etc. He has published one monograph, participated in the writing of six national and local standards, published more than 30 journal papers, and obtained 18 national patents.

Tao Ma is a full-time research professor and the vice dean of the School of Transportation at Southeast University. He is also the director of Road Engineering Department. His awards include the Young and Middle-Aged Leading Talent of Science And Technology Innovation In Transportation by the Ministry of Transport of China, Fok Ying Tung fund by the Ministry of Education of China, 333 High-Level Talent Project, and the Six Talent Summit Project by Jiangsu Province. He is the deputy director of the National Engineering Laboratory for Advanced Road Materials, deputy director of National Teaching Center of Road Traffic Virtual Simulation, and director of Jiangsu

Key Laboratory for Long-term Service and Safety of Road Infrastructure. His research interests are in asphalt pavement design, road and pavement materials, asphalt pavement maintenance and pavement sustainable development technologies. Dr. Ma is now conducting the science project for outstanding young people founded by the National Natural Science Foundation of China (NSFC), and other innovative projects supported by NSFC and provincial departments. Dr. Ma has published two books, more than 100 technical and journal papers, and has been awarded more than 20 national invention patents.

Xueyan Liu is currently an Associate Professor in the Section of Pavement Engineering of the Faculty of Civil Engineering & Geosciences of TU Delft. He works in the areas of constitutive modelling, numerical modelling, and material experimental characterization. Within the research program of the Section Pavement Engineering, his research topics mostly relate to the development and implementation of constitutive models for the simulation of the static and dynamic response of various pavement engineering materials like soils, asphalt concrete, liner and reinforcing systems, and sustainable development technologies, i.e., multiscale modelling of asphaltic materials, warm/cold asphalt concrete technology, durability of asphalt surfacings on orthotropic steel deck bridge, accelerated pavement test, and pavement continuous monitoring. Dr. Liu was granted his doctoral thesis in 2003. During the same period, Dr. Liu participated in the team that developed the ACRe model for Asphalt Concrete Response currently implemented in the 3D Computer Aided Pavement Analysis system (CAPA-3D). Dr. Liu has published more than 100 technical and journal papers on the mechanics and the finite element modelling of granular, concrete, and asphaltic materials. Dr. Liu is a member of the RILEM Technical Committee of Cracking in Asphalt Pavements WG3 and a member of the Delft Centre for Materials (DCMat). He is also a member of ISAP, AAPT, APSE, and IACMAG. Dr. Liu is an Editorial Board Member of Geomaterials (GM). Dr. Liu was appointed as a Board member of the International Association of Chinese Infrastructure Professionals (IACIP) and a member of the Academic Committee of the Key Laboratory of Road Structure and Materials Transportation Industry of the China Ministry of Transport. He is also actively involved in organizing international and national workshops and conferences and was invited as a Scientific/Technical committee member of several international conferences.

materials

MDPI

Editorial

Sustainable Designed Pavement Materials

Yue Xiao [1,2], Sandra Erkens [3], Mingliang Li [1,*], Tao Ma [4] and Xueyan Liu [3]

1 Key Laboratory of Transport Industry of Road Structure and Material, Research Institute of Highway (RIOH), Ministry of Transport, Beijing 100088, China; xiaoy@whut.edu.cn
2 State Key Laboratory of Silicate Materials for Architectures, Wuhan University of Technology, Wuhan 430070, China
3 Faculty of Civil Engineering and Geosciences, Delft University of Technology, 2628 CN Delft, The Netherlands; s.m.j.g.erkens@tudelft.nl (S.E.); X.Liu@tudelft.nl (X.L.)
4 School of Transportation, Southeast University, Nanjin 210096, China; matao@seu.edu.cn
* Correspondence: ml.li@rioh.cn; Tel.: +86-1581-033-9871

Received: 20 February 2020; Accepted: 25 March 2020; Published: 29 March 2020

Abstract: This Special Issue "Sustainable Designed Pavement Materials" has been proposed and organized as a means to present recent developments in the field of environmentally-friendly designed pavement materials. For this reason, articles included in this special issue relate to different aspects of pavement materials, from industry solid waste recycling to pavement materials recycling, from pavement materials modification to asphalt performance characterization, from pavement defect detection to pavement maintenance, and from asphalt pavement to cement concrete pavement, as highlighted in this editorial.

Keywords: pavement materials; sustainable designed pavement materials; recycling; recycled pavement materials; ageing resistance; modified asphalt materials; rejuvenator; skid resistance; pavement surfacing

This Special Issue "Sustainable Designed Pavement Materials" has been proposed and organized as a means to present recent developments in the field of environmentally-friendly designed pavement materials. It covers a wide range of selected topics on pavement materials. In total, 40 papers passed the peer-review and got published in this Special Issue. Universities and institutes considered as the most successful organizations, such as Wuhan University of Technology (10 papers), Southeast University (7 papers), Changsha University of Science & Technology (7 papers), Chang'an University (6 papers), Delft University of Technology (3 papers), Harbin Institute of Technology (2 papers), RWTH Aachen University (2 papers), Pennsylvania State University, Washington State University, Purdue University, and Michigan Technological University, have contributed a lot to this Special Issue. A brief summary of the articles is given in this editorial.

Research on solid waste recycling in pavement materials is considered as one of the most economic ways to achieve sustainable designed pavements. Kong et al. [1,2] studied the possibility of using oxygen furnace slag filler in asphalt mixture, and the BOF (Basic Oxygen Furnace) slag coarse aggregate was also presented in his research for making asphalt concrete. Three types of BOF slag fillers were concluded in their research. Ye et al. [3] investigated the effects of different cooling and treatment processes on the morphological features of BOF steel slag, and the effect of slag morphologies on the performance of asphalt mixtures. Another article from Qian et al. [4] also focused on slag pavement materials. Phosphorous slag was used as asphalt mixture aggregates on cement concrete deck to improve the interface bonding strength. Quarry fines were proposed by Zhang et al. [5,6] for pavement construction materials, by evaluating the properties of basic quarry fines and stabilized quarry fine specimens prepared using the gyratory compactor. Besides using slags as aggregates, crumb rubber was another widely used solid waste in pavement materials. The short-term aging of microwave activation

crumb rubber was studied by Li et al. [7], the mixing and compaction temperatures of the crumb rubber modified asphalt mixture were discussed in the research from Li et al. [8], while Gu et al. [9] developed a meso-structure-based finite element model of rubber modified mixture to predict both the dynamic modulus and phase angle properties.

Reuse of pavement materials is another eco-efficient method for sustainable pavement design. Long-term ageing resistance and healing properties of pavement materials were discussed in detail. The ageing characteristics of asphalt materials during their service life were evaluated by Wang et al. [10], which made them differ from ageing research on the lab-aged materials. Rejuvenators were designed by Zhang et al. [11] and Su et al. [12] using petroleum technology and encapsulating rejuvenator fiber, and then added into recycled pavement material and lab-aged material. They concluded that rejuvenators can soften aged pavement materials and consequently recover the road performance. Furthermore, self-healing characteristics of pavement materials were reported by Wu et al. [13], Li et al. [14], and Cai et al. [15]. Wu et al. [13] found that UV irradiation will weaken the macro-structure and lower the failure strength and healing index. Li et al. [14] designed steel fiber modified asphalt concrete to promote the induction heating technology, while Cai et al. [15] used engineered cementitious composites mortar to prepare flexible pavement materials with certain healing property. Numerical simulation models of microwave heating of asphalt mixture, which can be used for pavement maintenance, recycling, and deicing, were developed with finite element software by Wang et al. [16].

Environmental conditions such as higher temperature, UV radiation, and moisture can introduce significant deteriorations of asphalt-based pavement materials. Materials modification technologies are thus widely used in pavement engineering to improve the long-term performance of pavement materials. For instance, ethylene bis stearamide based graphene [17], styrene-butadiene-styrene latex [18], styrene-butadiene rubber [19], aged lignin [20] and bio-based polyurethane [21] were used as modifier and detailed explained in this special issue. The viscos-elastic behavior, storage property, fracture energy, rutting resistance, and anti-cracking property were presented. Studies on high-viscosity modified asphalt binder [22] and fire-retardant asphalt [23] were also discussed in this special issue.

Characterization research on pavement materials is of important for this Special Issue. Performance studies on stress absorbing membrane interlayer and semi-flexible composite mixture were discussed by Yang et al. [24] and Zhang et al. [25]. The former article investigated the phase transition characteristics by dynamic mechanical analysis, while the second article presented the engineering properties by means of thermal cracking, fatigue, rutting resistance, and moisture resistance. Asphalt-based materials are composed of binder, filler, and aggregates, and the interaction between each different compound is the key to get a better understanding of pavement performance. The effect of aggregate meso-structure on the permanent deformation of asphalt mixture was discussed by Zhang et al. [26], with the three-dimensional discrete element model. Their model can capture the aggregate morphologies of angularity, orientation, and surface texture. Chen et al. [27] investigated the asphalt-filler/aggregate interaction on self-designed interface specimens with dynamic shear rheometer. They concluded that asphalt mortar could be the closest subscale in terms of performance to that of asphalt mixtures, making it a vital scale to bridge the gap between asphalt binder and asphalt mixtures in multiscale performance analysis. A unified strength model, which can be used to overcome the design deviation caused by the randomness of the laboratory strength test and improve the accuracy degree, was described by Xia et al. [28]. Different loading stresses were investigated to conclude the unified strength model, as well as to study the asphalt mixture moduli in the research presented by Fan et al. [29].

Field investigation is the principal requirement to ensure safe and well-accepted driving conditions in pavement maintenance. In the study by Pan et al. [30], piezo-ultrasonic wave technology was used for damage detection, including groove damage and cylinder cutting damage, in road engineering. Pan found that factors such as temperature, defect size, and ultrasonic velocity would affect the detection accuracy. Zhang et al. [31] reported the field investigation in full-depth asphalt pavement.

Other researches focused on the wet skid resistance [32] and gradation design [33] of pavement surfacings. Lyu et al. [34] introduced an outstanding durable road surface marking material, using

persistent phosphors coated with silica-polymer hybrid shell. Cool coating materials for asphalt pavements were designed and discussed by Chen et al. [35]. These studies are critically important for pavement design and highway service. For instance, the cool coating can be widely used to solve the high-temperature-related defects in asphalt pavement.

Several other studies involved in this Special Issue look at cement concrete materials. Cement concrete and asphalt concrete are the two major materials in pavement engineering, so-called rigid pavement and flexible pavement. The micro-zone corrosion mechanism [36], cement mortar with super absorbent polymer [37], and exhaust-purifying cement [38] were discussed in detail. Polypropylene fiber was used in cement concrete and its performance was studied by Chen et al. [39] by dynamic compressive behavior analysis. Last, but not least, Yan et al. [40] presented their excellent work on anti-corrosion property of glass flake, which was designed for the reinforcement in chemically bonding phosphate ceramic coatings.

Author Contributions: Writing—original draft preparation, Y.X.; writing—review and editing, S.E., M.L., T.M. and X.L.; funding acquisition, Y.X. and T.M. All authors have read and agreed to the published version of the manuscript.

Funding: This research was funded by the National Natural Science Foundation of China (grant number No. 51922030, 51878164, and 51878526) and the 2019 Opening Funding Supported by the Key Laboratory of Transport Industry of Road Structure and Material in Research Institute of Highway, Ministry of Transport of China.

Acknowledgments: This Editorial was prepared by Yue Xiao at home, universities were closed due to the coronavirus, which has infected tens of thousands of people in China within these days. Revised by Sandra Erkens, Mingliang Li, Tao Ma, and Xueyan Liu. Many thanks to the doctors, nurses, and Chinese armies for their hard and unforgettable battle against the virus. They are the heroes who bring us hope and health. We wish China will receive the victory over novel coronavirus soon. Come on, Wuhan! Come on, China! We thank all the high-quality authors worldwide and reviewers for their contribution. Without their excellent work, this special issue would not get published successfully. We would also like to thank editors in MDPI for their assistance in managing this special issue.

Conflicts of Interest: The author declares no conflict of interest.

References

1. Kong, D.; Wu, S.; Chen, M.; Zhao, M.; Shu, B. Characteristics of Different Types of Basic Oxygen Furnace Slag Filler and its Influence on Properties of Asphalt Mastic. *Materials* **2019**, *12*, 4034. [CrossRef]
2. Kong, D.; Chen, M.; Xie, J.; Zhao, M.; Yang, C. Geometric Characteristics of BOF Slag Coarse Aggregate and its Influence on Asphalt Concrete. *Materials* **2019**, *12*, 741. [CrossRef] [PubMed]
3. Ye, Y.; Wu, S.; Li, C.; Kong, D.; Shu, B. Morphological Discrepancy of Various Basic Oxygen Furnace Steel Slags and Road Performance of Corresponding Asphalt Mixtures. *Materials* **2019**, *12*, 2322. [CrossRef] [PubMed]
4. Qian, G.; Li, S.; Yu, H.; Gong, X. Interlaminar Bonding Properties on Cement Concrete Deck and Phosphorous Slag Asphalt Pavement. *Materials* **2019**, *12*, 1427. [CrossRef] [PubMed]
5. Zhang, Y.; Korkiala-Tanttu, L.K.; Borén, M. Assessment for Sustainable Use of Quarry Fines as Pavement Construction Materials: Part I—Description of Basic Quarry Fine Properties. *Materials* **2019**, *12*, 1209. [CrossRef]
6. Zhang, Y.; Korkiala-Tanttu, L.K.; Borén, M. Assessment for Sustainable Use of Quarry Fines as Pavement Construction Materials: Part II-Stabilization and Characterization of Quarry Fine Materials. *Materials* **2019**, *12*, 2450. [CrossRef]
7. Li, B.; Zhou, J.; Zhang, Z.; Yang, X.; Wu, Y. Effect of Short-Term Aging on Asphalt Modified Using Microwave Activation Crumb Rubber. *Materials* **2019**, *12*, 1039. [CrossRef]
8. Li, Y.; Lyu, Y.; Xu, M.; Fan, L.; Zhang, Y. Determination of Construction Temperatures of Crumb Rubber Modified Bitumen Mixture Based on CRMB Mastic. *Materials* **2019**, *12*, 3851. [CrossRef]
9. Gu, L.; Chen, L.; Zhang, W.; Ma, H.; Ma, T. Mesostructural Modeling of Dynamic Modulus and Phase Angle Master Curves of Rubber Modified Asphalt Mixture. *Materials* **2019**, *12*, 1667. [CrossRef]
10. Wang, X.; Guo, H.; Yang, B.; Chang, X.; Wan, C.; Wang, Z. Aging Characteristics of Bitumen from Different Bituminous Pavement Structures in Service. *Materials* **2019**, *12*, 530. [CrossRef]

11. Zhang, C.; Ren, Q.; Qian, Z.; Wang, X. Evaluating the Effects of High RAP Content and Rejuvenating Agents on Fatigue Performance of Fine Aggregate Matrix through DMA Flexural Bending Test. *Materials* **2019**, *12*, 1508. [CrossRef] [PubMed]
12. Shu, B.; Bao, S.; Wu, S.; Dong, L.; Li, C.; Yang, X.; Norambuena-Contreras, J.; Liu, Q.; Wang, Q. Synthesis and Effect of Encapsulating Rejuvenator Fiber on the Performance of Asphalt Mixture. *Materials* **2019**, *12*, 1266. [CrossRef] [PubMed]
13. Wu, S.; Ye, Y.; Li, Y.; Li, C.; Song, W.; Li, H.; Nie, S. The Effect of UV Irradiation on the Chemical Structure, Mechanical and Self-Healing Properties of Asphalt Mixture. *Materials* **2019**, *12*, 2424. [CrossRef] [PubMed]
14. Li, H.; Yu, J.; Wu, S.; Liu, Q.; Li, Y.; Wu, Y.; Xu, H. Investigation of the Effect of Induction Heating on Asphalt Binder Aging in Steel Fibers Modified Asphalt Concrete. *Materials* **2019**, *12*, 1067. [CrossRef]
15. Cai, X.; Huang, W.; Wu, K. Study of the Self-Healing Performance of Semi-Flexible Pavement Materials Grouted with Engineered Cementitious Composites Mortar based on a Non-Standard Test. *Materials* **2019**, *12*, 3488. [CrossRef]
16. Wang, H.; Zhang, Y.; Zhang, Y.; Feng, S.; Lu, G.; Cao, L. Laboratory and Numerical Investigation of Microwave Heating Properties of Asphalt Mixture. *Materials* **2019**, *12*, 146. [CrossRef]
17. Zhang, X.; He, J.X.; Huang, G.; Zhou, C.; Feng, M.M.; Li, Y. Preparation and Characteristics of Ethylene Bis(Stearamide)-Based Graphene-Modified Asphalt. *Materials* **2019**, *12*, 757. [CrossRef]
18. Ren, S.; Liu, X.; Fan, W.; Wang, H.; Erkens, S. Rheological Properties, Compatibility, and Storage Stability of SBS Latex-Modified Asphalt. *Materials* **2019**, *12*, 3683. [CrossRef]
19. Fan, X.; Lu, W.; Lv, S.; He, F. Improvement of Low-Temperature Performance of Buton Rock Asphalt Composite Modified Asphalt by Adding Styrene-Butadiene Rubber. *Materials* **2019**, *12*, 2358. [CrossRef]
20. Zhang, Y.; Liu, X.; Apostolidis, P.; Gard, W.; van de Ven, M.; Erkens, S.; Jing, R. Chemical and Rheological Evaluation of Aged Lignin-Modified Bitumen. *Materials* **2019**, *12*, 4176. [CrossRef]
21. Leng, C.; Lu, G.; Gao, J.; Liu, P.; Xie, X.; Wang, D. Sustainable Green Pavement Using Bio-Based Polyurethane Binder in Tunnel. *Materials* **2019**, *12*, 1990. [CrossRef] [PubMed]
22. Li, M.; Zeng, F.; Xu, R.; Cao, D.; Li, J. Study on Compatibility and Rheological Properties of High-Viscosity Modified Asphalt Prepared from Low-Grade Asphalt. *Materials* **2019**, *12*, 3776. [CrossRef] [PubMed]
23. Xu, G.; Chen, X.; Zhu, S.; Kong, L.; Huang, X.; Zhao, J.; Ma, T. Evaluation of Asphalt with Different Combinations of Fire Retardants. *Materials* **2019**, *12*, 1283. [CrossRef] [PubMed]
24. Yang, G.; Wang, X.; Zhou, X.; Wang, Y. Experimental Study on the Phase Transition Characteristics of Asphalt Mixture for Stress Absorbing Membrane Interlayer. *Materials* **2020**, *13*, 474. [CrossRef]
25. Zhang, W.; Shen, S.; Goodwin, R.D.; Wang, D.; Zhong, J. Performance Characterization of Semi-Flexible Composite Mixture. *Materials* **2020**, *13*, 342. [CrossRef]
26. Zhang, D.; Gu, L.; Zhu, J. Effects of Aggregate Mesostructure on Permanent Deformation of Asphalt Mixture Using Three-Dimensional Discrete Element Modeling. *Materials* **2019**, *12*, 3601. [CrossRef]
27. Chen, M.; Javilla, B.; Hong, W.; Pan, C.; Riara, M.; Mo, L.; Guo, M. Rheological and Interaction Analysis of Asphalt Binder, Mastic and Mortar. *Materials* **2019**, *12*, 128. [CrossRef]
28. Xia, C.; Lv, S.; You, L.; Chen, D.; Li, Y.; Zheng, J. Unified Strength Model of Asphalt Mixture under Various Loading Modes. *Materials* **2019**, *12*, 889. [CrossRef]
29. Fan, X.; Lv, S.; Zhang, N.; Xia, C.; Li, Y. Characterization of Asphalt Mixture Moduli under Different Stress States. *Materials* **2019**, *12*, 397. [CrossRef]
30. Pan, W.-H.; Sun, X.D.; Wu, L.M.; Yang, K.K.; Tang, N. Damage Detection of Asphalt Concrete Using Piezo-Ultrasonic Wave Technology. *Materials* **2019**, *12*, 443. [CrossRef]
31. Zhang, W.; Lee, J.; Ahn, H.J.; Le, Q.; Wu, M.; Zhu, H.; Zhang, J. Field Investigation of Clay Balls in Full-Depth Asphalt Pavement. *Materials* **2019**, *12*, 2879. [CrossRef] [PubMed]
32. Yan, B.; Mao, H.; Zhong, S.; Zhang, P.; Zhang, X. Experimental Study on Wet Skid Resistance of Asphalt Pavements in Icy Conditions. *Materials* **2019**, *12*, 1201. [CrossRef] [PubMed]
33. Cui, W.; Wu, K.; Cai, X.; Tang, H.; Huang, W. Optimizing Gradation Design for Ultra-Thin Wearing Course Asphalt. *Materials* **2020**, *13*, 189. [CrossRef] [PubMed]
34. Lyu, L.; Chen, Y.; Yu, L.; Li, R.; Zhang, L.; Pei, J. The Improvement of Moisture Resistance and Organic Compatibility of SrAl2O4: Eu2+, Dy3+ Persistent Phosphors Coated with Silica–Polymer Hybrid Shell. *Materials* **2020**, *13*, 426. [CrossRef]

35. Chen, Y.; Hu, K.; Cao, S. Thermal Performance of Novel Multilayer Cool Coatings for Asphalt Pavements. *Materials* **2019**, *12*, 1903. [CrossRef]
36. Wang, F.; Zhang, Z.; Wu, S.; Jiang, J.; Chu, H. Effect of Inhibitor on Adsorption Behavior and Mechanism of Micro-Zone Corrosion on Carbon Steel. *Materials* **2019**, *12*, 1901. [CrossRef]
37. Tan, Y.; Tan, Y.; Chen, H.; Wang, Z.; Xue, C.; He, R. Performances of Cement Mortar Incorporating Superabsorbent Polymer (SAP) Using Different Dosing Methods. *Materials* **2019**, *12*, 1619. [CrossRef]
38. He, R.; Huang, X.; Zhang, J.; Geng, Y.; Guo, H. Preparation and Evaluation of Exhaust-Purifying Cement Concrete Employing Titanium Dioxide. *Materials* **2019**, *12*, 2182. [CrossRef]
39. Chen, M.; Ren, C.; Liu, Y.; Yang, Y.; Wang, E.; Liang, X. Effects of Polypropylene Fibre and Strain Rate on Dynamic Compressive Behaviour of Concrete. *Materials* **2019**, *12*, 1797. [CrossRef]
40. Yan, G.; Wang, M.; Sun, T.; Li, X.; Wang, G.; Yin, W. Anti-Corrosion Property of Glass Flake Reinforced Chemically Bonded Phosphate Ceramic Coatings. *Materials* **2019**, *12*, 2082. [CrossRef]

materials

MDPI

Article

Characteristics of Different Types of Basic Oxygen Furnace Slag Filler and its Influence on Properties of Asphalt Mastic

Dezhi Kong [1], Shaopeng Wu [1], Meizhu Chen [1,*], Meiling Zhao [2] and Benan Shu [1]

[1] State Key Laboratory of Silicate Materials for Architectures, Wuhan University of Technology, Wuhan 430070, China; kongdz@whut.edu.cn (D.K.); wusp@whut.edu.cn (S.W.); shuba@whut.edu.cn (B.S.)
[2] Research Institute of Highway of Ministry of Transport, Beijing 100088, China; zhaoml@whut.edu.cn
* Correspondence: chenmzh@whut.edu.cn

Received: 24 October 2019; Accepted: 29 November 2019; Published: 4 December 2019

Abstract: The fillers of ordinary and pyrolytic basic oxygen furnace (BOF) slag were selected to investigate the properties of their asphalt mastic. XRF (X-Ray Fluorescence) was used to analyze chemical composition of fillers. Meanwhile, SEM (Scanning Electron Microscope) and AIMS (Aggregate Image Measurement System) were utilized to explore meso-morphology, angularity and sphericity. Penetration, softening point and viscosity of asphalt mastic were discussed, while the rheological properties of asphalt mastic were studied by means of DSR (dynamic shear rheometer) and BBR (bending beam rheometer) tests. The experimental results show that chemical composition of different types of BOF slag is similar. The grinding energy consumption of pyrolytic BOF slag is higher than that of limestone and ordinary BOF slag. It is not recommended that pyrolytic BOF slag filler is produced by grinding process. The micro-texture structure of ordinary BOF slag filler is more abundant and their angularity index is about 15% higher than that of limestone filler. The stiffness modulus and rutting factor of asphalt mastic with ordinary BOF slag filler is higher than that of limestone filler. Meanwhile the incorporation of BOF slag filler will further reduce the low-temperature flow performance of asphalt mastic. The effect of pyrolytic BOF slag filler on the performance of asphalt mastic is less than that of ordinary BOF slag. Ordinary BOF slag filler can effectively improve high temperature anti-rutting stability of asphalt mixture. Ordinary BOF slag has a useful application prospect as filler in asphalt mixture.

Keywords: BOF slag filler; asphalt mastic; morphological characteristics; rheological properties

1. Introduction

Steel slag is a common by-product of the steelmaking industry, and its output is about 10% to 15% of steel production in the world [1–3]. As a major type of steel slag, basic oxygen furnace (BOF) slag has strong alkalinity, rich angularity, tough surface characteristics and relatively good mechanical properties [4]. BOF slag is widely used as aggregate in asphalt mixtures in related research [5–7]. Pasetto et al. and Wu et al. [8–10] demonstrated that BOF slag aggregates improve performance of asphalt mixtures, such as moisture stability, high temperature deformation resistance, abrasion and skid resistance. BOF slag is an ideal substitute for natural aggregates in asphalt mixture.

Asphalt mixtures consist of asphalt binder, aggregate, and mineral filler. Asphalt mastic, which refers to mixture of asphalt binder and mineral filler, determines the final mechanical properties of asphalt mixture. Previous studies [11,12] have demonstrated that the properties of asphalt mastic are the factors influencing the rutting resistance and low-temperature crack resistance of asphalt mixtures, while the properties of filler are closely associated with the asphalt mastic. Many researchers [13–17] have proved that performances of asphalt mastic are affected by the volume content of fillers and

performances of fillers like surface characteristics, alkalinity and size, as well as physical-chemical interaction between asphalt and fillers.

Xiao et al [18,19] discussed the feasibility of BOF slag as mineral filler in asphalt mixtures and the results show that the asphalt mastic with BOF slag filler has better high-temperature rheological properties than that of limestone filler. Qiu et al [20] examined the low-temperature fracture properties of asphalt mastic using steel slag powder. The results showed that the steel slag powder–asphalt system had higher fracture resistance than conventional systems and steel slag powder can diminish the severity of low-temperature reversible aging of modified asphalt. Song et al [21] demonstrated that the steel-making dust would be an alternative to the ordinary mineral filler to improve the performance of asphalt mortars and reduce the harm of the dust to the environment at the same time.

With the rapid development of highway construction projects and the consequential deterioration in high-quality mineral filler, there is an urgent need to broaden the source of the fillers that can be used in asphalt mixtures. Meanwhile, lots of numerous micro fillers are produced in the crushing process and magnetic separation of BOF slag [22]. The utilization of BOF slag as filler in asphalt mixture has attracted more concern. Furthermore, different types of BOF slag have different properties. Meanwhile, the difference in physicochemical properties of fillers and their influence on asphalt mastic is still unknown.

This study attempted to evaluate the feasibility of different types of BOF slag used as mineral filler to replace limestone filler (LF) in asphalt mixtures. All types of fillers were obtained by grinding 3–5 mm particle size range aggregates with the same processing conditions. It was found that 90% of all types of fillers could pass through 0.075 mm sieve. Figure 1 illustrates the research program on the characteristics of different types of BOF slag filler and their influence on properties of asphalt mastic. Firstly, chemical composition of different types of BOF slag filler was evaluated by XRF. Secondly, the geometrical properties of BOF slag filler were examined, such as meso-morphology and angularity and sphericity. Thirdly, the basic physical properties of asphalt mastic were discussed including penetration, softening point and viscosity. Finally, the rheological properties of asphalt mastic were studied at both low and high temperatures.

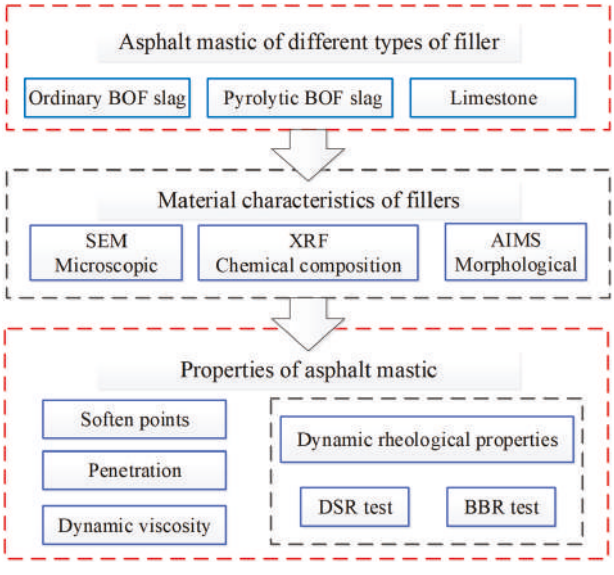

Figure 1. Finalized research program.

2. Materials and Methods

2.1. Raw Materials

Pen 60/80 bitumen binder, provided by Panjin Co., Ltd., Liaoning, Panjin, China, was used in this research. The basic properties of bitumen binder are shown in Table 1. They are all within the requirement specifications of China.

Table 1. Basic properties of the bitumen binder in this research.

Properties	Values	Specifications
Penetration [0.1 mm]	64	60–80
Penetration index	−0.6	−1.5–1.0
Softening point [°C]	46.9	≥46
Ductility, 5 cm/min, 15 °C [cm]	167	≥100
Dynamic viscosity (60 °C) [Pa·s]	172	≥160
Density [g/cm^3]	1.021	

Three types of BOF slag fillers and limestone filler were employed in this research. The limestone (L) was provided by Hubei province in China. Type A BOF slag (BS-A) was obtained from ironworks in Hubei province in China, while Type B BOF slag (BS-B) and pyrolytic BOF slag (PBS) were obtained from ironworks of Baotou in Inner Mongolia, China. BS-A and BS-B were basic oxygen furnace slag, and PBS was pyrolytic BOF slag which was treated with a hot stuffing process during the BOF slag cooling step.

All types of fillers in this research were obtained by grinding 3–5 mm particle size range aggregates with the same processing conditions. A ball mill was used and the time of the grinding was 60 min, 5,000 g for each sample and the rotating speed was 120 r/min. After grinding, more than 90% of all types of fillers could pass through the 0.075 mm sieve. The labels are as follows: limestone filler (LF), type A BOF slag filler (BSF-A), type B BOF slag filler (BSF-B), pyrolytic BOF slag filler (PBSF).

The basic properties of the four types of fillers are shown in Table 2. It can be deduced that the density of BOF slag is higher than that of LF. The density of BSF-A and BSF-B is almost equal, while they are about 18% higher than that of LF. Among them, the density of PBSF is the highest, which is attributed to the higher content of Fe_2O_3 and the hot stuffing process during BOF slag cooling step. The difference in hydrophilic coefficient of the four fillers is virtually negligible. However, the water absorption of BOF slag fillers is higher than that of LF, which is due to the particular pore structure of the surface of BOF slag.

Table 2. Basic properties of four types of fillers.

Property	Density (kg/m^3)	Hydrophilic Coefficient	Water Absorption (%)
LF	2725	0.64	0.53
BSF-A	3217	0.69	0.67
BSF-B	3244	0.73	0.63
PBSF	3478	0.65	0.64

2.2. Experimental Methods

2.2.1. Properties of Fillers

The chemical compositions of the four types of filler were evaluated by X-Ray Fluorescence (PANalytical. B.V., Zetium, Almelo, Netherlands). The surface characteristics of four types of fillers were evaluated using scanning electron microscope (JSM-IT300, SEM-JEOL, Tokyo, Japan). The aggregate image measurement system (AIMS) was used to analyze the morphological features of each type of

filler. Meanwhile, the laser particle size analyzer (Mastersizer-2000, Malvern, England) was utilized to analyze the difference of particle size of four types of fillers.

2.2.2. Preparation of Asphalt Mastic

Specific amounts of each type of filler were incorporated into pen 60/80 asphalt binder to prepare the asphalt mastic. Firstly, asphalt binder was preheated to 150 °C for 30 min. Then, filler was gradually incorporated with a high shear instrument of the shear speed of 4000 rpm for 30 min. Homogeneous dispersion of the filler in the asphalt binder was required for further research. the filler–asphalt volume ratio of asphalt mastic used in this research was 0.4. The mass–volume conversions of four fillers were calculated by the density values in Table 2. After calculation, the filler-asphalt weight ratios of LF was 1.113, BSF-A was 1.314, BSF-B was 1.32, and PBSF was 1.42.

2.2.3. Properties of Asphalt Mastic

The penetration and softening point test were used to assess the basic properties of the asphalt mastic. In the preparation process of asphalt mixture, the workability is closely linked to the viscosity of asphalt mastic. A Brickfield viscometer was used to analyze the difference of four types of asphalt mastic. Test methods of penetration, softening point and dynamic viscosity refer to Chinese official standard JTG E20-2011 [23].

A dynamic shear rheometer (MCR101, DSR, Anton Paar, Graz, Austria) was utilized to evaluate the rheological properties of asphalt mastics. The DSR test was performed at a fixed frequency of 10 rad/s under variation of temperature from −10 °C to 80 °C with increments of 2 °C/min. In −10 °C to 3 °C, specimens were placed on a parallel plate geometry whose diameter was 8 mm, the thickness was 2 mm and strain level was 0.2%. In 30 °C to 80 °C, specimens were placed on a parallel plate geometry whose diameter was 25 mm, the thickness was 1 mm and strain level was 2.0%. The BBR (TE-BBR, Cannon, New York, NY, USA) was used to examine the rheological properties at a low temperature, which relates to the low-temperature cracking resistance. Preheated asphalt mastic was filled into an aluminum mold to prepare a mastic beam 102.0 ± 0.5 mm in length, 12.7 ± 0.5 mm in width, and 6.25 ± 0.5 mm in thickness. Drawing on the research of Xiao et al [18,19], tests were performed at a definite temperature (15 °C). Specimens were tested under a constant stress of 0.985 N for 250 s. Each test for different mastic included five duplicate specimens and the average value was adopted.

3. Results and Discussion

3.1. Material Characteristics of Fillers

3.1.1. Chemical Compositions of Fillers

The chemical compositions of the four types of filler from X-ray fluorescence analysis are shown in Table 3. Limestone is an alkali aggregate because the chemical composition of CaO was higher than fifty percent. The chemical composition of Fe_2O_3 in three types of BOF slags is more than 20%. Three types of BOF slag contain less SiO_2 and more than 30% CaO making them alkali aggregates.

Table 3. Chemical composition of the fillers in this research.

Composition [%]	SiO_2	CaO	MgO	Al_2O_3	Fe_2O_3	MnO	P_2O_5	Other	LOI
LF	0.86	51.2	2.36	0.85	0.12	0.7	1.02	0.19	42.7
BSF-A	19.2	42.7	5.19	3.25	23.9	1.77	1.41	0.22	2.36
BSF-B	17.7	39.7	5.56	2.91	24.4	4.55	1.68	0.09	3.41
PBSF	15.4	34.4	6.22	1.95	30.8	4.46	2.15	0.16	4.46

3.1.2. Microscopic Characteristics of Fillers

Figure 2 shows the diversity between limestone filler and three types of BOF slag fillers in SEM images. Compared with the micrographs of LF, BOF slag has different surface texture particularly due to the size and number of numerous tiny particles which are adhered to its surface s and its rough surface. The surface of LF is relatively smoother than that of BOF slag filler, where the latter is irregular shaped, rough, and bumpy, which might result in effective cohesion with asphalt binder and consequently lead to improved strength and water resistance. From practical viewpoint, the rough surface of BOF slag filler will cause an increase in the amount of asphalt required when BOF slag filler is used as filler in asphalt mixtures.

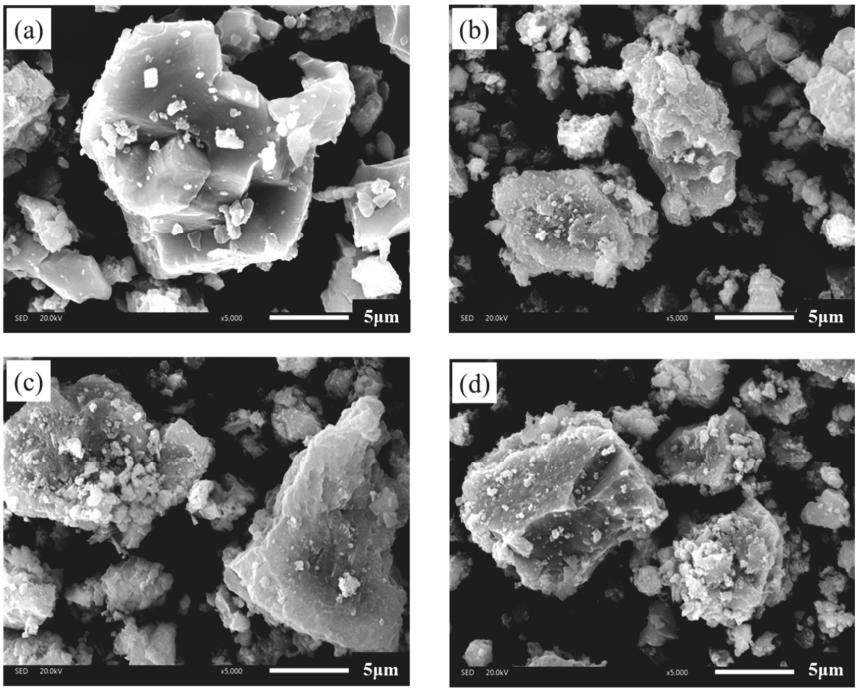

Figure 2. SEM images of investigated fillers: (**a**) limestone filler; (**b**) type A basic oxygen furnace (BOF) slag filler; (**c**) type B BOF slag filler; and (**d**) pyrolytic BOF slag filler.

3.1.3. Morphological Characteristics of Fillers

Morphological characteristics of fillers in this research were analyzed by AIMS, which is an integrated system comprising image acquisition hardware and a computer. Analysis of filler includes gradient angularity (the AIMS Angularity Index ranges from 1 to 10,000) and Form2D (AIMS Form2D Index ranges from 0 to 20).

Angularity is a description of edge sharpness of the boundary particles of aggregate. The angularity changes with filler granule boundary shape changes. The value of angularity is calculated based on the gradient on the particle boundary. Angularity is calculated with Equation (1) [24]. Its range is 0 to 10,000. The larger the value of angularity is, the boundary shape of filler is sharper.

$$Gradient\ Angularity = \frac{1}{\frac{n}{3} - 1} \sum_{i=1}^{n-3} \left| \theta_i - \theta_{i+3} \right| \quad (1)$$

where θ is angle of orientation of the edge points, n is the total number of points, i is the ith point on the edge of the particle.

Figure 3 shows the comparison of distributions of gradient angularity indexes of four types of fillers. It can be clearly seen that LF has the lowest gradient angularity indexes while BSF-B has the highest gradient angularity indexes. The distribution range of the angularity index of LF is narrower than that of BSF-A, BSF-B and PBSF. Such differences illustrate that the distribution of gradient angularity index of LF is more uniform. By comparing three types of BOF slag filler, it can be found that the gradient angularity index of PBSF is smaller than that of ordinary BOF slag. The gradient angularity index of ordinary BOF slag is about 15% higher than that of LF. In summary, the particle shape of the BOF slag filler has more angular structure than that of limestone filler under the same grinding process conditions.

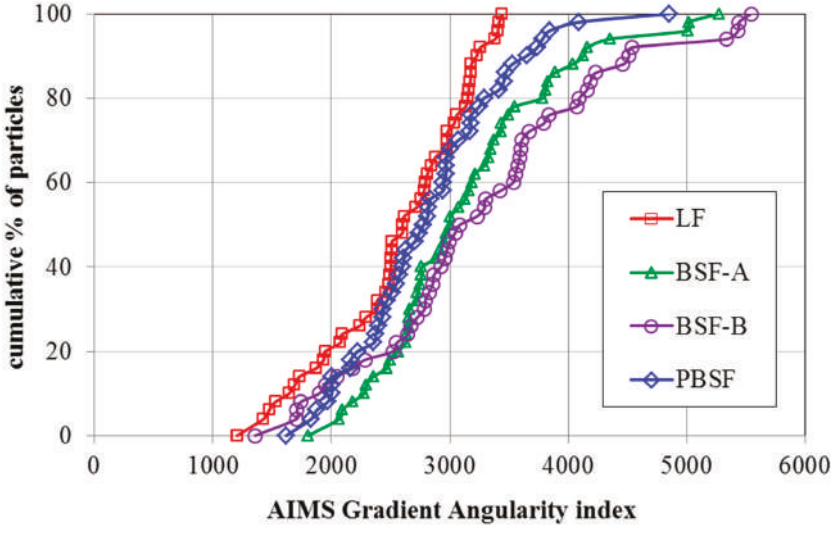

Figure 3. Comparison of distributions of angularity indexes of four types of fillers.

AIMS Form2D is applicable only to fine-sized aggregate and it quantifies the relative form from 2D images of aggregate particles. Form2D is calculated with Equation (2) [25] and its range is 0 to 20. A perfect circle has a Form2D value of 0. According to the definition of Form2D, a higher Form2D value would imply a relatively rougher surface, which would consequently indicate a positive contribution towards adhesive mechanical bonding of asphalt binder to filler.

$$Form\ 2D = \sum_{\theta=0}^{\theta=360-\Delta\theta} \left[\frac{R_{\theta+\Delta\theta} - R_{\theta}}{R_{\theta}} \right] \quad (2)$$

where R_θ is the radius of the particle at an angle of θ, $\Delta\theta$ is the incremental difference in the angle.

As shown in Figure 4, the Form2D values of four types of fillers have a wide distribution range of 5–12. For each type of BSF, nearly 80% of the particles have moderate and higher Form 2D values while about 40% of LF has lower Form 2D values. The Form2D values of LF is the lowest and the Form 2D of BOF slag is about 10% higher than that of LF. In summary, the surface of BOF slag filler was rougher and sharper than that of limestone filler. These results agree with the SEM results.

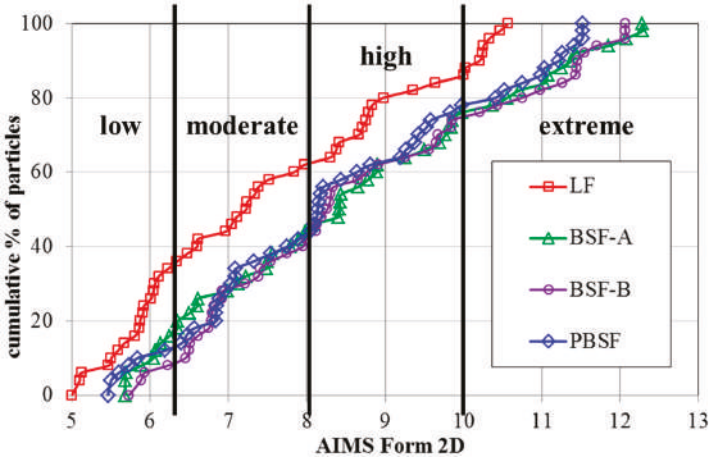

Figure 4. Distributions of Form2D values of four types of fillers.

3.1.4. Particle Size Analysis of Fillers

Figure 5 shows the particle size distribution of four types of filler. It reveals that the particle size of the four types of fillers is different under the same grinding process conditions. The particle size of LF is minimal, while the particle size of PBSF is maximal. Slight differences exist between LF and BSF-A in particle size. The order of particle size from small to large is LF, BSF-A, BSF-B and PBSF. The grinding efficiency of BOF filler is relatively lower than that of LF. The grinding efficiency of different kinds of BOF filler is also different. Pyrolytic BOF slag has the maximum particle size among the four types of fillers, indicating that pyrolytic BOF slag is more difficult to grind than ordinary BOF slag. In order to achieve the same particle size, the grinding process of pyrolytic BOF slag needs to consume more grinding time and more energy consumption.

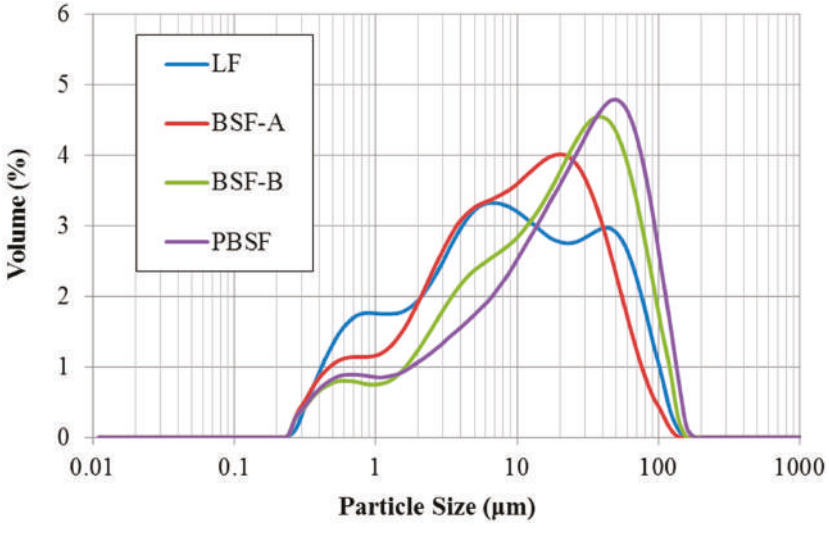

Figure 5. The particle size distribution of four types of filler.

3.2. Properties of Asphalt Mastic

Four types of asphalt mastics and basic bitumen binder were investigated in this research. Both basic properties and dynamic rheological properties were analyzed.

3.2.1. Basic Properties of Asphalt Mastic

The basic properties of asphalt mastic investigated in this research include soften points, penetration and dynamic viscosity.

The bitumen binder has a typical viscosity property. The smaller the penetration value is, the greater the viscosity of the asphalt material under low temperature conditions is, and the corresponding elastic deformation performance and recovery performance are also better. The softening point of the asphalt mastic is larger, indicating that the high temperature performance is better.

In Table 4 the values of soften points and penetration of asphalt mastic are presented. Compared with LF asphalt mastic, the softening point of asphalt mastic with BOF slag filler is lower, while its penetration is higher. BOF slag filler has a better viscosity-increasing effect on asphalt mastic than LF. The softening point and penetration of asphalt mastic with three types of BOF slag filler are similar. Although the PBSF has the largest particle size, its effect on softening point increase and penetration reduction is still effective. The particle size factor and morphological characteristics of BOF slag filler has little effect on the soften points and penetration of asphalt mastic.

Table 4. The soften points and penetration of asphalt mastic.

Property	Soften Points (°C)	15 °C Penetration (0.1 mm)	25 °C Penetration (0.1 mm)
LF	55.3	13.5	31.5
BSF-A	58.3	12.1	28.4
BSF-B	57.1	11.9	29.3
PBSF	58.5	12.5	29.8

The dynamic viscosity of asphalt is very important for asphalt mixture. The reasonable construction temperature is determined by the dynamic viscosity temperature range of 0.17 Pa s ± 0.02 Pa s, and construction rolling temperature is determined by the dynamic viscosity temperature range of 0.28 Pa s ± 0.03 Pa s [26]. The consistency of asphalt mastic in asphalt mixture construction is deeply influenced by the dynamic viscosity [27].

Viscosity–temperature value for bitumen binder and four types of asphalt mastic are shown in Table 5. In the case of limestone filler, the viscosity of asphalt mastic at different temperatures is approximately five times higher than that of bitumen binder. The addition of filler can effectively improve the viscosity of asphalt mastic. Compared with LF asphalt mastic, the viscosity of BSF asphalt mastic is higher, mainly because BOF slag filler has higher alkalinity and rougher micro-texture. The dynamic viscosity of the three types of asphalt mastic from large to small is BSF-A, BSF-B and PBSF. It is believed that the bigger particle size, more regular shape and smoother microscopic surface of PBSF result in a relatively lower dynamic viscosity of asphalt mastic.

Table 5. The dynamic viscosity test results of asphalt mastic.

Property	Dynamic Viscosity (Pa s)				
	90 °C	105 °C	120 °C	135 °C	150 °C
Bitumen binder	11.80	3.40	1.26	0.51	0.23
LF	52.00	14.25	4.95	1.97	0.94
BSF-A	78.00	22.25	7.25	3.00	1.40
BSF-B	77.00	21.05	7.15	2.80	1.38
PBSF	71.00	19.30	6.82	2.63	1.25

3.2.2. Dynamic Rheological Properties of Asphalt Mastic

As a typical viscoelastic material, the dynamic rheological properties of asphalt are closely related to its load and temperature conditions [28]. The viscoelastic characteristics of different types of asphalt and asphalt mastic are complex in different temperature conditions. Dynamic shear rheometer (DSR) tests were used to study dynamic rheological properties of asphalt mastic in this research. Complex shear modulus (G*) and phase angle (δ) are recorded and calculated by performing the DSR test at varying temperatures. G* can be decomposed into storage shear modulus (G′ = G*cosδ) and loss shear modulus (G′′ = G*sinδ), which is used to characterize the ability of asphalt mastic to resist deformation under repeated shear loads. The larger of the G* is, the higher of the resistance of asphalt mastic is in deformation. δ is the time lag of the applied stress and the resulting strain. The tangent value of δ is the ratio of the loss modulus to the storage modulus. A smaller δ indicates that there are more elastic components in the asphalt G*, and a larger δ indicates that there are more viscous components in the asphalt G*. For a fully elastic material, the phase angle δ is zero, at which point all deformations are recoverable. However, for viscous materials, the phase angle is close to 90°, at which point all deformation is permanent. G*/sinδ (the ratio of the complex modulus to phase angle sine) characterizes the ability of asphalt to resist high temperature rutting. G*/sinδ is called the rutting factor. Under the same temperature conditions, asphalt mastic with larger G*/sinδ has better rutting resistance [29].

Effect of different fillers on G* of asphalt mastic are shown in Figures 6 and 7. The G* of the asphalt mastic and asphalt decreases with the increase of temperature, which indicates that the rheological properties of the asphalt are greatly affected by the temperature. When the temperature rises, the volume of free asphalt increases, and the pitch changes from a high elastic state at a low temperature to a viscous state at a high temperature. As a result, the maximum shear stress and the maximum shear strain of the asphalt are increased when the shear force is applied, and therefore the G* is lowered.

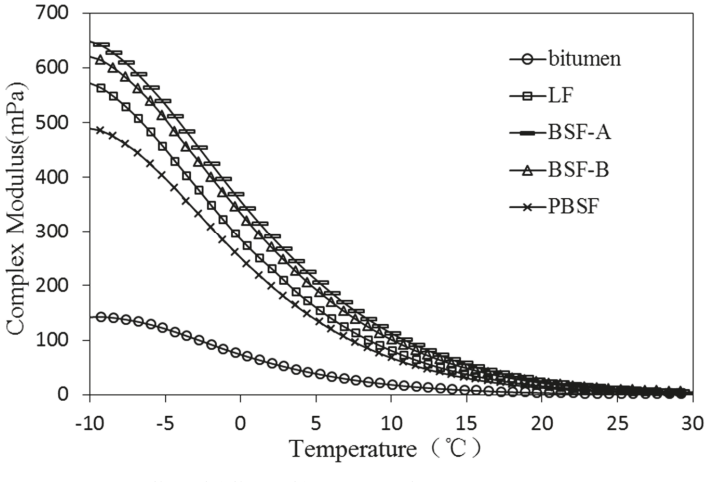

Figure 6. Effect of different fillers on G* of asphalt mastic (−10~30 °C).

In the temperature range of −10~30 °C, the higher the G* of the asphalt mastic is, the better the crack resistance of the asphalt under low temperature conditions. As shown in Figure 6, the values of complex modulus of BSFA are highest and PBSF has the worst effect on the increase of complex modulus. The values of PBSF are lower than that of LF, mainly due to a small alkalinity, a large particle size, a large specific surface area, less adsorbed asphalt, and relatively more free asphalt. Ordinary BOF slag filler has a good effect, improving the low temperature crack resistance of asphalt mastic.

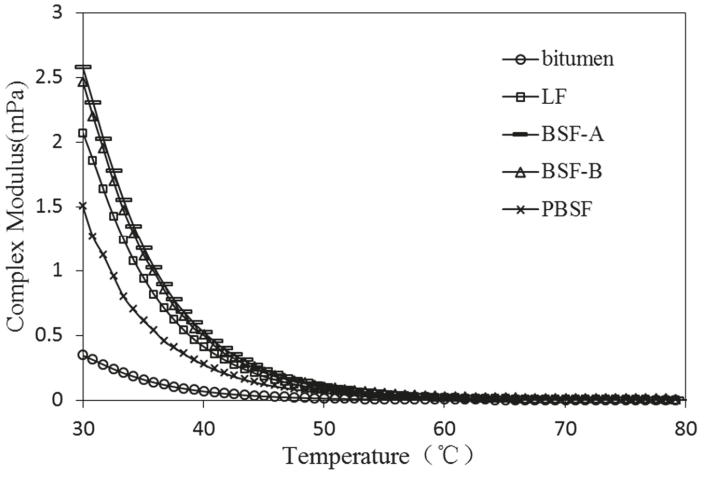

Figure 7. Effect of different fillers on G* of asphalt mastic (30~80 °C).

In Figure 7, the effect of different fillers on G* of asphalt mastic (30~80 °C) is presented. After adding BSF-A and BSF-B, the G* of asphalt mastic is higher than that of LF, which indicates that the high temperature stability of ordinary BOF slag filler asphalt mastic is better than that of LF.

In Figures 8 and 9 the values of different fillers on δ of asphalt mastic (−10~80 °C) are presented. The δ of asphalt mastic with different types of fillers increases with the increase of temperature, and the difference of δ values of asphalt mastic decreases with the increase of temperature. The sensitivity of the δ of the filler is continuously reduced with the temperature increasing. The phase angles of asphalt mastics with different types of fillers are arranged from large to small in order, pure asphalt, PBSF, LF, BSF-B and BSF-A. It is shown that ordinary BOF slag can effectively improve the elastic properties of asphalt mastic, and is beneficial, improving the anti-permanent deformation performance of asphalt mastic.

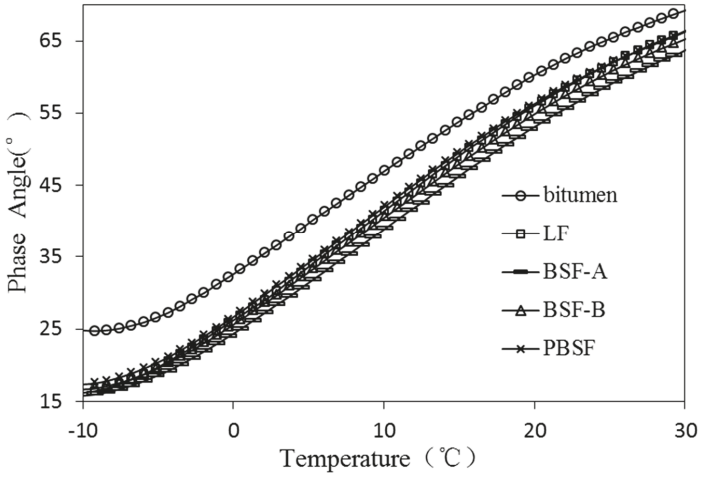

Figure 8. Effect of different fillers on δ of asphalt mastic (−10~30 °C).

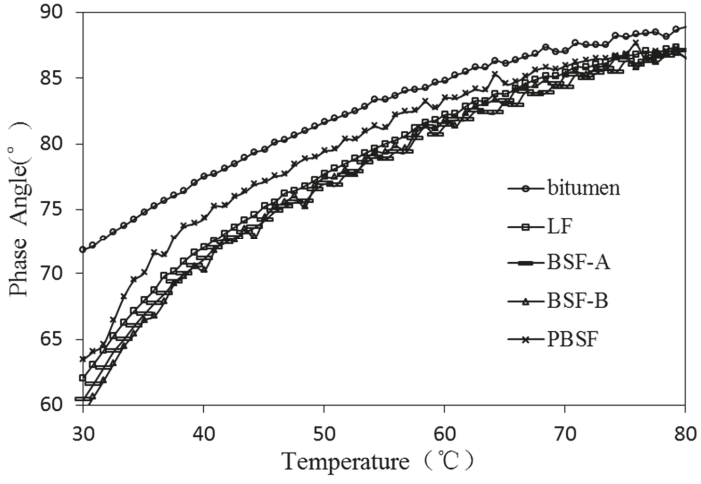

Figure 9. Effect of different fillers on δ of asphalt mastic (30~80 °C).

As shown in Figure 10, the rutting factor of the asphalt mastics with BSF-A and BSF-B are similar and larger than that of corresponding PBSF asphalt mastic. It demonstrates that all asphalt mastics containing ordinary BOF slag fillers have better high-temperature deformation resistance than ones with LF. BSF mastic presents the best deformation resistance. This was due to the chemical effect between alkaline components in ordinary BOF slag fillers and asphaltic acid in bitumen. The stiffness of BOF slag makes mastic structure more stable to resist permanent deformation.

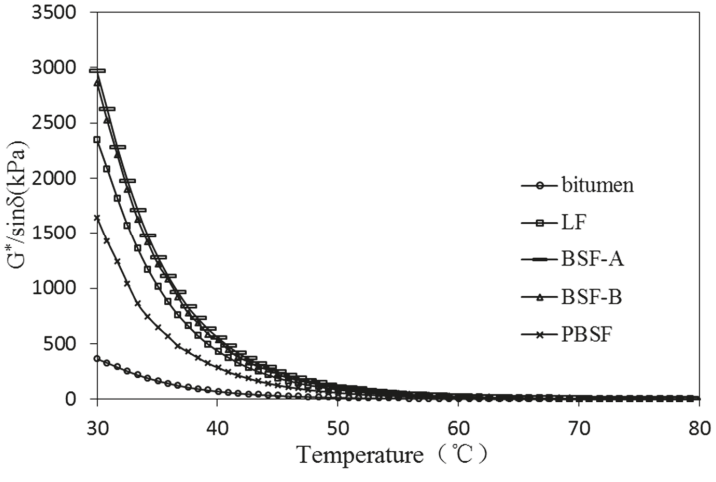

Figure 10. Effect of different fillers on G*/sinδ of asphalt mastic (30~80 °C).

3.2.3. Anti-Cracking Properties of Asphalt Mastic at Low Temperature

Bending beam rheometer (BBR) testing was used to investigate the low-temperature rheological properties of asphalt mastic in this research. Tests were performed at a fixed temperature (−15 °C) to discuss the different of low temperature performance of asphalt mastic with different filler, meanwhile the m-value and creep stiffness (S(t), MPa) were evaluated. The S(t) was calculated on the basis of Equation (3). The m-value signifies the rate that S(t) changes during loading time. Creep stiffness indicates the thermal stress of asphalt mastic under low temperature. Lower creep stiffness implies

that the specimen has better rheological properties at lower temperatures. Scientifically, lower creep stiffness is positive because it corresponds to lower deformation stress. M-value reflects the stress relaxation property of asphalt mastic at low temperatures. A higher m-value is required since asphalt with a higher m-value has better ability to disperse deformation stress [30].

$$S(t) = \frac{PL^3}{4bh^3\Delta(t)} \tag{3}$$

where b, h and L are the width (mm), height (mm), length (mm) of specimen. P is the constant applied load. $\Delta(t)$ is the deflection of beam (mm) at different times (t).

The creep stiffness and m-value of asphalt mastic with different types of filler are shown in Figure 11. The change of m-value is similar to the stiffness. It can be clearly seen that the introduction of fillers increases the $S(t)$ and m-value. The $S(t)$ values of LF are about four times that of pure asphalt, so asphalt will become stiffer at a low temperature after mixing with fillers. Considering the value of stiffness, the stiffness of PBSF is smaller than that of LF, which indicates that pyrolytic BOF slag filler has a positive effect on the low-temperature crack resistance performance of asphalt mastic. Asphalt mastics with BSF-A and BSF-B are higher than ones with LF. It indicates that ordinary BOF slag filler has a certain increase in the stiffness of asphalt mastic, but has a negative influence on its low-temperature rheological properties. The incorporation of ordinary BOF slag filler reduces the low-temperature crack resistance performance of asphalt mastic compared with LF.

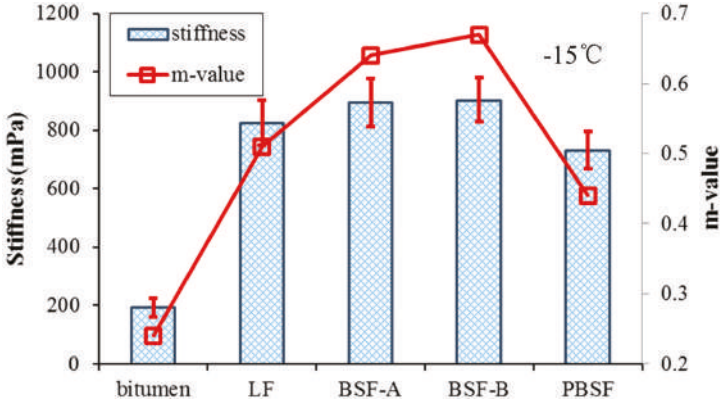

Figure 11. Bending beam rheometer (BBR) test results of four asphalt mastic and pure bitumen.

4. Conclusions

The microscopic characteristics, morphological characteristics (angularity and Form2D) and chemical properties of three types of BOF slag filler were investigated in the first part of this research. Then the basic physical properties and rheological properties of their asphalt mastic were studied. The overall conclusions are elaborated upon hereunder:

(1) The chemical composition of BOF slag is more complicated than that of limestone, which includes SiO_2, CaO, MgO, Al_2O_3, Fe_2O_3 and other components. The chemical composition of different types of BOF slag is similar. The micro-texture structure of BOF slag filler is more complex than that of LF. The angularity index of ordinary BOF slag is about 15% higher than that of LF. The angularity index, Form2D and micro texture of different types of BOF slag filler are also different.

(2) The asphalt mastic with BOF slag has higher soften points, lower penetration and higher dynamic viscosity than one with LF. The incorporation of BOF slag filler can significantly improve the high-temperature stability of asphalt mastic.

(3) Compared with rheological properties, asphalt mastic with BOF slag filler has higher stiffness modulus and rutting factor than that of LF asphalt mastic. The effect of pyrolytic BOF slag filler on the performance of asphalt mastic is less than that of ordinary BOF slag because of the bigger particle size, more regular shape and relatively clean surface. The incorporation of BOF slag filler will reduce the low temperature flow performance of asphalt.

(4) The grinding energy consumption of pyrolytic BOF slag is higher than that of limestone and ordinary BOF slag, meanwhile its chemical performance is relatively inactive. It is not recommended that pyrolytic BOF slag filler is produced by grinding technology. Ordinary BOF slag filler can effectively improve high temperature anti-rutting stability when used as filler in asphalt mixture. BOF slag filler has a good prospects for application as part of asphalt mixtures.

Author Contributions: D.K., M.Z., S.W. and B.S. conceived and designed the experiments; D.K., M.Z. and B.S. performed the experiments; D.K., M.C. and B.S. analyzed the data; M.C. and S.W. contributed reagents/materials/analysis tools; D.K., M.C. and M.Z. wrote the paper.

Funding: This work was financially supported by the Fundamental Research Funds for the Central Universities (WUT: 2017IVA083), Technological Innovation Major Project of Hubei Province (No. CXZ2016000024), Technological Innovation Major Project of Hubei Province (No. CXZ2019ACA147) and the Science and Technology Major Project of Inner Mongolia Autonomous Region (No. ZDZX2018029).

Acknowledgments: The authors gratefully acknowledge many important contributions from the researchers of all reports cited in our paper.

Conflicts of Interest: The authors declare no conflict of interest.

References

1. Han, F.; Zhang, Z.; Wang, D.; Yan, P. Hydration heat evolution and kinetics of blended cement containing steel slag at different temperatures. *Thermochim. Acta* **2015**, *605*, 43–51. [CrossRef]
2. Reddy, A.S.; Pradhan, R.K.; Chandra, S. Utilization of Basic Oxygen Furnace (BOF) slag in the production of a hydraulic cement binder. *Int. J. Miner. Process.* **2006**, *79*, 98–105. [CrossRef]
3. Shen, D.H.; Wu, C.M.; Du, J.C. Laboratory investigation of basic oxygen furnace slag for substitution of aggregate in porous asphalt mixture. *Constr. Build. Mater.* **2009**, *23*, 453–461. [CrossRef]
4. Chen, Z.; Wu, S.; Yue, X.; Zeng, W.; Yi, M.; Wan, J. Effect of hydration and silicone resin on Basic Oxygen Furnace slag and its asphalt mixture. *J. Clean. Prod.* **2015**, *112*, 392–400. [CrossRef]
5. Xue, Y.; Wu, S.; Hou, H.; Zha, J. Experimental investigation of basic oxygen furnace slag used as aggregate in asphalt mixture. *J. Hazard. Mater.* **2006**, *138*, 261–268. [CrossRef]
6. Iacobescu, R.I.; Angelopoulos, G.N.; Jones, P.T.; Blanpain, B.; Pontikes, Y. Ladle metallurgy stainless steel slag as a raw material in Ordinary Portland Cement production: A possibility for industrial symbiosis. *J. Clean. Prod.* **2016**, *112*, 872–881. [CrossRef]
7. Li, C.H.; Xiang, X.D.; Qin, X.X. Utilization of Steel Slag as Aggregates for SMA-13. *Appl. Mech. Mater.* **2015**, *768*, 402–405. [CrossRef]
8. Pasetto, M.; Baldo, N. Experimental evaluation of high performance base course and road base asphalt mixture with electric arc furnace steel slags. *J. Hazard. Mater.* **2010**, *181*, 938–948. [CrossRef]
9. Pasetto, M.; Baldo, N. Fatigue Performance of Asphalt Mixtures with RAP Aggregates and Steel Slags. *Rilem Bookseries* **2012**, *4*, 719–727.
10. Wu, S.; Xue, Y.; Ye, Q.; Chen, Y. Utilization of steel slag as aggregates for stone mastic asphalt (SMA) mixtures. *Build. Environ.* **2007**, *42*, 2580–2585. [CrossRef]
11. Antunes, V.; Freire, A.C.; Quaresma, L.; Micaelo, R. Effect of the chemical composition of fillers in the filler–bitumen interaction. *Constr. Build. Mater.* **2016**, *104*, 85–91. [CrossRef]
12. Wang, H.; Alqadi, I.L.; Faheem, A.F.; Bahia, H.U.; Yang, S.H.; Reinke, G.H. *Effect of Mineral Filler Characteristics on Asphalt Mastic and Mixture Rutting Potential*; Transportation Research Board: Washington, DC, USA, 2011.
13. Antunes, V.; Freire, A.C.; Quaresma, L.; Micaelo, R. Influence of the geometrical and physical properties of filler in the filler–bitumen interaction. *Constr. Build. Mater.* **2015**, *76*, 322–329. [CrossRef]
14. Faheem, A.F.; Wen, H.; Stephenson, L.; Bahia, H.U. Effect of Mineral Filler on Damage Resistance Characteristics of Asphalt Binders (With Discussion). *J. Assoc. Asph. Paving Technol.* **2008**, *1*, 77.

15. Geber, R.; Simon, A.; Kocserha, I.; Buzimov, A. In Microstructural and rheological analysis of fillers and asphalt mastics. *J. Phys. Conf. Ser.* **2017**, *790*, 012009. [CrossRef]
16. Grabowski, W.; Wilanowicz, J. The structure of mineral fillers and their stiffening properties in filler-bitumen mastics. *Mater. Struct.* **2008**, *41*, 793–804. [CrossRef]
17. Wang, D.; Zhou, G. Fatigue of asphalt binder, mastic and mixture at low temperature. *Front. Struct. Civ. Eng.* **2012**, *6*, 166–175.
18. Li, C.; Chen, Z.; Wu, S.; Li, B.; Xie, J.; Xiao, Y. Effects of steel slag fillers on the rheological properties of asphalt mastic. *Constr. Build. Mater.* **2017**, *145*, 383–391. [CrossRef]
19. Tao, G.; Xiao, Y.; Yang, L.; Cui, P.; Kong, D.; Xue, Y. Characteristics of steel slag filler and its influence on rheological properties of asphalt mortar. *Constr. Build. Mater.* **2019**, *201*, 439–446. [CrossRef]
20. Li, Q.; Qiu, Y.; Rahman, A. Application of Steel Slag Powder to Enhance the Low-temperature Fracture Properties of Asphalt Mastic and its Corresponding Mechanism. *J. Clean. Prod.* **2018**, *184*, 21–31. [CrossRef]
21. Song, L.; Wang, X.; Li, X.; Yang, Q.; Wang, P. Influence of the steel-making dust on high temperature and fatigue performance of asphalt mortars. *J. Wuhan Univ. Technol. Mater. Sci. Ed.* **2019**, *34*, 361–367. [CrossRef]
22. Topkaya, Y.; Sevinç, N.; Günaydın, A. Slag treatment at Kardemir integrated iron and steel works. *Int. J. Miner. Process.* **2004**, *74*, 31–39. [CrossRef]
23. Ministry of Transport. *Standard Test Methods of Bitumen and Bituminous Mixtures for Highway Engineering: JTGE20-2011*; China Communications Press: Beijing, China, 2011.
24. Kong, D.; Chen, M.; Xie, J.; Zhao, M.; Yang, C. Geometric Characteristics of BOF Slag Coarse Aggregate and its Influence on Asphalt Concrete. *Materials* **2019**, *12*, 741. [CrossRef]
25. Yue, X.; Feng, W.; Peide, C.; Lei, L.; Juntao, L.; Mingwei, Y. Evaluation of fine aggregate morphology by image method and its effect on skid-resistance of micro-surfacing. *Materials* **2018**, *11*, 920.
26. Geng, J.G.; Dai, J.L.; Sheng, Y.P. The Determination of Mixing and Compaction Temperature of Recycled Asphalt Mixtures. In Proceedings of the International Workshop on Energy & Environment in the Development of Sustainable Asphalt Pavements, Xi'an, China, 6–8 June 2010; pp. 44–49.
27. Tan, Y.; Meng, G. Study on the phase behavior of asphalt mastic. *Constr. Build. Mater.* **2013**, *47*, 311–317. [CrossRef]
28. Li, X.; Shan, L.; Tan, Y. Analysis of different indices for high- and low-temperature properties of asphalt binder. *Constr. Build. Mater.* **2015**, *83*, 70–76. [CrossRef]
29. Zu-Zhong, L.I.; Man, X.Y.; Chen, S.F. Study on Viscosity-temperature Characteristics of Asphalt Binder for Stress Absorbing Layers and Determination of Construction Temperature. *J. Wuhan Univ. Technol.* **2012**, *34*, 37–41.
30. Moon, K.H.; Falchetto, A.C.; Marasteanu, M.O. Investigation of limiting criteria for low temperature cracking of asphalt mixture. *KSCE J. Civ. Eng.* **2014**, *18*, 172–181. [CrossRef]

materials

MDPI

Article

Geometric Characteristics of BOF Slag Coarse Aggregate and its Influence on Asphalt Concrete

Dezhi Kong [1], Meizhu Chen [1], Jun Xie [1,*], Meiling Zhao [2] and Chao Yang [1]

[1] State Key Laboratory of Silicate Materials for Architectures, Wuhan University of Technology, Wuhan 430070, China; kongdz@whut.edu.cn (D.K.); chenmzh@whut.edu.cn (M.C.); hbyangc@whut.edu.cn (C.Y.)
[2] Research Institute of Highway of Ministry of Transport, Beijing 100088, China; 197791@whut.edu.cn (M.Z.)
* Correspondence: xiejun3970@whut.edu.cn

Received: 31 January 2019; Accepted: 27 February 2019; Published: 4 March 2019

Abstract: In order to examine the geometric characteristics of BOF (blast oxygen furnace) slag coarse aggregate, the aggregate image measurement system (AIMS) was used to analyze the sphericity, gradient angularity and micro texture. Both volumetric and mechanical properties were studied to evaluate the influence of geometric characteristics of BOF slag coarse aggregate on asphalt concrete. The experimental results show that the BOF slag coarse aggregate has the characteristics of high sphericity, good angular performance and rough surface texture. The geometric characteristics of BOF slag has obvious influence on the volume performance of asphalt concrete. the higher sphericity of BOF slag causes an increase of the air voids of asphalt mixture. BOF slag coarse aggregate can effectively improve the road performances of asphalt concrete. BOF slag's higher sphericity and angularity improve the moisture damage resistance and rutting resistance of asphalt concrete. Results indicate that better angularity can slightly enhance the moisture resistance property of asphalt concrete, but excessively high angularity of BOF slag coarse aggregates reduces the anti-rutting properties of asphalt mixture.

Keywords: BOF slag; coarse aggregate; geometric characteristics; asphalt concrete; road performance

1. Introduction

With the increasing development of the transportation industry in the past few decades, the consumption of natural aggregate resource has been a close concern of scholars in this field. By the end of 2017, the total mileage of expressway has reached 0.137 million kilometers in China [1]. More than 90% of this is asphalt pavement, which has the advantages of low vibration, low noise, short construction time and convenient maintenance [2,3]. Expressway need lots of construction and maintenance, and more than 90% of the components of asphalt pavement are aggregates, which causes the depletion of natural resources [4,5]. Therefore, recycling solid waste and industrial smelting waste are becoming an effective option to relieve the supply pressure of natural aggregate resources [6–8].

Steel slag is the main solid waste in steel industry, accounting for more than 10% of crude steel production [9–11]. According to the different steelmaking processes, steel slag can be classified into three types: Electric arc furnace (EAF) slag, basic oxygen furnace (BOF) slag and ladle furnace (BF) slag. The large capacity of steel slag can meet the needs of aggregates for road construction, and it has good mechanical properties and high alkalinity [12,13]. The steel slag asphalt mixture has become an increasingly popular research topic in the field of environmental protection road materials in recent years [14,15].

Ahmedzade et al. [16] discussed the application of BOF slag coarse aggregate in AC-10 and AC-5 asphalt mixture. The research showed that the use of BOF slag coarse aggregate in asphalt mixture has better performance than that of limestone. The mechanical properties of steel slag improve the moisture damage resistance and rutting resistance performance of asphalt mixture. Behnood et al. [17,18] used

steel slag coarse aggregate in stone mastic asphalt (SMA) mixture and found that steel slag applied in the stone mastic asphalt mixture is feasible. Using steel slag as coarse aggregate in SMA can effectively improve its water damage resistance and pavement durability. Pasetto et al. [19,20] evaluated high performance asphalt concrete with electric arc furnace steel slags. Their results showed that asphalt mixtures with EAF slags exhibited better mechanical characteristics than those of the asphalt mixtures with natural aggregates.

Wu et al. [21,22] studied the properties of BOF slag asphalt mixture from the viewpoint of physicochemical characteristics of basic oxygen furnace (BOF) slag. SEM, XRD, EPMA and other testing methods were used to analyze the physicochemical properties of BOF slag. The results showed that BOF slag has a rough surfaced micro texture, which is beneficial to the bonding properties of asphalt. The BOF slag has good angle properties and a rougher alkaline surface than natural aggregates. The asphalt mixture prepared by the BOF slag has better water damage resistance, and higher temperature rutting resistance, fatigue resistance and anti-skid resistance.

Although existing research has determined that the special physical properties of BOF slag can improve the performance of asphalt concrete, the geometric properties of BOF slag and its influence on asphalt mixture have not been effectively quantified. Nodes et al. [23] analyzed the performance of asphalt pavement with the effect of angularity on natural aggregate. The results showed that higher angularity of aggregates improved the interlocking interaction of coarse aggregates, which contributed to increased rutting resistance of asphalt pavement.

Digital image processing technology can solve this problem properly, as it has been used for accurately quantifying the sphericity, gradient angularity and micro texture of aggregates [24–26]. The aggregate image measurement system (AIMS) is a computer automation system that can accurately quantify the geometric properties of aggregates [27]. It uses a high resolution digital camera to quickly picture large numbers of aggregates, and then uses data processing software to calculate and process the shape and surface texture of each aggregate. Finally, quantitative properties, such as the angularity, sphericity and texture of the aggregates, can be obtained [28,29].

This research uses AIMS to quantify and analyze angularity, sphericity and texture of the BOF slag coarse aggregates, and then investigate the influence of geometric characteristics of coarse aggregates on asphalt concrete. The concept of effective density is used in this research to decrease the experimental error caused by the high density of BOF slag. Coarse aggregate of basalt, limestone and three types of BOF slag are used to prepare AC 13 (asphalt mixture with a maximum particle size of aggregate of 13 mm). Volumetric and mechanical properties are discussed to investigate the influence of geometric characteristics of BOF slag coarse aggregate on AC 13.

2. Materials and Methods

2.1. Aggregates

Two types of natural aggregates, basalt and limestone, were obtained from Hubei province in China for use in this research. Three types of BOF slag were used in this research: BOF slag #1 was obtained from Wuhan Iron and Steel Company in Hubei province, China; BOF slags #2 and #3 were obtained from Baotou Iron and Steel Company in Inner Mongolia. BOF slags 1 and 2 were basic oxygen furnace slag, while BOF slag #3 was pyrolytic BOF slag (basic oxygen furnace slag treated with hot stuffing process). Table 1 lists the chemical compositions based on X-ray fluorescence analysis.

Basalt and limestone are naturally available aggregates. As Table 1 shows, the chemical composition of SiO_2 in basalt is 47.9%, while chemical composition of CaO in limestone is more than 50%. Compared with naturally available aggregates, the chemical composition of Fe_2O_3 in the three types of BOF slag is more than 20%. The SiO_2 content in the three types of BOF slag is less than 30%.

The basic engineering properties of aggregates were tested according to ASTM standards [30–32] and the results are showed in Table 2. They all meet requirements.

Table 1. Chemical composition of the aggregates.

Aggregate Type	Composition (%)							
	SiO_2	CaO	MgO	Al_2O_3	Fe_2O_3	MnO	P_2O_5	LOI
Basalt	47.9	8.23	4.34	18.3	9.82	3.6	2.25	5.27
Limestone	0.86	51.2	2.36	0.85	0.12	0.7	1.02	42.7
1# BOF slag	19.2	42.7	5.19	3.25	23.9	1.77	1.41	2.36
2# BOF slag	17.7	39.7	5.56	2.91	24.4	4.55	1.68	3.41
3# BOF slag	15.4	34.4	6.22	1.95	30.8	4.46	2.15	4.46

Table 2. The basic engineering properties of the aggregates in this research.

Parameter Measured	Basalt	Limestone	BOF Slag			Requirements
			#1	#2	#3	
Los Angeles abrasion (%)	10.2	11.8	16.5	15.6	15.6	≤28
Aggregate Crushing Value (%)	9.1	14.1	14.3	15.2	13.9	≤26
Flakiness and elongation (%)	13.2	10.7	6.6	5.8	4.3	≤18
Fine aggregate angularity (%)	42	46.3	NA	NA	NA	≥30
Sand equivalent (%)	68.5	74.2	NA	NA	NA	≥60

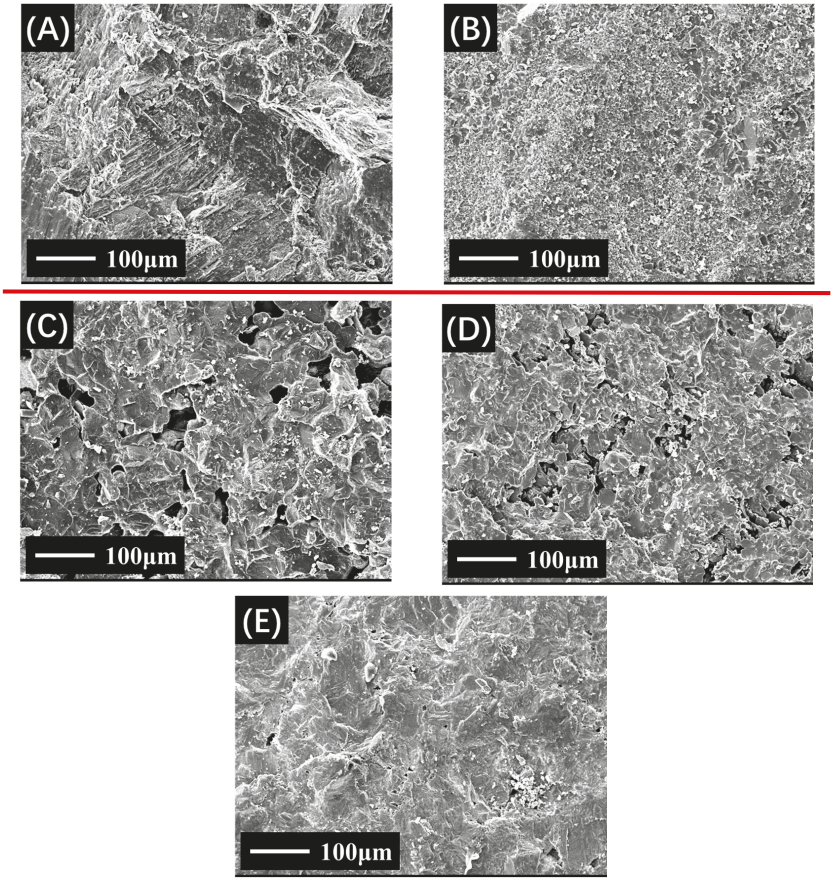

Figure 1. SEM images of investigated aggregates. **A**: Basalt; **B**: Limestone; **C**: #1 BOF slag, **D**: #2 BOF slag, **E**: #3 BOF slag).

Figure 1 shows the diversity between two types of naturally aggregates and three types of BOF slags in SEM images. According to the micrographs of basalt and limestone, the microscopic texture of basalt is relatively dense because it is a volcanic rock, while the microscopic surface of limestone consists of a clastic texture and tiny grain structure as it belongs to the carbonate sedimentary rocks. Comparing micrographs of BOF slags and natural aggregates, BOF slags show different surface textures, particularly on the size and number of surface microscopic pore structures. Micrographs of BOF slags #1 and #2 show that large numbers of pore structures with sizes of approximately 10–50 μm appear on the BOF slag surface. Micrographs of BOF slag #3 shows that the surface microscopic imaging of pyrolytic BOF slag is between basalt and BOF slag, which has a considerable number of pore structures of 1–10 μm in size. The greater the number of surface microscopic pore structures in BOF slag represents higher water absorption and asphalt absorption.

2.2. Asphalt Binder and Filler

Asphalt binder was used in this research and its optimum asphalt content is 4.7% in the mixture. Its characteristics are shown in Table 3. Table 4 presents the features of the used limestone filler in this research.

Table 3. Basic properties of the asphalt binder.

Properties		Values	Specifications
Penetration (0.1 mm)		63	60–80
Penetration index		−0.7	−1.5–1.0
Softening point (°C)		47.7	≥46
Ductility, 5 cm/min, 15 °C (cm]		>160	≥100
Dynamic viscosity (60 °C) (Pa·s)		179	≥160
Density (g/cm^3)		1.023	
After RTFOT (rotating thin film over test) ageing	Weight loss (%)	−0.05	−0.8–0.8
	Penetration ratio (%)	67.5	≥61
	Residual ductility 5 cm/min, 10 °C (cm)	11.5	≥6

Table 4. Basic properties of limestone filler in this research.

Properties		Values	Specifications
Apparent specific gravity		2.816	≥2.5
Sieves passing percentage (%)	<0.6 mm	100	100
	<0.15 mm	98.4	90–100
	<0.075 mm	92.2	75–100
Hydrophilic coefficient		0.4	<1.0

3. Experimental Details

3.1. Gravity Characteristics of Coarse Aggregate

Aggregate gravity is the first factor to be considered in asphalt mixture design. It includes apparent specific gravity, bulk specific gravity and water absorption.

The specific gravity of BOF slag and natural aggregates is quite different. The purpose of this research is to design an asphalt mixture with different types of coarse aggregates and fine aggregates. Insufficient consideration of aggregate specific gravity will lead to adverse influence on the volumetric and road performance of the asphalt mixture [33].

3.1.1. Aggregate Specific Gravity

Aggregate specific gravity is the ratio of the aggregate's density to water density at 23 °C. It is quite different between BOF slag and natural aggregate. The apparent specific gravity (Gsa) measures

the volume of aggregate particle and impervious voids. The bulk specific gravity (Gsb) measures the volume of aggregate particle, impervious voids and water permeable voids. Water absorption refers to the amount of water absorbed by the void of the aggregate.

Aggregate with different grain size ranges have different aggregate specific gravity. Table 5 shows the Gsb and Gsa of aggregates at different grain size ranges according to the JTG42-2005 standard of China. Table 5 shows that the Gsb and Gsa of BOF slag is higher than that of basalt and limestone. Among three types of BOF slags, the Gsb and Gsa of BOF slag #1 and BOF slag #2 are similar. Due to the self-slaking process of BOF slag by pyrolytic and processing technology, BOF slag #3 (pyrolytic BOF slag) has the highest specific gravity. It is at least 15% higher than the basalt's specific gravity in each grain size. In the same types of aggregates, the Gsb increase with the increase of aggregate particle size range.

Table 5. Specific gravities of coarse aggregates at different size ranges.

Aggregate	Gravity	Grain Size (mm)			
		2.36–4.75	4.75–9.5	9.5–13.2	13.2–16.0
Basalt	Gsa	2.923	2.918	2.915	2.912
	Gsb	2.863	2.881	2.886	2.899
Limestone	Gsa	2.723	2.716	2.705	2.701
	Gsb	2.663	2.676	2.684	2.689
1#BOF slag	Gsa	3.308	3.302	3.293	3.306
	Gsb	3.092	3.102	3.125	3.153
2#BOF slag	Gsa	3.275	3.263	3.302	3.293
	Gsb	3.098	3.124	3.179	3.186
3#BOF slag	Gsa	3.543	3.587	3.563	3.582
	Gsb	3.379	3.426	3.453	3.517

Figure 2 shows the water absorption of the five types of aggregates at different grain size ranges. Immersion duration of aggregates is 24 h. Apparently, with the decrease of aggregate grain size, the water absorption becomes larger. Smaller grain size is logically related to bigger specific surface area, which will therefore decrease the ration of closed voids in aggregates and increase the ratio of open voids. Basalt and limestone have similar water absorption at different grain size ranges. Meanwhile, BOF slag has higher water absorption than natural aggregate. The order of their water absorption from large to small is: #1BOF slag, #2BOF slag and #3BOF slag.

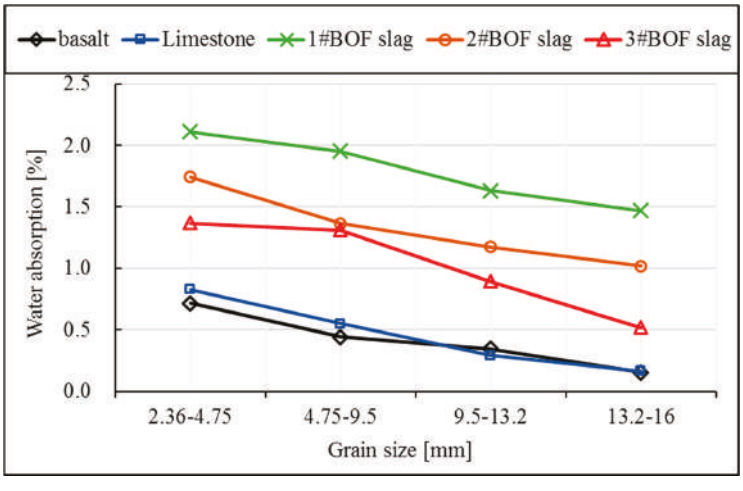

Figure 2. Water absorptions of aggregates.

3.1.2. Effective Specific Density

The mix ratio of asphalt mixture with single type of aggregate was based on aggregate weight. However, in the experimental design of this research, four types of aggregates were used to replace basalt coarse aggregate. The aggregate specific gravity results illustrate that big differences appear on specific gravities and water absorption between different aggregate types. Due to the difference in specific gravity, the gradation and optimum asphalt content in the design of asphalt mixture will change.

In the asphalt mixture, the asphalt can partly fill open voids on the surface of aggregate; therefore, the apparent density or bulk density of aggregates cannot effectively represent the density of aggregates in asphalt. It is more effective to use the specific density (Dse), taking into account the volume effect between aggregate types for designing asphalt mixture. The Dse of the different aggregates are shown in Table 6. Coarse aggregate was replaced by the ratio of effective specific density of different aggregates, aiming to reduce the inaccuracy of the test caused by aggregate density.

Table 6. Dse of aggregates at different grain size range.

Aggregate	Grain Size (mm)			
	2.36–4.75	**4.75–9.5**	**9.5–13.2**	**13.2–16**
Basalt	2.691	2.694	2.695	2.696
Limestone	2.896	2.905	2.902	2.904
#1BOF slag	3.272	3.264	3.217	3.186
#2BOF slag	3.214	3.197	3.245	3.153
#3BOF slag	3.474	3.513	3.498	3.421

3.2. Preparation of Asphalt Mixture

AC 13 asphalt mixture was selected to investigate the combination of two natural aggregates and three BOF slags. In order to reduce experimental errors, the aggregate gradation was kept constant. The aggregates distribution of basalt was used in the basic aggregate gradation, as shown in Table 7.

Table 7. Aggregate composite gradation of AC 13 asphalt mixture.

Coarse Aggregates (mm)		Weight Ratio (%)	Fine Aggregates (mm)		Weight Ratio (%)
9.5–16	13.2–16	4.1	0–2.36	1.18–2.36	6.3
	9.5–13.2	22.6		0.6–1.18	7.7
2.36–9.5	4.75–9.5	28.7		0.3–0.6	4.6
	2.36–4.75	13.3		0–0.3	8.7
Filler					4%

The coarse aggregate and fine aggregate play different roles in the asphalt mixture. Coarse aggregates play a major role in supporting and reinforcing the construction of asphalt mixture, while fine aggregates are mainly used to fill the gaps between coarse aggregates. For the AC 13 asphalt mixture, the dividing sieve size between coarse aggregate and fine aggregate is 2.36 mm.

A coarse–fine composition method was proposed and used to keep fine aggregates such as basalt unchanged, while the coarse aggregates were fully replaced basing on effective specific density. Figure 3 explains the detail of coarse–fine composition.

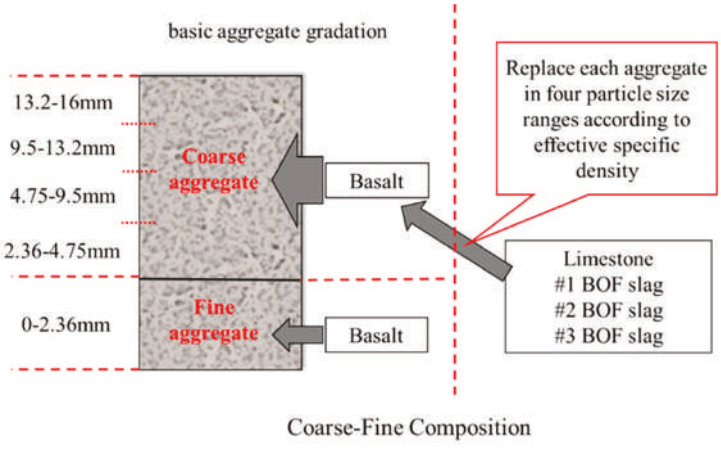

Figure 3. The coarse–fine composition method.

In asphalt concrete, the geometric characteristics of coarse aggregate, such as angularity, sphericity, surface texture, have a great influence on its performance. A marshall stability test was used to characterize the water resistance of asphalt mixture in 60 °C water; this test is still currently used in the road laboratories for the mechanical characterization of asphalt concretes. In order to change geometric characteristics of the coarse aggregate, a ball mill is used to process the coarse aggregate, which imitates the Los Angeles abrasion test. The time of the specific processing was 30 min, at a weight of 3000 g for each sample; the rotating speed was 120 rpm; and using abrasion with 8 steel balls (500 g each). In this research, #1 BOF slag was treated using the above method and named as processed #1BOF slag (SP1). AIMS (aggregate image measurement system) was used to analyze the angularity, sphericity and surface texture of each aggregate.

In this research, the coarse–fine composition of asphalt mixture method was applied, with 0% of coarse aggregates and 100% of fine aggregates passing through sieves of 2.36 mm. Table 8 lists the labels for every coarse–fine composition of asphalt mixture. Four specimens were tested in each and the average data were used for analysis.

Table 8. Labels for every coarse–fine composition of asphalt mixture.

Fine Aggregate	Coarse Aggregate	Label
Basalt	Basalt (B)	BB
	Limestone (L)	BL
	#1BOF slag (S1)	BS1
	#2BOF slag (S2)	BS2
	#3BOF slag (S3)	BS3
	processed #1BOF slag (SP1)	BSP1

3.3. Experimental Methods

3.3.1. Aggregates Morphology Test

Shape, angularity, and surface texture of aggregates have been shown to directly affect the engineering properties of highway construction such as HMA (hot mix asphalt concrete) and concrete. The aggregate image measurement system (AIMS) was used to analyze the angularity, sphericity and surface texture of coarse aggregates of each types of aggregate.

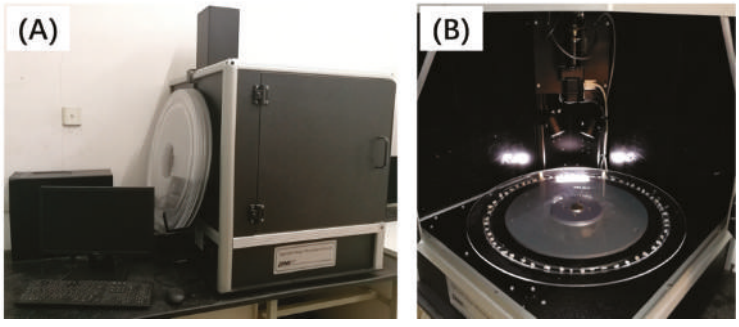

Figure 4. Aggregate image measurement system (**A**), and the tested coarse aggregate placed on tray (**B**).

As shown in Figure 4, the aggregate image measurement system is comprised of image acquisition hardware and a computer to run the system and process data. The image acquisition hardware used a high-resolution digital camera and a variable magnification microscope to collect digital images and measure aggregates. The system used a tray to place the aggregate under the view of the camera. The first scan used backlighting to describe a profile image of the aggregate particle, from which dimensions and angularity gradients of the edges were measured. The second scan utilized top-lighting and variable magnification to capture texture images and measure each aggregate particle's height. AIMS then used the computer to process the acquired images.

Angularity is a description of edge sharpness of the boundary particles of aggregate. The angularity changes with aggregate boundary shape changes. The value of angularity is calculated based on the gradient of the particle boundary. Angularity is calculated with Equation (1) and its range is from 0 to 1000. The lager the value of angularity, the sharper the boundary shape of the aggregate.

$$Angularity = \frac{1}{\frac{n}{3} - 1} \sum_{i=1}^{n-3} |\theta_i - \theta_{i+3}| \quad (1)$$

where θ is angle of orientation of the edge points, n is the total number of points, i is the ith point on the edge of the particle.

Sphericity is used to characterize the degree of similarity between the aggregate shape and the ideal sphere. Sphericity is calculated with Equation (2), its range is 0 to 1. If the value of sphericity is closer to 1, the shape of aggregate is more similar to the ideal sphere.

$$Sphericity = \sqrt[3]{\frac{d_S d_I}{d_L^2}} \quad (2)$$

where, d_S is particle shortest dimension, d_I is particle intermediate dimension, d_L is particle longest dimension.

3.3.2. Marshall Stability Test

The Marshall stability test is used to characterize the water resistance of asphalt mixture in 60 °C water. The compacted specimens were divided into two groups according to the numerical average of VV (percent air voids in asphalt mixtures). The first group was put in the water at 60 °C for 30 min. The second group was placed in water at 60 °C for 48 h. The specimens were then placed in a testing machine at a constant displacement load rate of 50 mm/min. We recorded the Marshall stability (MS, maximum load) and Marshall flow (the maximum load starts to decrease when the deformation is mm).

The retained Marshall stability (RMS) is defined as the ratio of the sample to Marshall stability after immersion in hot water for 48 h (MS1, kN) and 30 min (MS, kN). The larger the RMS, the better the water resistance performance of asphalt mixture.

3.3.3. Freeze-Thaw Splitting Test

The freeze-thaw splitting test can be used to measure the ability of moisture resistance of asphalt mixture at low temperatures. The main evaluation index is the splitting strength ratio TSR (%). The larger the value of TSR, the better the moisture resistance of asphalt mixture of the water at freezing and thawing environmental conditions.

Splitting strength ratio (TSR) is defined as the ratio between ITS after F-T circles and ITS of nor-freeze. Among them, the environmental conditions of F-T circles are freezing at −20 °C for 16 h.

3.3.4. Rutting Test

The rutting test was used to characterize the high temperature rutting resistance of asphalt mixture. The size of the rut specimen was 300 × 300 × 50 mm, and the specimen density was controlled at 100 + 1.0% of the Marshall density. The rutting experiment temperature was 60 °C, the wheel pressure was 0.7 MPa, and the experimental wheel round-trip speed was 42 times/min. The dynamic stability (DS) is expressed by the rutting depth change rate of 45–60 min.

3.4. Research Program

Figure 5 illustrates the research program on the influence of geometric characteristics of BOF slag coarse aggregate on asphalt concrete. Firstly, the aggregate image measurement system (AIMS) was used to analyze the angularity, sphericity and surface texture of coarse aggregates. Then, the effective specific density was conducted during the asphalt mixture design. Basalt was used to create the AC 13 mixture, and the coarse aggregate was replaced by limestone and BOF slags by coarse-fine composition method, respectively. Volumetric and mechanical properties were studied to evaluate the influence of geometric characteristics of BOF slag coarse aggregate on asphalt concrete.

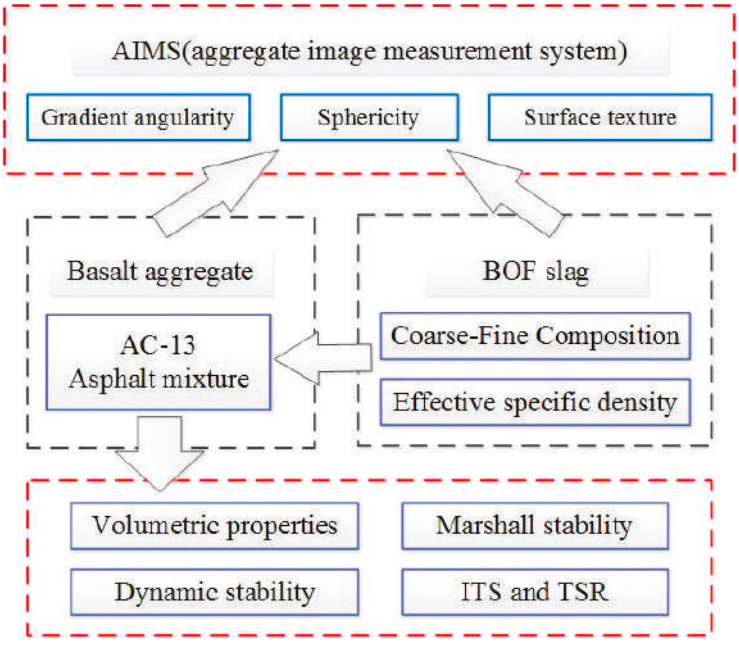

Figure 5. Finalized research program.

4. Results and Discussion

4.1. Geometric Characteristics of Coarse Aggregate

Coarse aggregates with sizes of 9.5–13.2 mm and 4.75–9.5 mm in total, account for 51.3% by the weight of the asphalt mixture. Therefore, the geometric characteristics of coarse aggregate were represented by the angularity, sphericity and surface texture of aggregates with those two sizes. Each test selected 200 aggregate samples, and the illustration of angularity, sphericity and texture is shown in Figure 6.

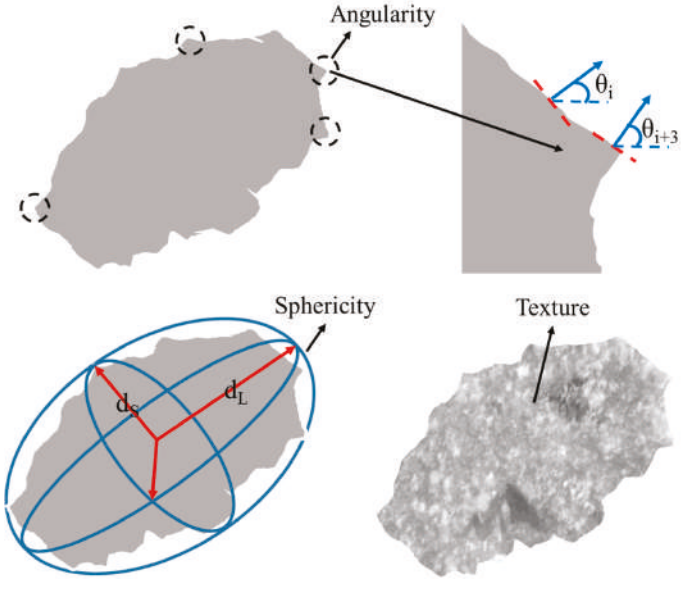

Figure 6. Illustration of angularity, sphericity and texture.

4.1.1. Angularity

Angularity is a description of edge sharpness of the boundary particles of aggregate. Profile images of different types of aggregate particle from the first scan of AIMS are shown in Figure 7.

The angularity of investigated coarse aggregates is shown in Table 9. This was obtained from the average values of 200 aggregate samples. The results show that the angularity of BOF slag is higher than that of natural aggregates. Different types of BOF slag have different angularity. Among them, in the same place of production, the angularity of basic oxygen furnace slag is higher than pyrolytic BOF slag. Meanwhile, limestone has the lowest angularity and #2 BOF slag has the highest angularity.

Table 9. Angularity of investigated coarse aggregates.

Grain Size (mm)	Basalt	Limestone	S1	S2	S3	SP1
9.5–13.2 mm	2965	2896	3064	3770	3180	2886
4.75–9.5 mm	2846	2733	3051	3283	2829	2765

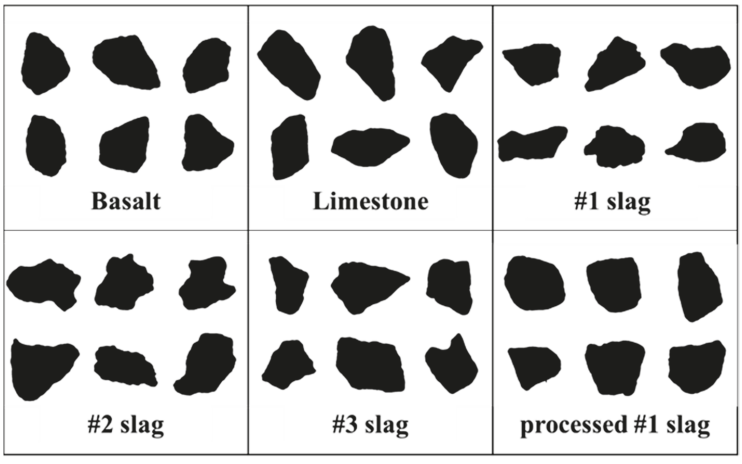

Figure 7. Parts of the profile image of different types aggregate particles.

4.1.2. Sphericity

The sphericity of the investigated coarse aggregates is shown in Table 10. The results were calculated from the 200 aggregate samples. It can be observed from Table 10 that the limestone had the lowest sphericity and #2 BOF slag had the highest sphericity. BOF slag had a higher degree of sphericity than natural aggregates.

Table 10. Sphericity of investigated coarse aggregate.

Grain Size (mm)	Basalt	Limestone	S1	S2	S3	SP1
9.5–13.2 mm	0.706	0.662	0.749	0.759	0.739	0.768
4.75–9.5 mm	0.639	0.609	0.693	0.718	0.726	0.729

4.1.3. Texture

Texture represents the relative roughness and smoothness of aggregate surfaces. The second scan utilized top-lighting and variable magnification to capture texture images of aggregates; these are shown in Figure 8.

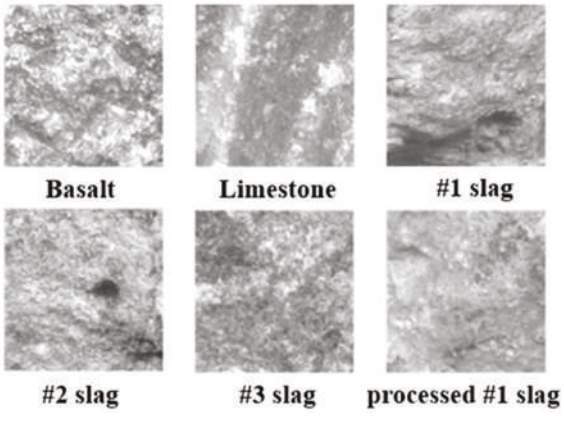

Figure 8. Parts of the surface texture images of aggregates.

The texture value of an ideal smooth surface is defined as zero. The AIMS texture analysis uses the wavelet method in the calculation and analysis of texture.

The texture of investigated coarse aggregate is shown in Table 11. From the texture values of six types of aggregate, the highest texture value is basalt. The texture value of BOF slag is smaller. As the surface of BOF slag has formed uniform color carbonized layers during the aging process, the photos taken by the digital camera of AIMS cannot represent the surface texture of the BOF slag. With reference to the water absorption of each aggregates in Table 8, #1 BOF slag is considered to be the most texture.

Table 11. Texture of investigated coarse aggregate.

Grain Size (mm)	Basalt	Limestone	S1	S2	S3	SP1
9.5–13.2 mm	708	450	349	356	407	419

4.2. Volumetric Properties of BOF Slag Coarse Aggregate Asphalt Concrete

In traditional asphalt mixture gradation designs the air voids in the asphalt mixture are the most important index of volumetric properties, which can also affect the performance of asphalt concrete. The skeleton structure of AC 13 asphalt mixture is a suspension-compact structure with 3–5% percent air voids in the asphalt mixture.

The percentage of air voids in the asphalt mixture (VV) is defined as the volume percentage of air voids in compacted asphalt mixtures. It is calculated with Equation (2).

$$VV = 100 \times \left[1 - \left(\frac{G_f}{G_t}\right)\right] \quad (3)$$

where G_t is the theoretical maximum specific gravity of bituminous mixture and G_f is bulk specific gravity of bituminous mixture.

Table 12 shows the volumetric properties of AC 13. Compare with group BB, the theoretical maximum density decrease and porosity decrease by about 40% in terms of limestone aggregate. The VV of BS2 is similar with BB, and the use of other groups of BOF slag can effectively improve the value of VV; the highest VV of BSP1 reached 5.83%.

Table 12. Volumetric properties with different coarse aggregates.

Aggregate Categories	Theoretical Maximum Density [g/cm^3]	Apparent Density [g/cm^3]	VV [%]
BB	2.689	2.585	3.873
BL	2.601	2.545	2.154
BS1	2.828	2.708	4.262
BS2	2.812	2.706	3.769
BS3	2.958	2.831	4.285
BSP1	2.827	2.662	5.832

When combining the volumetric properties analysis with geometric characteristics of aggregate, four types of BOF slags have higher sphericity than basalt. Among them, BSP1 has the highest sphericity and the lowest angularity and it has the largest value of VV. BS2 has the highest angularity when compared with BS1, but its VV is lower. This shows that the excessively high angularity reduces the value of VV.

The geometric characteristics of coarse aggregates have a great effect on the volumetric properties of asphalt mixture. Firstly, the rough surface texture and high water absorption of BOF slag coarse aggregate can absorb more free asphalt in the mixture and increase air voids of the asphalt mixture. Secondly, the high sphericity of the BOF slag contributes more skeleton support in the asphalt mix skeleton structure. In addition, BOF slag has a higher angularity than natural aggregate, so the larger

sphericity of the BOF slag leads to a higher VV of the asphalt mixture. Lastly, if BOF slag has excessive angularity value, the edge angle of BOF slag would be destroyed during the compaction of the asphalt mixture, which would result in the decrease of the air voids of the asphalt mixture.

Using BOF slag coarse aggregates will result in a significant increase in the percentage of air voids in asphalt mixture. The rough surface texture and higher sphericity of BOF slag will cause the increase of the air voids of asphalt mixture. Besides, if the BOF slag has excessively high angularity, it will have an adverse effect on the increase of air voids.

4.3. Mechanical Properties of BOF Slag Coarse Aggregate Asphalt Concrete

The Marshall stability test, freeze-thaw (F-T) splitting test and rutting test were employed to evaluate the influence of geometric characteristics of BOF slag coarse aggregate on asphalt concrete.

4.3.1. Marshall Stability Test Results

As shown in Figure 9, the values of Marshall stability are presented. The RMS of the basalt-based asphalt mixture has the lowest value of 80.37%. Coarse aggregate of limestone and coarse aggregate of BOF slag can significantly enhance the moisture resistance property. BS1 has the highest water absorption and non-outstanding value of angularity and sphericity. The results of BS1 and BSP1 are similar, showing that improving the sphericity of BOF slag and reducing the angularity of BOF slag have little effect on the moisture resistance property of asphalt mixture.

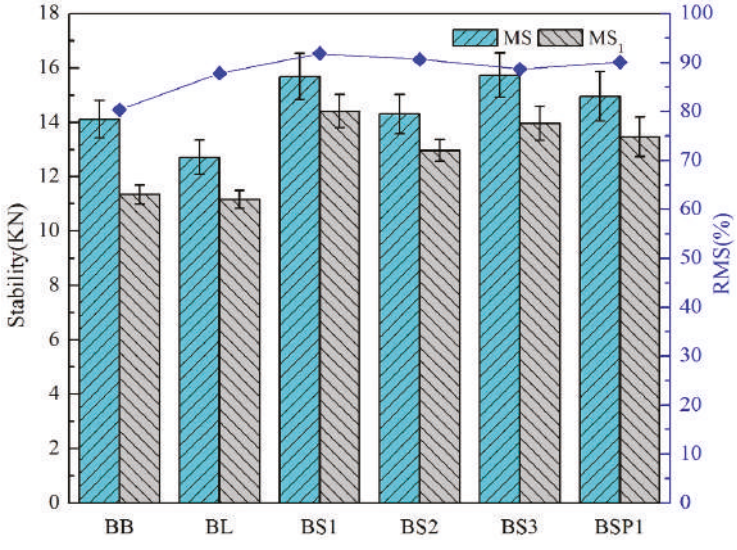

Figure 9. Marshall stability test results with different coarse aggregates.

As can be seen in Figure 10, there are close parabolic equation curve relationships between angularity or sphericity of BOF slag and Marshall stability test results. The R2 of angularity and sphericity is 0.99 and 0.78, respectively. Both of the correlations of angularity and sphericity tend to increase first and then decrease. The optimal angularity and sphericity of Marshall results is 3267 and 0.755, respectively.

AC 13 has a suspension-compactness skeleton structure. The rough surface texture (high water absorption) of BOF slag and good adhesion with asphalt result in a good moisture resistance property of the asphalt mixture. Changing the degree of sphericity or angularity of BOF slag has little influence on the beneficial effect of moisture resistance property on the asphalt mixture.

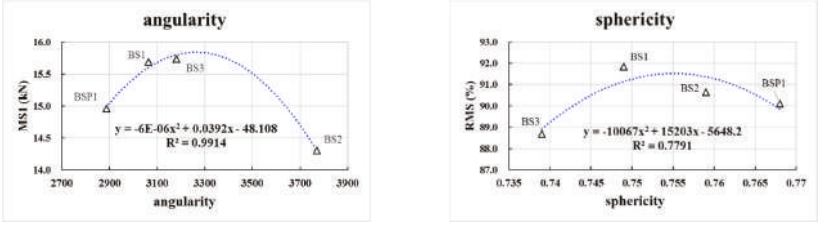

(**A**) (**B**)

Figure 10. Correlation between Marshall stability test results and aggregate geometric characteristics. (**A**) correlation between MS1 and angularity; (**B**) correlation between RMS and sphericity.

4.3.2. Freeze-Thaw Splitting Test Results

Figure 11 presents the splitting rest results of composite asphalt mixtures. The tendency of freeze-thaw splitting test is similar to the Marshall stability test. The TSR of BB is the lowest. All types of BOF slags coarse aggregates composite asphalt mixtures possess higher TSR values. There is little difference between the TSR values of BS1 and BSP1. It shows that improving the sphericity of BOF slag and reducing the angularity of BOF slag have little effect on the moisture resistance property of BOF slag coarse aggregate asphalt mixture. TSR value of BS2 is the lowest among the 4 types of asphalt mixture with BOF slag.

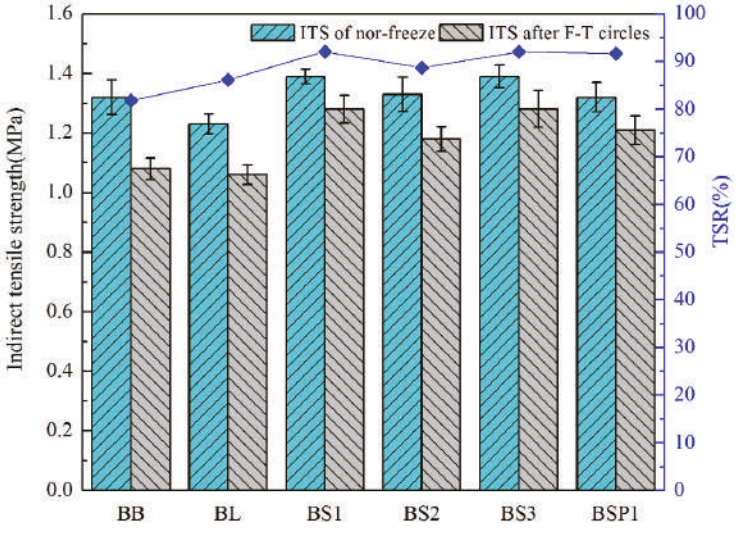

Figure 11. Splitting test results with different coarse aggregates.

As can be seen in Figure 12, there are close parabolic equation curves relationships between angularity of BOF slag and splitting test results, while R2 of angularity is 0.999. The correlations of angularity and TSR tend to increase first and then decrease. The optimal angularity of Marshall results is 3344. There is a weak linear relationship between sphericity and splitting test results.

BOF slag coarse aggregates have a rough surface and an alkaline surface, which enhances the moisture resistance under F-T circles of AC 13. Changing the degree of sphericity of BOF slag has little influence on the improving effect of low temperature moisture resistance property of asphalt mixture. The excessively high angularity of the aggregate can adversely affect the low temperature moisture resistance property of the asphalt mixture.

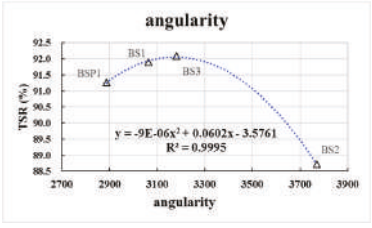

(**A**)

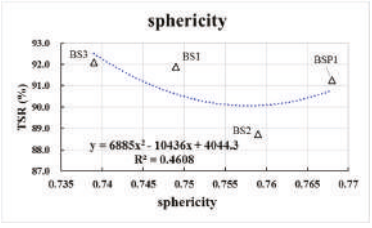

(**B**)

Figure 12. Correlation between splitting test results and aggregate geometric characteristics. (**A**) correlation between TSR and angularity; (**B**) correlation between TSR and sphericity.

4.3.3. Rutting Test Results

The Rutting test results are shown in Table 13. It can be clearly observed that the limestone coarse aggregate asphalt mixture has the lowest dynamic stability. Using four types of BOF slag coarse aggregates can improve the values of asphalt mixture dynamic stability in varying degrees, among which BS3 has the best high temperature rutting resistance of asphalt mixture. When compared with BS1, the dynamic stability of BSP1 and BS2 is decreased. This shows that the high sphericity and low angularity of BOF slag coarse aggregates will increase the dynamic stability of the asphalt mixture. Meanwhile, if the BOF slag has excessively high angularity, it will have an adverse effect on the increased dynamic stability.

Table 13. Rutting text results with different coarse aggregates.

Aggregate Categories	Rutting Depth (mm)	Dynamic Stability (mm)
BB	2.162	3056
BL	3.284	1863
BS1	1.952	4632
BS2	2.341	3517
BS3	1.842	4782
BSP1	2.080	4152

As can be seen in Figure 13, there are close parabolic equation curves relationships between angularity of BOF slag and dynamic stability, while R2 of angularity is 1.0. The curves of angularity tend to increase first and then decrease. The optimal angularity of dynamic stability is 3285. There is a weak linear relationship between sphericity and dynamic stability. With the rise of sphericity of BOF slag, dynamic stability has a slight reduction trend.

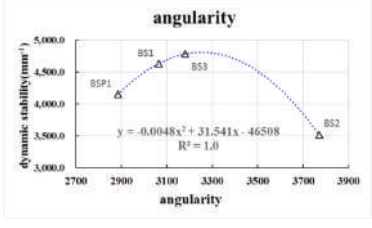

(**A**)

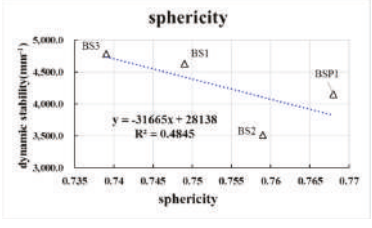

(**B**)

Figure 13. Correlation between rutting test results and aggregate geometric characteristics. (**A**) correlation between dynamic stability and angularity; (**B**) correlation between dynamic stability and sphericity.

5. Conclusions

This study investigated the geometric characteristics (sphericity, angularity and texture) of three types of BOF slag coarse aggregates by AIMS. A coarse-fine composition method and effective density were proposed and studied. Volumetric and mechanical properties of AC 13 were discussed to investigate the influence of geometric characteristics of BOF slag coarse aggregate. The following conclusions were obtained:

(1) Compared with natural aggregates, the microscopic surface of BOF slag has a pitted and vesicular texture and a porous structure with particle range of 1–50 μm. BOF slag coarse aggregates have higher sphericity and angularity than natural aggregates. The BOF slag coarse aggregate has higher water absorption and higher effective density, among which the pyrolytic BOF slag has the largest effective density.

(2) Using BOF slag coarse aggregates result in a significant increase on the VV of AC 13. The rough surface texture (higher water absorption) and higher sphericity of BOF slag causes the increase of the air voids in the asphalt mixture. The excessively high angularity of BOF slag can decrease the VV of AC 13 and the higher sphericity of BOF slag causes the increase of the air voids in the asphalt mixture.

(3) According to the result of the Marshall stability, freeze-thaw splitting, and Rutting tests, using the coarse aggregate of three types of BOF slag and the processed BOF slag can enhance the properties of moisture damage resistance and rutting resistance of the asphalt mixture. A higher sphericity of BOF slag coarse aggregates leads to better rutting resistance. Excessively high angularity of BOF slag coarse aggregates reduces the anti-rutting properties of asphalt mixture. The optimal angularity of BOF slag is about 3300 based on the analysis of the result of Marshall stability test, freeze-thaw (F-T) splitting test and rutting test.

(4) In the production of BOF slag coarse aggregates, the exorbitant angularity of coarse aggregates of BOF slag should be controlled. This will help to improve the service life of BOF slag asphalt pavement and the promotion of slag.

Author Contributions: Conceptualization, D.K.; data curation, D.K. and C.Y.; formal analysis, D.K., J.X., C.Y. and M.Z.; methodology, D.K., M.C. and C.Y.; project administration, J.X.; resources, M.C., J.X. and M.Z.; writing—review and editing, D.K., M.C. and J.X.

Funding: This research was funded by the National Key Research and Development Program of China grant number [2017YFE0111600] and the National Natural Science Foundation of China grant numbers [51708437 and 51778515].

Acknowledgments: The authors gratefully acknowledge many important contributions from the researchers of all reports cited in our paper.

Conflicts of Interest: The authors declare no conflict of interest.

References

1. Ministry of Transport of the People's Republic of China. The Annual Statistics of Traffic and Transportation. Available online: http://zizhan.mot.gov.cn/zfxxgk/bnssj/zhghs/201803/t20180329_3005087.html (accessed on 2 July 2018).
2. Skaf, M.; Manso, J.M.; Aragón, Á.; Fuente-Alonso, J.A.; Ortega-López, V. EAF slag in asphalt mixes: A brief review of its possible re-use. *Resour. Conserv. Recycl.* **2017**, *120*, 176–185. [CrossRef]
3. Zheng, J. Design Guide for Semirigid Pavements in China Based on Critical State of Asphalt Mixture. *J. Mater. Civ. Eng.* **2013**, *25*, 899–906. [CrossRef]
4. Ibrahim, A.; Faisal, S.; Jamil, N. Use of basalt in asphalt concrete mixes. *Constr. Build. Mater.* **2009**, *23*, 498–506. [CrossRef]
5. Pan, P.; Wu, S.; Xiao, Y.; Liu, G. A review on hydronic asphalt pavement for energy harvesting and snow melting. *Renew. Sustain. Energy Rev.* **2015**, *48*, 624–634. [CrossRef]

6. Kambole, C.; Paige-Green, P.; Kupolati, W.K.; Ndambuki, J.M.; Adeboje, A.O. Basic oxygen furnace slag for road pavements: A review of material characteristics and performance for effective utilisation in southern Africa. *Constr. Build. Mater.* **2017**, *148*, 618–631. [CrossRef]
7. Jiang, Y.; Ling, T.C.; Shi, C.; Pan, S.Y. Characteristics of steel slags and their use in cement and concrete—A review. *Resour. Conserv. Recycl.* **2018**, *136*, 187–197. [CrossRef]
8. Poulikakos, L.D.; Papadaskalopoulou, C.; Hofko, B.; Gschösser, F.; Falchetto, A.C.; Bueno, M.; Arraigada, M.; Sousa, J.; Ruiz, R.; Petit, C. Harvesting the unexplored potential of European waste materials for road construction. *Resour. Conserv. Recycl.* **2017**, *116*, 32–44. [CrossRef]
9. Han, F.; Zhang, Z.; Wang, D.; Yan, P. Hydration heat evolution and kinetics of blended cement containing steel slag at different temperatures. *Thermochim. Acta* **2015**, *605*, 43–51. [CrossRef]
10. Reddy, A.S.; Pradhan, R.K.; Chandra, S. Utilization of Basic Oxygen Furnace (BOF) slag in the production of a hydraulic cement binder. *Int. J. Miner. Process.* **2006**, *79*, 98–105. [CrossRef]
11. Shen, D.H.; Wu, C.M.; Du, J.C. Laboratory investigation of basic oxygen furnace slag for substitution of aggregate in porous asphalt mixture. *Constr. Build. Mater.* **2009**, *23*, 453–461. [CrossRef]
12. Iacobescu, R.I.; Angelopoulos, G.N.; Jones, P.T.; Blanpain, B.; Pontikes, Y. Ladle metallurgy stainless steel slag as a raw material in Ordinary Portland Cement production: a possibility for industrial symbiosis. *J. Cleaner Prod.* **2016**, *112*, 872–881. [CrossRef]
13. Chao, L.I.; Chen, Z.; Xie, J.; Shaopeng, W.U.; Xiao, Y. A Technological and Applicational Review on Steel Slag Asphalt Mixture. *Mater. Rev.* **2017**.
14. Ahmedzade, P.; Sengoz, B. Evaluation of steel slag coarse aggregate in hot mix asphalt concrete. *J. Hazard. Mater.* **2009**, *165*, 300–305. [CrossRef] [PubMed]
15. Xie, J.; Wu, S.; Zhang, L.; Xiao, Y.; Ding, W. Evaluation the deleterious potential and heating characteristics of basic oxygen furnace slag based on laboratory and in-place investigation during large-scale reutilization. *J. Cleaner Prod.* **2016**, *133*, 78–87. [CrossRef]
16. Ameri, M.; Behnood, A. Laboratory studies to investigate the properties of CIR mixes containing steel slag as a substitute for virgin aggregates. *Constr. Build. Mater.* **2012**, *26*, 475–480. [CrossRef]
17. Behnood, A.; Ameri, M. Experimental investigation of stone matrix asphalt mixtures containing steel slag. *Scientia Iranica* **2012**, *19*, 1214–1219. [CrossRef]
18. Chen, Z.; Wu, S.; Xiao, Y.; Zhao, M.; Xie, J. Feasibility study of BOF slag containing honeycomb particles in asphalt mixture. *Constr. Build. Mater.* **2016**, *124*, 550–557. [CrossRef]
19. Pasetto, M.; Baldo, N. Experimental evaluation of high performance base course and road base asphalt concrete with electric arc furnace steel slags. *J. Hazard. Mater.* **2010**, *181*, 938–948. [CrossRef] [PubMed]
20. Pasetto, M.; Baldo, N. Fatigue Performance of Asphalt Concretes with RAP Aggregates and Steel Slags. *RILEM Bookseries* **2012**, *4*, 719–727.
21. Wu, S.; Xue, Y.; Ye, Q.; Chen, Y. Utilization of steel slag as aggregates for stone mastic asphalt (SMA) mixtures. *Build. Environ.* **2007**, *42*, 2580–2585. [CrossRef]
22. Xue, Y.; Wu, S.; Hou, H.; Zha, J. Experimental investigation of basic oxygen furnace slag used as aggregate in asphalt mixture. *J. Hazard. Mater.* **2006**, *138*, 261–268. [CrossRef] [PubMed]
23. Zhu, H.; Nodes, J.E. Contact based analysis of asphalt pavement with the effect of aggregate angularity. *Mech. Mater.* **2000**, *32*, 193–202. [CrossRef]
24. Amarasiri, S.; Gunaratne, M.; Sarkar, S. Use of Digital Image Modeling for Evaluation of Concrete Pavement Macrotexture and Wear. *J. Transp. Eng.* **2012**, *138*, 589–602. [CrossRef]
25. Wang, H.N.; Hao, P.W.; Pang, L.G.; Di, J.H. Investigation into grading characteristic of coarse aggregate via digital image processing technique. *J. S. Chin. Univ. Technol.* **2007**, *35*, 54–59.
26. Xiong, Q.; Wang, X.D.; Zhang, L. Research Summary of Digital Image Processing Technology on Coarse Aggregate Morphology Characteristics. *Subgrade Eng.* **2012**.
27. Araujo, V.M.C.; Bessa, I.S.; Branco, V.T.F.C. Measuring skid resistance of hot mix asphalt using the aggregate image measurement system (AIMS). *Constr. Build. Mater.* **2015**, *98*, 476–481. [CrossRef]
28. Bessa, I.S.; Soares, J.B. Evaluation of polishing and degradation resistance of natural aggregates and steel slag using the aggregate image measurement system. *Road Mater. Pavement Des.* **2014**, *15*, 385–405. [CrossRef]
29. Mahmoud, E.; Gates, L.; Masad, E.; ErdoğAn, S.; Garboczi, E. Comprehensive Evaluation of AIMS Texture, Angularity, and Dimension Measurements. *J. Mater. Civ. Eng.* **2010**, *22*, 369–379. [CrossRef]

30. ASTM. Standard Test Method for Flat Particles, Elongated Particles, or Flat andElongated Particles in Coarse Aggregate. ASTM D4791. 2010.
31. ASTM. Standard Test Method for Resistance to Degradation of Small-sizeCoarse Aggregate by Abrasion and Impact in the Los Angeles Machine. ASTM C131. 2014.
32. ASTM. Standard Specification for Concrete Aggregates. ASTM C33. 2003.
33. Kong, D.; Xiao, Y.; Wu, S.; Tang, N.; Ling, J.; Wang, F. Comparative evaluation of designing asphalt treated base mixture with composite aggregate types. *Constr. Build. Mater.* **2017**, *156*, 819–827. [CrossRef]

materials

MDPI

Article

Morphological Discrepancy of Various Basic Oxygen Furnace Steel Slags and Road Performance of Corresponding Asphalt Mixtures

Yong Ye, Shaopeng Wu *, Chao Li *, Dezhi Kong and Benan Shu

State Key Laboratory of Silicate Materials for Architectures, Wuhan University of Technology, Wuhan 430070, China

* Correspondence: wusp@whut.edu.cn (S.W.); lic@whut.edu.cn (C.L.)

Received: 20 June 2019; Accepted: 19 July 2019; Published: 21 July 2019

Abstract: Due to the difference of cooling and treatment processes (rolling method, hot braised method, layer pouring method), basic oxygen furnace (BOF) steel slag can be mainly classified as roller steel slag (RSS), hot braised steel slag (HBSS) and layer pouring steel slag (LPSS). Treatment difference directly results in the performance variations of different BOF steel slag and corresponding asphalt mixtures. The primary purpose of this research was to examine the effects of different cooling and treatment processes on the morphological discrepancy of different BOF steel slag. Also, the road performances of corresponding asphalt mixtures, and mechanism between steel slag performance and road performance were studied. The results show that LPSS owns the largest variability of angular index and texture index, and RSS has the most balanced morphological parameters. The structure of RSS asphalt mixture is advantageous for improving the ability of the asphalt mixture to resist the deformation and enhancing the stability of structure. Higher content of CaO and lower content of SiO_2 make the acid-base reaction of RSS asphalt mixture most intense, which contribute to the best road performance of it.

Keywords: basic oxygen furnace steel slag; morphological discrepancy; road performance; mechanism research

1. Introduction

In recent years, rapid development of transportation infrastructure has aroused various obstacles [1], the lack of substantive natural aggregates which possess significant qualities is the most urgent one [2]. Substantive natural aggregates made asphalt mixtures inferior in moisture damage, crack resistance and rutting deformation in road construction [3,4]. The lack of them has made researchers to take other measures to alleviate the crisis, like the use of industrial waste [5].

Steel slag, one type of industrial wastes to replace superior natural aggregates, can be mainly classified as basic oxygen furnace (BOF) steel slag, electric arc furnace (EAF) steel slag, ladle refining (LF) steel slag, and casting residue according to the manufacturing types of steel production [2,6]. Among these, BOF steel slag has been widely utilized in producing numerous types of asphalt mixtures according to former researches [5,7,8]. Kambole reviewed common physical and mechanical characteristics of BOF slag and natural aggregates, and evaluated the influence of main aggregate performance on the properties of asphalt mixtures [9]. Results demonstrated that BOF steel slag owns very good technical and physical properties compared with natural stone aggregates, and proved its feasibility as a valuable resource for road pavements. In addition, mixtures of bitumen with BOF steel slag have yielded better resilient moduli, rutting resistance, bonding, moisture damage resistance and stripping resistance compared to mixes with natural aggregates [9–11]. López-Díaz used the BOF steel slag as coarse aggregate in asphalt concrete, and the results confirmed that it was feasible to use BOF

steel slag to partially replace conventional aggregates in road paving [12]. Qazizadeh evaluated the effects of BOF steel slags on the fatigue behavior of asphalt mixes and found that the addition of slags in the mixtures considerably enhanced fatigue life of asphalt mixes [13]. Xue explored the feasibility of using BOF steel slag as aggregates in stone mastic asphalt (SMA) mixtures, results indicated that BOF steel slag improved the high-temperature stability and the low-temperature cracking resistance of SMA mixture when compared with basalt [14]. Shen studied the influence of porous asphalt mixture contained BOF steel slag on the mixture performance and sound absorption characteristic, results demonstrated that BOF steel slag enhanced the skid resistance, moisture susceptibility, rutting resistance, and sound absorption of porous asphalt mixtures [15].

Nevertheless, former researches neglected the influence of cooling and treatment techniques on the properties of BOF steel slag after being produced from furnace, and just placed different BOF steel slag in the same bracket indistinctly. Actually on the basis of different cooling and treatment techniques in China, the BOF steel slag can be mainly classified as roller steel slag (RSS), hot braised steel slag (HBSS) and layer pouring steel slag (LPSS) [16]. To obtain the RSS, firstly the liquid BOF steel slag is dumped into the rotating roller along the chute, steel balls are then added into the roller. By controlling the amount of water, finally steel slag can undergo heating, pulverizing, grinding, and cooling in the roller. The manufacture of HBSS is in accordance with the steps that liquid BOF steel slag is firstly dumped into the pit with the sprinkler and cover, and then smashed by mixing many saturated steams in the confined pit. Comparing to the former two treatments and cooling processes, the production of LPSS is much easier. The liquid BOF steel slag only needs to be pumped onto the slag bed (or inside the slag pit) firstly. Then, a proper amount of water is sprayed and LPSS is weathered in the natural environment.

Above treatment difference directly results in the performance variations of different BOF steel slag, such as the chemical composition, and morphology [17]. The chemical composition and morphology are directly related to the road performance of corresponding asphalt mixtures [18,19]. Therefore, in line with the properties aroused by different cooling and treatment techniques to select suitable application, this paper focused on the utilization of three BOF steel slags in asphalt mixtures, including RSS, HBSS, and LPSS, so that the BOF steel slag could have a broader utilization prospects in transportation infrastructure based on their difference. Firstly, both the surface texture of three BOF steel slags were investigated. Secondly, their chemical composition and morphological discrepancy were also included. Thirdly, three types of asphalt mixtures contained different steel slags were designed, and their road performances were tested. Finally, the mechanism between the BOF steel slag performance and road performance were also analyzed.

2. Materials and Methods

2.1. Raw Materials

The asphalt binder with penetration of 68.3 (0.1 mm at 25 °C), ductility of 151 cm (5 cm/min, 15 °C), and softening point of 47.5 °C, which supplied by Guochuang Co., Ltd., Wuhan, China, was used in this research [20]. Limestone aggregates with different particle size (0 mm–2.36 mm, 2.36 mm–4.75 mm, 4.75 mm–9.5 mm) and filler were supplied by Agoura Stone Processing Factory, Inner Mongolia and their properties were all met the standard specifications. Three types of basic oxygen furnace (BOF) steel slag, including roller steel slag (RSS), hot braised steel slag (HBSS), and layer pouring steel slag (LPSS), were supplied by Baotou Steel with particle size ranging from 9.5 mm to 19 mm, the basic properties of them were shown in Table 1. From the results of Los Angeles abrasion and crushing value, it can be seen that the mechanical properties of steel slag are better than natural aggregates. As these mechanical properties can reflect the hardness, wear resistance and anti-slip properties of aggregates closely related to the performance of asphalt mixtures [9]. Additionally, as shown in Figure 1, it can be seen that the three types of steel slag all have irregular shapes and porous structure. Among them, the surface texture of LPSS is the most abundant. This is because the aging process of LPSS occurs in

natural conditions with no high temperature and high-pressure treatments. Therefore, the formation process of LPSS is uneven, slow and the pores are not fully filled with aged materials, which results in a topographical feature of the surface texture.

Table 1. Basic properties of used aggregates. RSS: roller steel slag; LPSS: layer pouring steel slag; HBSS: hot braised steel slag.

Aggregate	Properties [21]					
	Size	Water Absorption (%)	Apparent Specific Gravity	Log Angeles Abrasion (%)	Crushing Value (%)	f-CaO Content (%)
RSS	9.5–16 mm	1.16	3.220	12.9	18.5	0.40
LPSS	9.5–16 mm	1.44	3.260	14.5	13.9	1.17
HBSS	9.5–16 mm	1.75	3.100	13.2	16.8	0.81
Basalt [22]	9.5–16 mm	0.40	2.774	16.8	20.0	N/A
Limestone [23]	9.5–16 mm	1.10	2.650	20.4	N/A	N/A
Granite [22]	9.5–16 mm	0.60	2.723	21.6	21.9	N/A
Limestone	4.75–9.5 mm	1.30	2.726	N/A	9.3	N/A
Limestone	2.36–4.75 mm	1.50	2.822	N/A	9.3	N/A
Requirements [24]	N/A	≤3.00	≥2.500	≤30.0	≤26.0	≤2.00

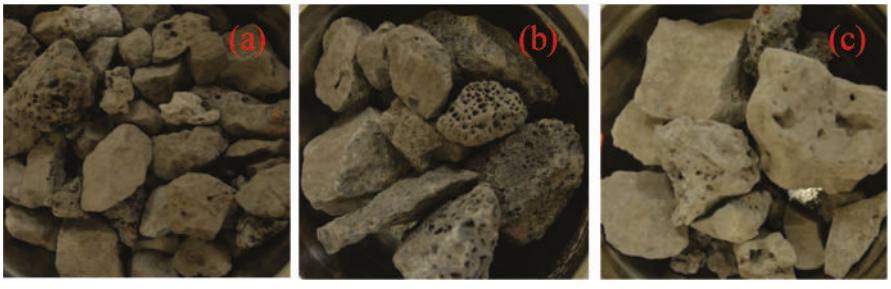

Figure 1. Appearance of different basic oxygen furnace (BOF) steel slag: (**a**) RSS; (**b**) LPSS; (**c**) HBSS.

2.2. Asphalt Mixture Design

In this research, two types of asphalt mixtures were designed based on standard Marshall Method and Superpave method. Three types of AC-13 asphalt mixtures were mixed with same limestone aggregates, asphalt binder and different BOF steel slag, the gradation curve was shown in Figure 2. Additionally, three types of Superpave-13 asphalt mixtures were mixed the same materials as the AC-13 asphalt mixtures, and the gradation curve was shown in Figure 3.

2.3. Experimental Methods

2.3.1. Characterization

The surface textures of different steel slags were detected by a JSM-5610LV Scan Electronic Microscope (SEM) manufactured by JEOL, Tokyo, Japan [25]. The resolution of SEM in the high-vacuum and low-vacuum mode was 3.0 nm and 4.0 nm separately; the magnification of 1000× was adopted in this research. Chemical composition changes of different steel slags were determined using an AXIOS X-ray fluorescence spectrometer (XRF) manufactured by PANalytical B.V., Amsterdam, The Netherlands [26].

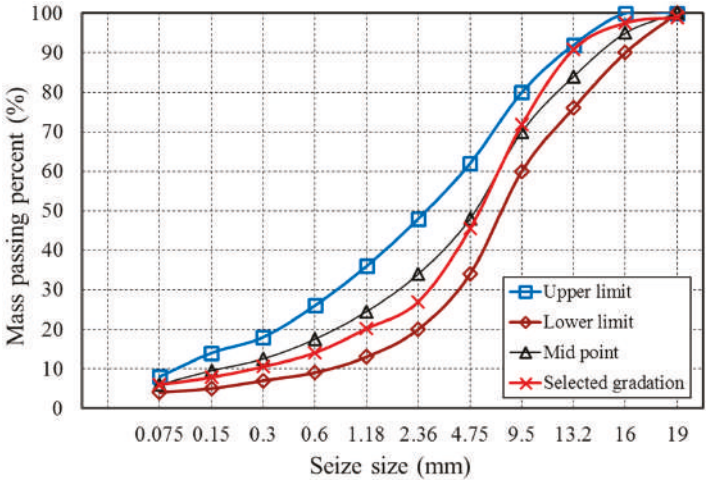

Figure 2. Gradation curve of AC-13 asphalt mixtures.

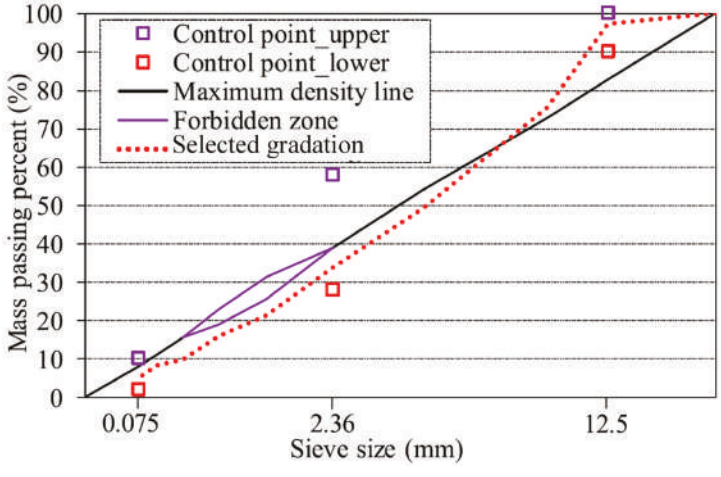

Figure 3. Gradation curve of Superpave-13 asphalt mixtures.

2.3.2. Morphological Discrepancy

AFA2 Aggregate Imaging System (AIMS) (PINE, New York, USA) was utilized to analyze the morphological properties of steel slag in this research, including angularity and texture. AIMS captures images of aggregates at different resolutions through a simple setup that consists of one camera and two different types of lighting schemes [27,28]. The image acquisition setup is configured to capture a typical image of 640 by 480 pixels at these resolutions in order to analyze the aggregates, and export the angularity index and texture index.

2.3.3. Road Performance

In this paper, high temperature stabilities of AC-13 asphalt mixtures were performed by using the wheel tracking device, which was normally used for HMA testing and the dimension of tested slab specimen was 300 mm × 300 mm × 50 mm [29]. A solid rubber wheel with a wheel pressure of 0.7 MPa is used to walk on the specimen at 60 °C. When measuring the deformation period of the

test piece, the dynamic stability, which means the number of times it needs to walk for every 1 mm augment, was obtained to evaluate the high temperature stabilities [30].

Based on ASTM D1075 and AASHTO T283, the moisture resistance abilities of three steel slag asphalt mixtures were evaluated by the water immersion Marshall test and the freeze-thaw split test. Both AC-13 asphalt mixtures and Superpave-13 asphalt mixtures were evaluated [31].

To evaluate the low temperature cracking resistance abilities of AC-13 asphalt mixtures, specimen was loaded under a universal material testing machine (IPC, Sydney, Australia) based on the single axes compression test at 0 °C, and the stress–strain curves were obtained automatically by the data acquisition system. The maximum compressive strain energy density was used to evaluate the low temperature cracking resistance abilities and calculated according to the Equation (1) [14].

$$\frac{dW}{dV} = \int_0^{\varepsilon_0} \sigma_{ij} d\epsilon_{ij} \tag{1}$$

where dW/dV represents the compressive strain energy density function; σ_{ij} represents the stress fraction; ε_{ij} represents the strain fraction; and ε_0 represents the strain at maximum compressive stress.

3. Results and Discussions

3.1. Characterization

The SEM results of different types of steel slags are shown in Figure 4, it can be indicated that all steel slags have rough surface and numerous pores. This morphological property contributes to improve the bonding performance between aggregate and asphalt binder, resulting in the enhancement of asphalt concrete structural stability. The shape characteristics of RSS and HBSS are similar with little pits and gullies on the surface, which are relatively smoother than the surface texture of LPSS. LPSS not only contains numerous pits, but also has a very uneven surface contained crystal materials with regular shapes. This is because aging process of LPSS is in the natural environment, in which the free calcium oxide slowly forms a calcium carbonate with a crystal structure under the action of water and carbon dioxide. The formed calcium carbonate crystal gradually fills the original pores of LPSS, and due to the uneven distribution of the free material on the surface of LPSS, large amounts of pores still exist on the surface of LPSS. In contrast, under the condition of high temperature and high pressure, RSS and HBSS have been fully aged, the resulting aged products are fully fused with original components of steel slag and formed into a whole, so the surface textures of RSS and HBSS are relatively smoother than LPSS.

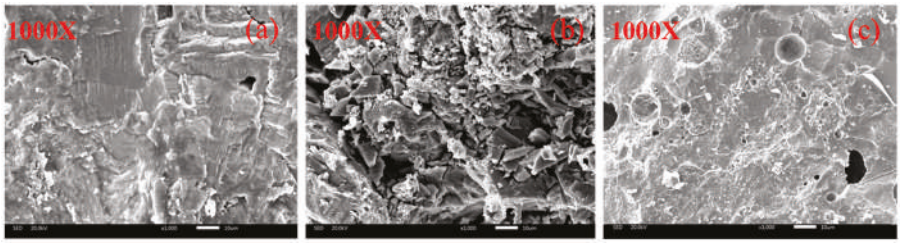

Figure 4. SEM results of different steel slags: (**a**) RSS; (**b**) LPSS; (**c**) HBSS.

The XRF results of different steel slags are shown in Figure 5, it can be inferred that the chemical composition of three steel slags mainly contains CaO, SiO_2 and Fe_3O_4, which accounts for more than 80% of the total composition. Compared with the main chemical composition of CaO obtained by the XRF test of traditional aggregate limestone, the steel slag contains a certain amount of silicate and iron-containing compounds due to the iron ore composition and the steel slag treatment process. Limestone is an excellent alkaline rock with good adhesion to asphalt binder. For steel slag, alkalinity

which calculated by $M = w(CaO)/[w(SiO_2) + w(P_2O_5)]$, is used to evaluate the acidity and alkalinity of steel slag [32]. Wang Q divided BOF steel slags into three grades based on alkalinity: low alkalinity slag ($M < 1.8$), intermediate alkalinity slag ($1.8 < M < 2.5$) and high alkalinity slag ($M > 2.5$) [33]. Chen indicated that intermediate alkalinity slag and high alkalinity slag had better adhesion to asphalt binder [3]. Therefore, It can be seen from the XRF results, all three steel slags are medium-high alkalinity steel slags ($M > 1.8$) and has good adhesion to asphalt binder. In addition, M value of RSS is 26.84% higher than that of HBSS, and 9.72% higher than that of LPSS, which caused by the higher content of CaO and lower content of SiO_2 in RSS.

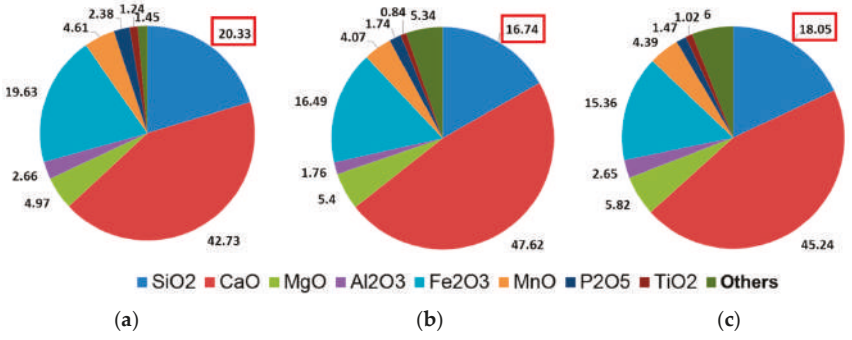

Figure 5. X-ray fluorescence spectrometer (XRF) results of different steel slags (**a**) LPSS; (**b**) RSS; (**c**) HBSS.

3.2. Morphological Discrepancy

Figure 6 shows the schematic diagram of morphological properties for coarse aggregates. Angularity is used to demonstrate variations at the corners, surface texture is used to describe the surface irregularity at a tiny scale to affect the overall shape. Because of different scales with respect to aggregate size, these two morphological properties can be distinguished and used to order them. Every property can be distinguished from other properties widely without necessarily affecting each other [28].

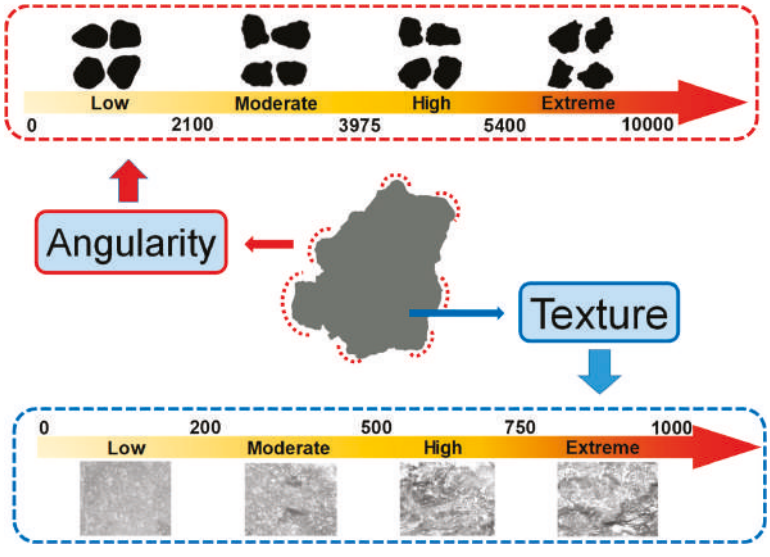

Figure 6. Schematic diagram of morphological properties.

With regard to angularity, the angularity index is calculated by the radius method [34]. Through measuring the difference between particle radius in a certain direction and that of an equivalent ellipse, the angularity index can be calculated according to the following Equation (2) [28]:

$$Angularity\ Index = \sum_{\theta=0}^{355} \frac{|R_\theta - R_{EE\theta}|}{R_{EE\theta}} \quad (2)$$

In the equation, R_θ represents the radius of the particle at an angle of θ, and $R_{EE\theta}$ represents the radius of the equivalent ellipse at an angle of θ. The equivalent ellipse has the same aspect ratio of the particle but has no angularity (smooth with no sharp corners). Normalization of the aspect ratio can minimize the effect of form on the angularity index [34]. The values of angularity index distribute from 0 to 10,000, and can also be divided into four levels: low level is from 0 to 2100 and particle is rounded, moderate level is from 2100 to 3975 and particle is sub-rounded, high level is from 3975 to 5400 and particle is sub-angular, extreme level is from 5400 to 10,000 and particle is angular. Additionally, the particle can be recognized to be more rounded if the angularity index is closer to 0.

Table 2 and Figure 7 summarize the angularity test results of different steel slags. It can be inferred that the angularity indexes of three steel slags are mainly distributed in the two levels of sub-rounded and sub-angular, and the distributions in sub-rounded account for the most. The average value and variance of the angularity of RSS are the smallest of three steel slags, while the average value and variance of LPSS are the largest. The results show that RSS owns the lowest angularity but the best control of variability. In contrast, LPSS owns the worst control of variability but the largest angularity.

Table 2. Aggregate Imaging System (AIMS) angularity index of tested steel slag particles.

Angularity Index						
Sample	**Average Value**	**Standard Deviation Value**	**Low (≤2100)**	**Moderate (2100–3975)**	**High (3975–5400)**	**Extreme (5400–10,000)**
RSS	2946.5	609.6	0%	95%	5%	0%
HBSS	3292.0	862.2	5%	75%	15%	5%
LPSS	3725.8	1226.1	0	60%	30%	10%

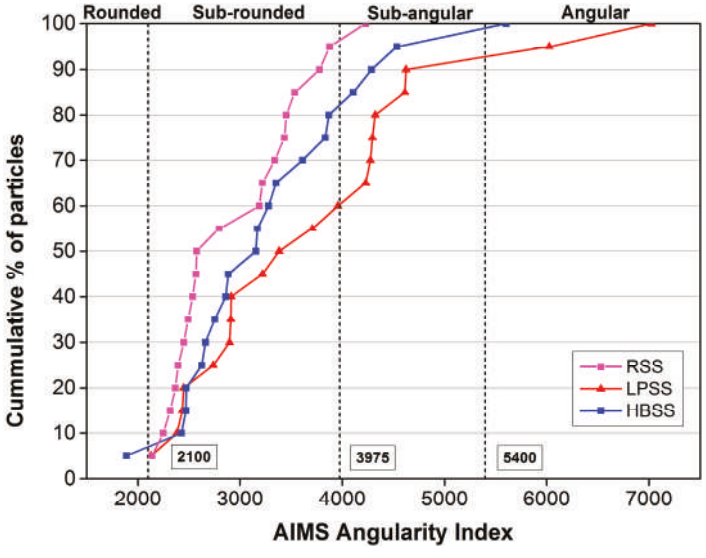

Figure 7. AIMS angularity index curve of tested steel slag particles.

Texture index is applied to characterize the texture distinction by wavelet analysis [35], the texture index at any given decomposition level is the arithmetic mean of the squared values of the detail coefficients of different level and can be calculated in the following Equation (3) [8]:

$$Texture\ Index = \frac{1}{3N}\sum_{i=1}^{3}\sum_{j=1}^{N}\left(D_{i,j}(x,y)\right)^2 \quad (3)$$

where N denotes the total number of coefficients in the detailed image of the aggregate; i takes a value of 1, 2, or 3, corresponding to three detailed images of the texture; J is the index of the wavelet coefficients, D means the transformed domain and (x, y) is the position of the coefficients in the texture scan area. The texture index can be divided into four levels: 0 to 200 accounts for the low grade, 200 to 500 accounts for the medium grade, 500 to 750 accounts for the high grade, and 750 to 1000 accounts for very high grade. Higher value of texture value represents the richer surface texture of aggregate.

Table 3 and Figure 8 summarize the results of different steel slag texture indexes. Results show that the texture indexes of three steel slags are mainly distributed in the medium grade. Among the three steel slags, only the HBSS is not distributed in the low grade of texture index, only the LPSS is distributed in the high grade of texture index. As with the results of angular index, LPSS owns the highest texture index, and its average texture index is 53.24% and 19.06% higher than that of RSS and HBSS, respectively. However, the texture index value of LPSS is distributed in all four grades, its standard deviation of texture index is 94.83% and 78.58% higher than that of RSS and HBSS, respectively, showing poor texture variability.

Table 3. AIMS texture index values of tested steel slag particles.

Texture Index						
Sample	**Average Value**	**Standard Deviation**	**Low (≤200)**	**Moderate (200–500)**	**High (500–750)**	**Extreme (750–1000)**
RSS	311.4	81.3	15%	85%	0%	0%
HBSS	400.8	88.7	0%	75%	25%	0%
LPSS	477.2	158.4	5%	60%	25%	10%

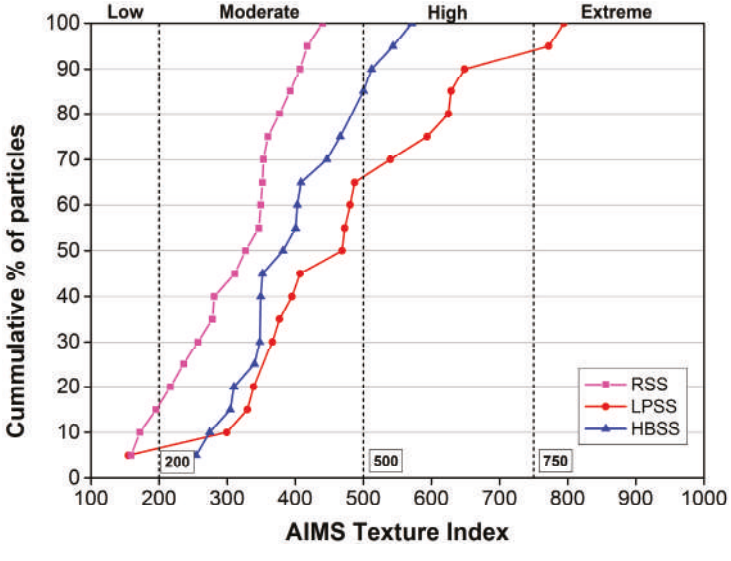

Figure 8. AIMS texture index curve of tested steel slag particles.

Both the results of angular index and texture index show that LPSS has higher geometrical characteristics, this is mainly because that the cooling and treatment of RSS and HBSS experience both aging and stable processes in the initial formation of steel slag. Most free components have been digested into calcium carbonate, the composition and material properties of the steel slag have been relatively stable. However, cooling and treatment process of LPSS cannot guarantee that the aging of free components was finished completely during the slag splashing. Therefore, during the stacking period of LPSS, the free components continuously react with the moisture and carbon dioxide in the air, and the uneven distribution of aging products lead to the rugged surface texture of the aggregate, which increases the angular index and texture index of LPSS.

3.3. Road Performance

3.3.1. High Temperature Stability

The high temperature stability of asphalt pavement represents the ability of the asphalt mixture to resist permanent deformation after being subjected to vehicle load and repeated rolling under high temperature conditions. The rutting test is currently the mainstream method for evaluating the high temperature stability. If the high temperature stability of asphalt mixture does not meet the requirements of the standard design, the road surface will be damaged due to insufficient stability and low load loading rate at high temperature. The research shows that the dynamic stability of the rutting test has a good correlation with the rutting depth of the asphalt mixture [36]. By comparing the dynamic stability, the high temperature stability of the asphalt mixture can be evaluated.

Figure 9 shows the results of high temperature stability of different BOF steel slag asphalt mixture. It shows that the dynamic stability values of three steel slag asphalt mixtures are all higher than 2800 times/mm, which meets the requirements of the specification of China properly. Excellent material characteristics of BOF steel slag make its dynamic stability far greater than the specification requirements. Among them, the RSS asphalt mixture has the highest dynamic stability, which is 25.48% and 14.44% higher than that of LPSS asphalt mixture and HBSS asphalt mixture, respectively. The high temperature stability of LPSS is the worst, representing that although the LPSS has highest geometric parameters, it also has larger geometric variability and smaller crushing value, also the residual free material in LPSS affects the high temperature stability of asphalt mixture.

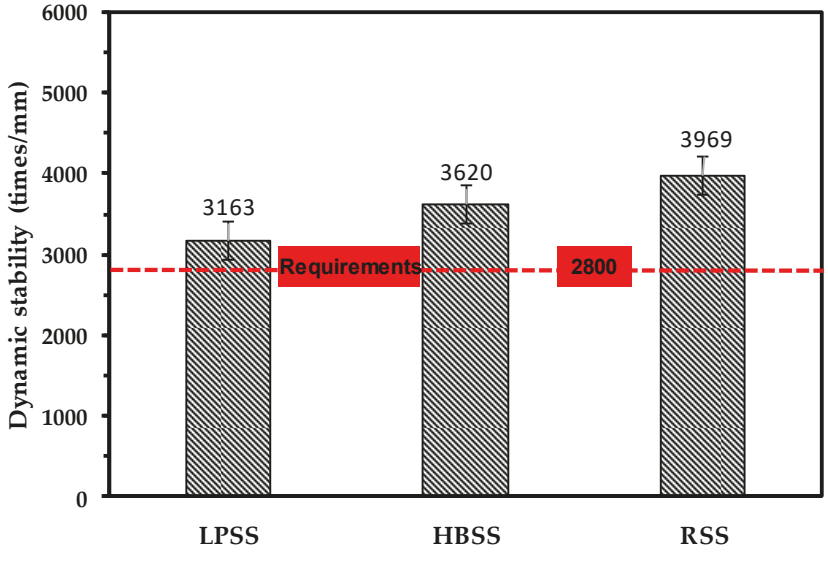

Figure 9. High-temperature stability test results of different steel slag asphalt mixtures.

3.3.2. Moisture Resistance Ability

Moisture resistance is recognized as the ability to resist the peeling of bitumen, which adhering to the aggregate surface in asphalt mixture after being corroded by water. In this paper, according to ASTM D1075 and AASHTO T283, the moisture resistance abilities of steel slag asphalt mixtures were evaluated by the water immersion Marshall test and the freeze-thaw split test. The moisture resistance test results of Superpave-13 steel slag asphalt mixtures are shown in Figures 10 and 11, it can be seen that the RMS values of three steel slag asphalt mixtures are all greater than 80%, and the TSR values of them were more than 75%, which are fully meeting the requirements of the specification. The RMS value of RSS asphalt mixture is 4.97% and 1.22% higher than that of LPSS asphalt mixture and HBSS asphalt mixture. In addition, the TSR value of RSS asphalt mixture is 5.51% and 1.68% higher than that of LPSS asphalt mixture and HBSS asphalt mixture. The moisture resistance test results of AC-13 steel slag asphalt mixtures are shown in Table 4. In consistent with the results of the Superpave-13 steel slag asphalt mixtures, the RMS values of three AC-13 steel slag asphalt mixture are all more than 80%, and the TSR values are greater than 75%. LPSS asphalt mixture still behaves the worst moisture resistance. Results show that three steel slag asphalt mixtures have good water stability, the main reason is that the steel slag shows coarse, porous surface texture that enhances the bonding performance between BOF steel slag and bitumen. In addition, the alkali metal cations such as Ca^{2+}, Mg^{2+}, Fe^{2+}, Al^{2+} and Mn^{2+} contained in the steel slag can react with the bituminous acid, and the formed materials further increases the bonding property of the steel slag asphalt mixtures. In contrast to LPSS asphalt mixture and HBSS asphalt mixture, RSS asphalt mixture behaves the best moisture resistance, and the reason is that the more advanced treatment methods make the RSS more uniform and stable than the other two steel slags during aging process, and the produced silicate compounds (like $CaCO_3$) improved the ability of asphalt mixture to resist water erosion.

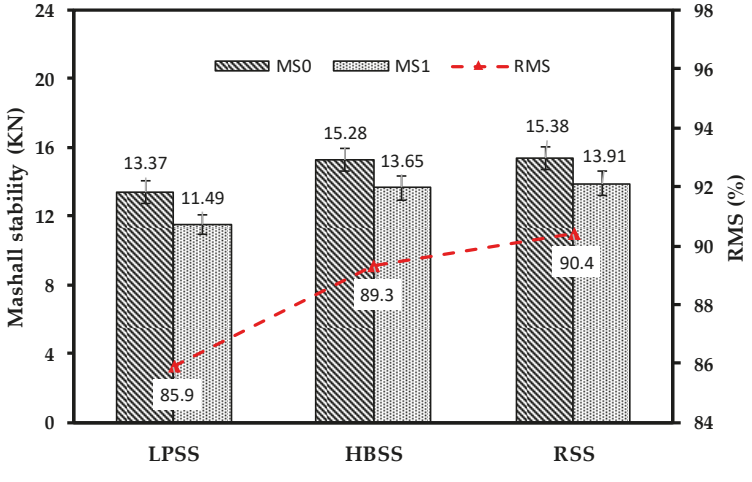

Figure 10. Water immersion Marshall test of Superpave-13 steel slag asphalt mixtures.

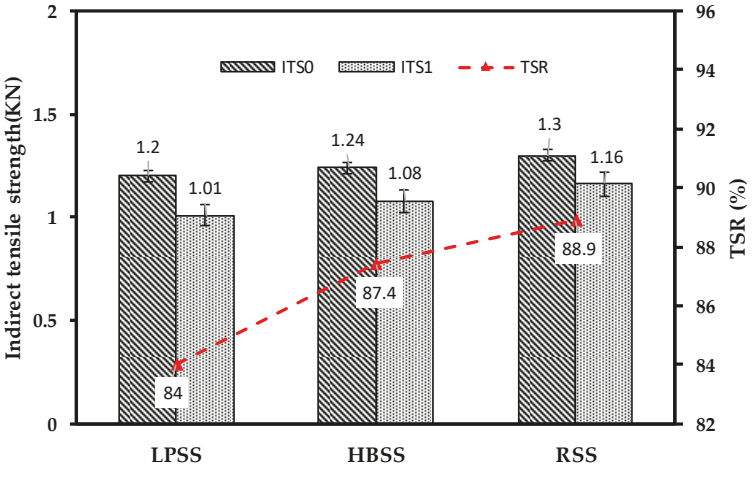

Figure 11. Freeze–thaw split test of Superpave-13 steel slag asphalt mixtures.

Table 4. Moisture resistance results of AC-13 steel slag asphalt mixtures.

AC-13 Asphalt Mixture	RMS Test			ITS Test		
	MS_0 (KN)	MS_1 (KN)	RMS (%)	ITS_0 (MPa)	ITS_1 (MPa)	TSR (%)
RSS	16.92	15.59	92.1	1.65	1.49	90.3
HBSS	15.82	14.37	90.8	1.53	1.35	88.1
LPSS	14.10	12.44	88.2	1.49	1.28	85.6

3.3.3. Low Temperature Cracking Resistance Ability

Low temperature crack resistance is the ability to characterize the asphalt mixture to resist temperature-shrinkage cracks at low temperatures. According to the measured relationship between compressive stress and strain of asphalt mixture shown in Equation (4) [14], it was found that the strain-stress relationship of asphalt mixture was quadratic parabola.

$$\sigma = A\varepsilon^2 + B\varepsilon + C \tag{4}$$

where $\sigma$is the stress, MPa: $\varepsilon$is the strain; A, B, and C are constants, which are related to the type of material. So, the compressive strain energy density function can be transformed into the Equation (5) [17]:

$$\frac{dW}{dV} = \int_0^{\varepsilon_0} \sigma_{ij} d\epsilon_{ij} = \frac{A}{3}{\varepsilon_0}^3 + B{\varepsilon_0}^2 + C\varepsilon_0 \tag{5}$$

where ε_0 is the strain at the peak point of compression stress–strain curve, and the stress–strain curves were obtained automatically by the data acquisition system. As shown in Figure 12, it can be clearly seen that the RSS asphalt mixture owns the largest ε_0 while LPSS asphalt mixture has the lowest ε_0. After substituting the ε_0 values into the Equation (5), the critical value dW/dV is obtained in Table 5. Observations reveal that the critical value of dW/dV is 42.7 KJ/m^3 for LPSS asphalt mixture, while RSS asphalt mixture owns the highest critical value of dW/dV and about 41.83% higher than that of LPSS asphalt mixture. Results confirm that LPSS asphalt mixture has the best ability to resist low temperature deformation.

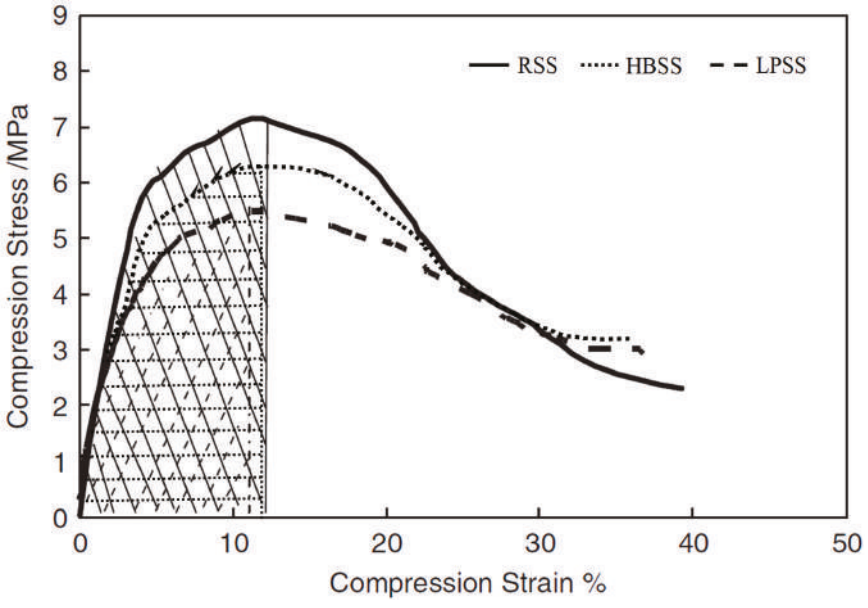

Figure 12. Compression stress–strain curves of AC-13 steel slag asphalt mixtures.

Table 5. ε_0 and critical value of dW/dV at peak poiont.

Mixture Type	Aggregate Type	dW/dV–Strain Function	ε_0	Critical Value of dW/dV (KJ/m^3)
AC-13 Asphalt mixture	LPSS	$dW/dV = -3 \times 10 - 5\varepsilon^5/5 + 0.0015\varepsilon^4/4 - 0.0882\varepsilon^3/3 + 1.128\varepsilon^2/2 + 0.5047\varepsilon$	12.0	42.7
	HBSS	$dW/dV = -3 \times 10 - 5\varepsilon^5/5 + 0.0019\varepsilon^4/4 - 0.0904\varepsilon^3/3 + 1.39\varepsilon^2/2 + 0.6116\varepsilon$	12.9	69.8
	RSS	$dW/dV = -3 \times 10 - 5\varepsilon^5/5 + 0.002\varepsilon^4/4 - 0.0959\varepsilon^3/3 + 1.44\varepsilon^2/2 + 0.8109\varepsilon$	13.3	73.4

3.4. Mechanism between Steel Slag Performance and Road Performance

The road performance of steel slag asphalt mixture is closely related to the performance of steel slag. The reasons for the difference in road performance of asphalt mixtures prepared by different steel slag mainly include two aspects: the difference of the skeleton structure after the formation of steel slag asphalt mixture, and the difference of the adhesion performance between bitumen and steel slag. According to the results of the morphological discrepancy, Figure 13 shows the structural sketch of different steel slag asphalt mixtures. In morphological discrepancy section, RSS owns the best control of variability, in contrast, LPSS owns the worst control of variability. Thus, compared with HBSS and LPSS, RSS has a lower length-to-particle ratio and a smaller number of needle-like particles. At the same time, RSS has good angularity, while the shape variability is small, and the size between the particles is relatively balanced. Therefore, after the formation of asphalt mixtures, the RSS particles have more skeleton support points and are more likely to form a tight skeleton structure. The structure of RSS asphalt mixture is advantageous for improving the ability of the asphalt mixture to resist the deformation and enhancing the stability of structure.

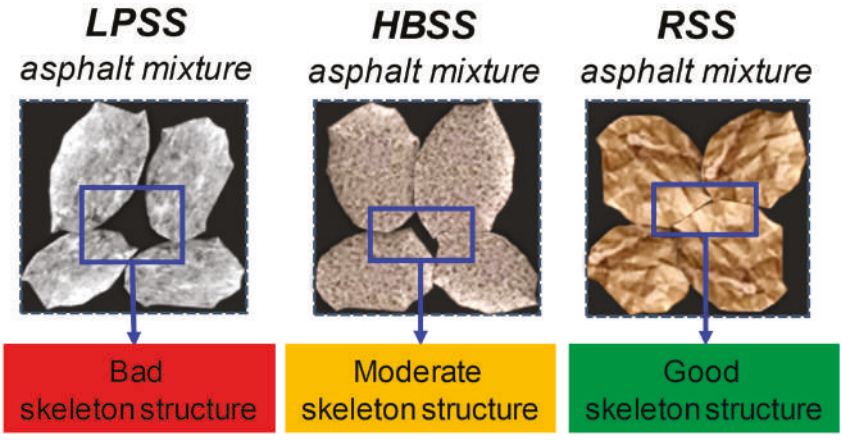

Figure 13. Structural sketch of different steel slag asphalt mixtures.

Figure 14 reveals the schematic diagram of adhesion between steel slag and bitumen. According to the XRF results, the BOF steel slag contains alkaline components like dicalcium silicate (C_2S), tricalcium silicate (C_3S), calcium hydroxide ($Ca(OH)_2$), and free calcium oxide (f-CaO). The bitumen contains some acidic groups like R-COOH, R-SO_XH, and R-COSH, which can react with the alkaline components in the steel slag to form an acid-base neutralization reaction, and the resulting product enhances the adhesion between the bitumen and steel slag. In addition, *M* value of RSS is 26.84% higher than that of HBSS, and 9.72% higher than that of LPSS, which caused by the higher content of CaO and lower content of SiO_2 in RSS. This make the acid-base reaction of RSS asphalt mixture most intense, which contribute to the best road performance of it [5].

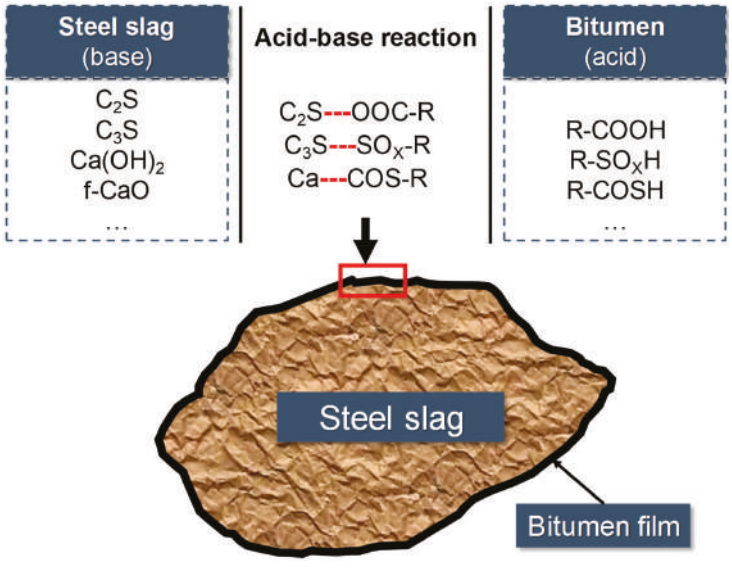

Figure 14. Schematic diagram of adhesion between steel slag and bitumen.

4. Conclusions

The primary purpose of this research was to examine the effects of different cooling and treatment processes on the morphological discrepancy of different BOF steel slag, including roller steel slag (RSS), hot braised steel slag (HBSS), and layer pouring steel slag (LPSS). Also, the road performances of corresponding asphalt mixtures were studied. On account of the results above, the following conclusions can be obtained.

RSS owns the lowest angularity but the best control of variability. In contrast, LPSS owns the worst control of variability but the highest angularity. Average texture index of LPSS is 53.24% and 19.06% higher than that of RSS and HBSS, respectively.

The RSS asphalt mixture has the highest dynamic stability, which is 25.48% and 14.44% higher than that of LPSS asphalt mixture and HBSS asphalt mixtures, respectively. The high temperature stability of LPSS asphalt mixture is the worst, representing that although the LPSS has higher geometric properties, it also has larger geometric variability and smaller crushing value, also the residual free material in LPSS affects the high temperature stability of asphalt mixture.

RSS asphalt mixture and LPSS asphalt mixture still behave the best and worst moisture resistance. Surface texture and alkali metal cations enhance the bonding performance between steel slag and bitumen. Observations reveal that the critical value of dW/dV is 42.7 KJ/m^3 for LPSS asphalt mixture, while RSS asphalt mixture owns the highest critical value of dW/dV and about 41.83% higher than that of LPSS asphalt mixture.

The structure of RSS asphalt mixture is advantageous for improving the ability of the asphalt mixture to resist the deformation and enhancing the stability of structure. Higher content of CaO and lower content of SiO_2 make the acid-base reaction of RSS asphalt mixture most intense, which contribute to the best road performance of it.

Author Contributions: D.K. and C.L. conceived and designed the experiments. B.S. and S.W. performed the experiments. C.L. analyzed the data. Y.Y. contributed reagents/materials/analysis tools. Y.Y. and C.L. wrote the paper.

Funding: This research was funded by National Key R&D Program of China (No. 2018YFB1600200), National Natural Science Foundation of China (71961137010), the Fundamental Research Funds for the Central Universities (No. 195201013), Fundamental Research Funds for the Central Universities (WUT:182459009) and State Key Laboratory of Silicate Materials for Architectures (Wuhan University of Technology) (No. SYSJJ2019-19).

Acknowledgments: The authors gratefully acknowledge Wuhan University of Technology and the shiyanjia lab (www.shiyanjia.com), for their materials and experimental instruments supports.

Conflicts of Interest: The authors declare no conflict of interest.

References

1. Cui, P.Q.; Wu, S.P.; Xiao, Y.; Wan, M.; Cui, P.D. Inhibiting effect of layered double hydroxides on the emissions of volatile organic compounds from bituminous materials. *J. Clean. Prod.* **2015**, *108*, 987–991. [CrossRef]
2. Skaf, M.; Manso, J.M.; Aragón, Á.; Fuente-Alonso, J.A.; Ortega-López, V. EAF slag in asphalt mixes: A brief review of its possible re-use. *Resour. Conserv. Recycl.* **2017**, *120*, 176–185. [CrossRef]
3. Chen, Z.W.; Wu, S.P.; Wen, J.; Zhao, M.L.; Yi, M.W.; Wan, J.M. Utilization of gneiss coarse aggregate and steel slag fine aggregate in asphalt mixture. *Constr. Build. Mater.* **2015**, *93*, 911–918. [CrossRef]
4. Shu, B.A.; Zhang, L.; Wu, S.P.; Dong, L.J.; Liu, Q.T.; Wang, Q. Synthesis and characterization of compartmented Ca-alginate/silica self-healing fibers containing bituminous rejuvenator. *Constr. Build. Mater.* **2018**, *190*, 623–631. [CrossRef]
5. Zongwu, C.; Yuyong, J.; Shaopeng, W.; Fubin, T. Moisture-induced damage resistance of asphalt mixture entirely composed of gneiss and steel slag. *Constr. Build. Mater.* **2018**, *177*, 332–341.
6. Yi, H.; Xu, G.; Cheng, H.; Wang, J.; Wan, Y.; Chen, H. An overview of utilization of steel slag. *Procedia Environ. Sci.* **2012**, *16*, 791–801. [CrossRef]
7. Chao, L.; Chen, Z.; Wu, S.; Bo, L.; Xie, J.; Yue, X. Effects of steel slag fillers on the rheological properties of asphalt mastic. *Constr. Build. Mater.* **2017**, *145*, 383–391.

8. Li, C.; Wu, S.L.; Chen, Z.; Tao, G.; Xiao, Y. Enhanced heat release and self-healing properties of steel slag filler based asphalt materials under microwave irradiation. *Constr. Build. Mater.* **2018**, *193*, 32–41. [CrossRef]
9. Kambole, C.; Paige-Green, P.; Kupolati, W.K.; Ndambuki, J.M.; Adeboje, A.O. Basic oxygen furnace slag for road pavements: A review of material characteristics and performance for effective utilisation in southern Africa. *Constr. Build. Mater.* **2017**, *148*, 618–631. [CrossRef]
10. Xie, J.; Wu, S.; Lin, J.; Cai, J.; Chen, Z.; Wei, W. Recycling of basic oxygen furnace slag in asphalt mixture: Material characterization & moisture damage investigation. *Constr. Build. Mater.* **2012**, *36*, 467–474.
11. Ko, M.S.; Chen, Y.L.; Jiang, J.H. Accelerated carbonation of basic oxygen furnace slag and the effects on its mechanical properties. *Constr. Build. Mater.* **2015**, *98*, 286–293. [CrossRef]
12. López-Díaz, A.; Ochoa-Díaz, R.; Grimaldo-León, G.E. Use of BOF slag and blast furnace dust in asphalt concrete: an alternative for the construction of pavements. *Dyna* **2018**, *85*, 24–30.
13. Qazizadeh, M.J.; Farhad, H.; Kavussi, A.; Sadeghi, A. Evaluating the fatigue behavior of asphalt mixtures containing electric arc furnace and basic oxygen furnace slags using surface free energy estimation. *J. Clean. Prod.* **2018**, *188*, 355–361. [CrossRef]
14. Wu, S.P.; Xue, Y.J.; Ye, Q.S.; Chen, Y.C. Utilization of steel slag as aggregates for stone mastic asphalt (SMA) mixtures. *Build. Environ.* **2007**, *42*, 2580–2585. [CrossRef]
15. Shen, D.H.; Wu, C.M.; Du, J.C. Laboratory investigation of basic oxygen furnace slag for substitution of aggregate in porous asphalt mixture. *Constr. Build. Mater.* **2009**, *23*, 453–461. [CrossRef]
16. Zhang, Z.H.; Liao, J.L.; Ju, J.T.; Dang, Y.J. Treatment process and utilization technology of steel slag in China and Abroad. *J. Iron. Steel Res.* **2013**, *25*, 1–4. [CrossRef]
17. Guo, H. Selection of steel slag processing technology. *Energy Metall. Ind.* **2011**, *25*, 14–20.
18. Juckes, L.M. The volume stability of modern steelmaking slags. *Miner. Process. Extr. Metall. Trans.* **2003**, *112*, 177–197. [CrossRef]
19. Zhou, Z.; Ming, H. Analysis of affecting factors on thermal stability of asphalt mixtures. *J. Highw. Transp. Res. Dev.* **2004**, *6*, 15–21.
20. Xue, Y.J.; Wang, C.; Hu, Z.H.; Zhou, Y.; Liu, G.; Hou, H.B. Thermal treatment on sewage sludge by electromagnetic induction heating: Methodology and drying characterization. *Waste Manag.* **2018**, *78*, 917–928. [CrossRef]
21. Li, C.; Wu, S.; Chen, Z.; Shu, B.; Li, Y.; Xiao, Y.; Liu, Q. Synthesis of Fe3O4-decorated Mg-Al layered double hydroxides magnetic nanosheets to improve anti-ultraviolet aging and microwave absorption properties used in asphalt materials. *Constr. Build. Mater.* **2019**, *220*, 320–328. [CrossRef]
22. Chen, Z.W.; Xie, J.; Xiao, Y.; Chen, J.Y.; Wu, S.P. Characteristics of bonding behavior between basic oxygen furnace slag and asphalt binder. *Constr. Build. Mater.* **2014**, *64*, 60–66. [CrossRef]
23. Ziaee, S.A.; Kavussi, A.; Jalili Qazizadeh, M.; Mohammadzadeh Moghadam, A. Avaluation of long term ageing of asphalt mixtures containing eaf and bof steel slags. *Int. J. Transp. Eng.* **2015**, *5*, 65–72.
24. Ameri, M.; Hesami, S.; Goli, H. Laboratory evaluation of warm mix asphalt mixtures containing electric arc furnace (EAF) steel slag. *Constr. Build. Mater.* **2013**, *49*, 611–617. [CrossRef]
25. Shu, B.; Wu, S.; Dong, L.; Li, C.; Kong, D.; Yang, X. Synthesis and properties of microwave and crack responsive fibers encapsulating rejuvenator for bitumen self-healing. *Mater. Res. Express* **2019**, *6*, 30–35. [CrossRef]
26. Shu, B.; Wu, S.; Dong, L.; Norambuena-Contreras, J.; Yang, X.; Li, C. Microfluidic synthesis of polymeric fibers containing rejuvenating agent for asphalt self-healing. *Constr. Build. Mater.* **2019**, *219*, 176–183. [CrossRef]
27. Prowell, B.D.; Zhang, J.; Brown, E.R. Aggregate properties and the performance of superpave-designed Hot Mix Asphalt. *Nchrp Report.* **2005**, *4*, 93–101.
28. Masad, E.A. Aggregate Imaging System (AIMS): Basics and Applications. *Blending* **2005**, *23*, 453–461.
29. Ma, T.; Wang, H.; He, L.; Zhao, Y.L.; Huang, X.M.; Chen, J. Property characterization of asphalt binders and mixtures modified by different crumb rubbers. *J. Mater. Civ. Eng.* **2017**, *29*, 50–55. [CrossRef]
30. Ma, T.; Zhang, D.Y.; Zhang, Y.; Wang, S.Q.; Huang, X.M. Simulation of wheel tracking test for asphalt mixture using discrete element modelling. *Road Mater. Pavement Des.* **2018**, *19*, 367–384. [CrossRef]
31. Pan, P.; Wu, S.P.; Xiao, Y.; Liu, G. A review on hydronic asphalt pavement for energy harvesting and snow melting. *Renew. Sustain. Energy Rev.* **2015**, *48*, 624–634. [CrossRef]
32. Mason, B. The constitution of some basic open-hearth slags. *J. Iron Steel Inst.* **1994**, *12*, 69–80.

33. Wang, Q.; Yan, P.; Han, S. The influence of steel slag on the hydration of cement during the hydration process of complex binder. *Sci. China Technol. Sci.* **2011**, *54*, 388–394. [CrossRef]
34. Masad, E.; Olcott, D.; White, T.; Tashman, L. Correlation of fine aggregate imaging shape indices with asphalt mixture performance. *Transp. Res. Rec.* **2001**, *1757*, 148–156. [CrossRef]
35. Mallat, S.G. A theory for multiresolution signal decomposition: the wavelet representation. *IEEE Trans. Pattern Anal. Mach. Intell.* **1989**, *158*, 231–242. [CrossRef]
36. Chen, Z.W.; Wu, S.P.; Xiao, Y.; Zeng, W.B.; Yi, M.W.; Wan, J.M. Effect of hydration and silicone resin on Basic Oxygen Furnace slag and its asphalt mixture. *J. Clean. Prod.* **2016**, *112*, 392–400. [CrossRef]

materials

MDPI

Article

Interlaminar Bonding Properties on Cement Concrete Deck and Phosphorous Slag Asphalt Pavement

Guoping Qian [1], Shunjun Li [2], Huanan Yu [1,*] and Xiangbing Gong [1]

[1] National Engineering Laboratory for Highway Maintenance Technology, School of Traffic and Transportation Engineering, Changsha University of Science & Technology, Changsha 410114, China; guopingqian@sina.com (G.Q.); xbgong@csust.edu.cn (X.G.)

[2] School of Traffic and Transportation Engineering, Changsha University of Science & Technology, Changsha 410114, China; shunjun.li@stu.csust.edu.cn

* Correspondence: huanan.yu@csust.edu.cn; Tel.: +86-13714470593

Received: 11 April 2019; Accepted: 29 April 2019; Published: 1 May 2019

Abstract: The slippage damage caused by weak interlaminar bonding between cement concrete deck and asphalt surface is a serious issue for bridge pavement. In order to evaluate the interlaminar bonding of cement concrete bridge deck and phosphorous slag (PS) asphalt pavement, the shear resistance properties of the bonding layer structure were studied through direct shear tests. The impact of PS as a substitute of asphalt mixture aggregate, interface characteristics, normal pressure, waterproof and cohesive layer types, temperature and shear rate on the interlaminar bonding properties were analyzed. The test results indicated that the interlaminar bonding of bridge deck pavement is improved after asphalt mixture fine aggregate was substituted with PS and PS powder, and the result indicated that the shear strength of grooved and aggregate-exposed interfaces is significantly higher than untreated interface, the PS micro-powder or anti-stripping agent can also improve the adhesion between layers when mixed into SBS asphalt. This study provided important theoretical and practical guidance for improving the shear stability of bridge deck pavement.

Keywords: asphalt mixture; cement concrete deck; phosphorous slag; interlaminar bonding; shear strength

1. Introduction

The early damage, especially the slippage and upheaval of asphalt pavement over cement concrete bridge deck is a serious issue for bridge operations. When the bridge is under an extensive heavy vehicle load, large shear stress is generated inside the bridge deck pavement which caused uncertain shear failure surface; or serious shear damage and diseases are caused because the horizontal shear resistance between the pavement layer and bridge deck is weak [1]. Among the factors affecting the interlaminar bonding of bridge deck pavement structure, the mixture aggregate characteristic plays a significant role in that [2]. However, the lack of high-quality aggregates is very common in many areas, the mining of raw aggregate have cost many environmental problems, and the problem has become more and more serious with the acceleration of the infrastructure construction process.

Phosphorous slag (PS) is an industrial by-product produced in the process of phosphorus ore in a high-temperature environment. At present, the global discharge of wasted PS is about 12 to 15 million ton each year. The accumulation of a large amount of PS not only occupies the land but also seriously pollutes the environment [3]. Therefore, the effective utilization of PS in the asphalt pavement would beneficial the highway construction and the environment from all prospects [4].

Many pieces of research have been carried out on the engineering application of PS. Allahverdi, et al. [5] found that PS powder can significantly improve the quality of cement after mechanical activation and chemical catalysis. Zhao, et al. [6] demonstrated that PS with appropriate

cement replacement dosage and specific area could improve the mechanical properties of sleeper concrete under steam curing. Xia, et al. [7] studied the crack resistance of PS concrete from the aspects of physical properties, hydration heat, shrinkage and creep and found that the crack resistance of PS concrete is approximate to, even to some extent better than, that of fly ash concrete. He, et al. [8] found that with the increase of granularity of PS additive, there are significant increases in the uniformity of particle sizes, slurry pH, and activity index, and the effects on cement paste are significantly mitigated. Jin [9] studied the influence of superfine PS as mineral filler on the long-term performance and durability of concrete. The results show that PS can improve the pore structure of concrete which is beneficial to the development of compressive strength and splitting tensile strength of concrete at a late age. Hamideh, et al. [10] predicted and optimized the compressive strength of PS cement at different ages (3, 7 and 28 days) based on the response surface method.

Qian, et al. [11] found that PS can be potentially used as an antistripping additive in asphalt mixture because the pH of the slag was alkaline and it was also hydrophobic and stable at high temperature. The viscoelasticity test also showed that PS filler improved the stiffness of asphalt. The mixture performance tests also indicated that PS filler significantly increases the resistance of HMA to rutting and moisture damage. Qian, et al. [12] further analyzed the influence of surface modified PS powder as a modifier on the mechanism of asphalt and asphalt mixture and found that TM-P modified PS powder can enhance the compatibility with asphalt, which improves the antiaging, rutting resistance and water damage resistance of asphalt mixture. Sheng, et al. [13] studied the effect of PS powder as mineral filler on the rheological properties of asphalt binder and the properties of asphalt mixture and found that it increased the binder viscosity resulting in enhanced mixture rutting resistance. In order to study the rutting and fatigue damage of asphalt pavement, Bazzaz, et al. [14,15] proposed a straightforward procedure to characterize the nonlinear viscoelastic response of asphalt concrete materials.

In addition, there are many pieces of research that have been carried out on asphalt pavement structure of cement concrete bridge deck which provided meaningful guidance on this research. Wang, et al. [16] have studied the interface shear characteristics between the asphalt pavement structure and the concrete bridge deck pavement and found that the shear strength of SBS modified asphalt pavement over concrete bridge deck is slightly greater than that of crumb rubber modified asphalt pavement. Li, et al. [17] studied the interlaminar failure modes and mechanisms of rubber powder modified asphalt, SBS modified asphalt and epoxy resin adhesive as waterproof bonding materials and found that the shear strength is greatly affected by the thickness of the waterproof adhesive layer. Liu, et al. [18] studied the bonding performance of waterproof bonding layer between the concrete bridge deck and asphalt mixture pavement by a lab test, field temperature monitoring and finite element method (FEM). The test results show that the safety factor (strength/stress) decreases significantly with increasing environmental temperatures. Sheng, et al. [19] established a simplified formula for calculating the extreme temperature (maximum and minimum temperature) stress of bridge deck pavement structures. The results have shown a strong linear correlation between the bridge deck pavement maximum principal stress and the elastic modulus.

He, et al. [20] proposed typical structural types of cement concrete bridge deck pavement based on waterproof cohesive layer material test and bridge deck pavement composite structure test. Jia [21] proposed using the interlayer shear test as a method to study the shear performance of the interlayer structure layer of bridge deck pavement. And have proposed design method and design standard of asphalt mixture based on that. Ren, et al. [22] analyzed the influence of chip-sprinkling interlayer treatment technology on the shear resistance of cement concrete bridge deck asphalt pavement layers, and recommended the optimal chip-sprinkling technique parameters. Xu, et al. [23] evaluated the improvement effect of aggregate-exposed interface on the stability of bridge deck pavement structure by direct shear test and pull-out test. They found that exposed-aggregate showed better shear performance than other interfacial treatment methods under various positive pressures. Liu, et al. [24] proposed the environmental simulation bubble test and used MatchID-3D structural deformation analysis system to measure bubble deformation, and studied the deformation characteristics and mechanism of bubbles

in bridge deck waterproofing membrane. It found that the test temperature, initial debonding aperture, and water have great influences on the performance of bridge deck pavement. Lee, et al. [25] have studied the feasibility of reducing early temperature shrinkage crack and dry shrinkage crack of low melting point concrete with shrinkage reducing agent. And confirmed the durability can be increased without affecting other properties by adding a shrinkage reducing agent.

Although there are many pieces of research on the application of PS in HMA, research on the interlaminar shear resistance of cement concrete bridge deck PS asphalt pavement is relatively limited. In this paper, interlaminar shear strength is used as evaluation indexes, and the bonding performance of the interlayer structure is evaluated through the direct shear test with normal pressure. The impact of PS as a substitute for the asphalt mixture aggregate, interface types, normal pressure levels, waterproof bonding layer types, temperature and shear rate on interlaminar bonding shear performance are analyzed.

2. Experimental Plan

2.1. Mixture Design

In this research, "Shell" SBS modified asphalt binder was used in the design of pavement surface layer and an interlaminar bonding layer. The conventional test of asphalt and asphalt mixture was following the procedures of "standard test methods for bitumen and bituminous mixture for highway engineering" (JTG E20-2011) [26]. The conventional asphalt binder test results are shown in Table 1, as shown in the table that the asphalt binder satisfied the specification requirement. The asphalt mixture was designed following the steps of "technical specification for construction of highway asphalt pavement" (JTG F40-2017) [27], the aggregate used was limestone, the filler was limestone mineral powder, the optimum asphalt content was 5.4%, and the pavement mixture gradation was widely-used AC-16C. The gradation curve of the asphalt mixture is shown in Figure 1 and the design and volumetric parameters of asphalt mixture are shown in Table 2. In order to evaluate the influence of PS on the shear resistance of asphalt mixture, the fine limestone aggregate of 0.075 mm–4.75 mm was replaced with PS and PS powder for comparative tests.

Table 1. Technical indexes of (Styrene-Butadiene-Styrene) SBS modified asphalt binder.

Properties		Test Value	Technical Index
Penetration at 25 °C, 100 g, 5 s (0.1 mm)		51.5	30-60
Ductility at 5 °C, 5 cm/min (cm)		28.5	≥20
Softening Point (°C)		87	≥60
After RTFOT	Weight Change (%)	−0.053	≤± 1.0
	Penetration Ratio (%)	80	≥65
	Residual Ductility at 5 °C, 5 cm/min	16	≥15

Table 2. Marshall test results of SBS modified asphalt.

Asphalt Content (%)	Void Ratio (%)	VMA* (%)	VFA* (%)	Stability (kN)	Flow Value (mm)
5.4	4.7	15.2	69	16.3	31.4

* VMA = Voids in Mineral Aggregate, VFA = Voids Filled with Asphalt.

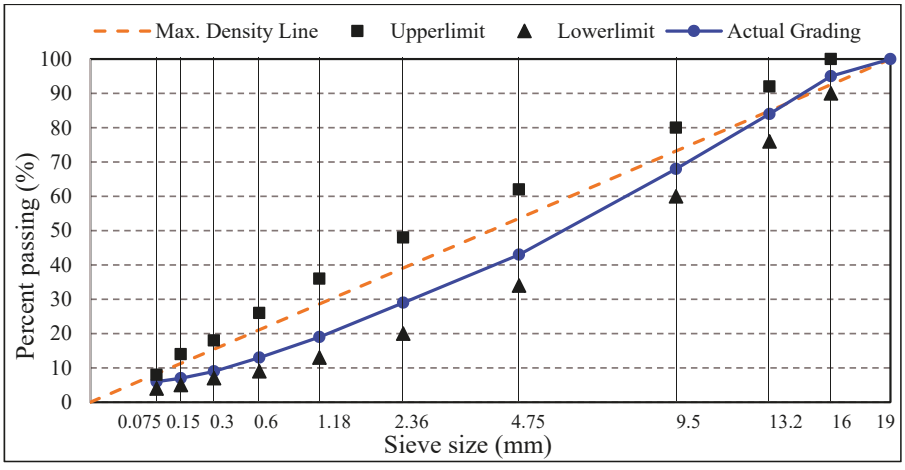

Figure 1. The gradation of dense-graded AC-16C asphalt mixtures.

2.2. Experiment Design

The interlaminar shear resistance of bridge deck pavement specimens was studied by direct shear test under normal pressure. The specimens used were prismatic specimens of 80 mm × 80 mm × 100 mm. The test design and test equipment (Material Testing Systems—MTS 810, USA) are shown in Figure 2.

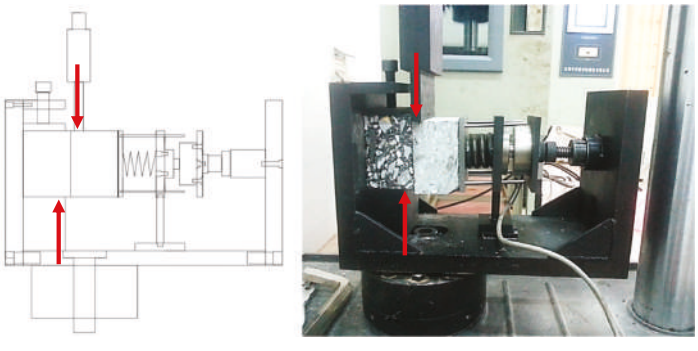

Figure 2. Direct shear test design and test device.

Four duplicate specimens were prepared for each test, and the test results were illustrated with the average of four specimens. The test specimens preparation steps were as follows:

(1) Cement concrete test specimens were formed indoor following the construction process with a size of 300 mm × 300 mm × 50 mm. Then, specimens were placed in the standard curing room for curing of 28 days, and the cement concrete panels were prepared with three types of interface: untreated (without any surface treatment), grooved and aggregate-exposed, the sample preparation process of the grooved interface and aggregate-exposed interface were shown below:

(a) Grooved interface. The grooves were notched according to the pavement anti-slide requirements in the technique guidelines for construction of highway cement concrete pavement [28]. The grooves were notched in a depth of 2–4 mm, in a width of 3–5 mm, and a groove spacing of about 15 mm.

(b) Aggregate-exposed interface. The first step prepares the aggregate-exposed concrete was to spray retarder on the surface of the cement concrete layer after paving, which delayed the setting and hydration of the surface mortar layer but did not affect the normal setting and hydration of the main

body. After the main-body concrete reaches a certain strength, the surface laitance was washed out to expose part of coarse aggregate.

After curing, the cement concrete slabs of the three interface types are shown in Figure 3, which displays as the untreated interface, the grooved interface and the aggregated-exposed interface from left to right.

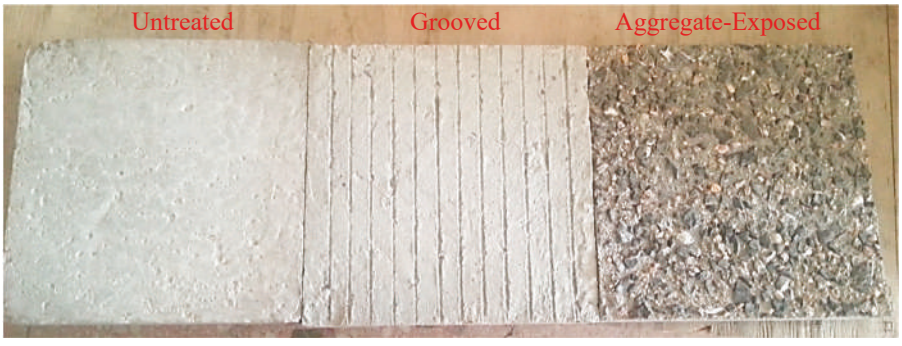

Figure 3. Cement concert slabs with three interface types.

(2) After the cement concrete slabs were cured, the surface of each type was coated with three different types of interlayer bonding materials separately, which included SBS modified asphalt, SBS modified asphalt mixed with PS micro-powder, and SBS modified asphalt mixed with surfactant (anti-stripping agent). The content of PS micro-powder and anti-stripping agent was 10% and 0.4% of the mass of asphalt, respectively. As the surface area of each type of interface was different, in order to make sure that all surfaces were coated well, the dosage of waterproof cohesive bonding material for untreated, grooved and aggregate-exposed interfaces was 1.0 kg/m^2, 1.2 kg/m^2 and 1.5 kg/m^2 respectively.

(3) Then, put the cement concrete specimen into a 300 mm × 300 mm × 100 mm rutting plate test mold, and poured the mixed asphalt mixture over it and applied the rutting wheel to compact it into the desired compaction level. Finally, the composite specimens were cut into 80 mm × 80 mm × 100 mm small prism specimens. The specimens with different interfacial treatment are shown in Figure 4.

Figure 4. Specimens for the direct shear test with different interfacial treatment.

For the direct shear test, the shear strength corresponding to the peak value of the load-displacement curve is the shear strength of the interface. The calculation method is shown in Equation (1):

$$\tau = P/S. \quad (1)$$

In which: τ is the interlaminar interface shear strength (MPa); P is the peak value of shear load in the direct shear test (kN); S is the interfacial area (mm^2).

As the surface roughness of cement concrete slabs with three interface types of untreated, grooved and aggregate-exposed was different, the roughness characteristics were evaluated by the texture depth (*TD*) index. The *TD* was measured by sand spreading method following the field test methods of subgrade and pavement for highway engineering (JTG E60-2008) [29] which was described below: Firstly, spread the standard sand on the cement slab into a circle, then scrape the surface of the standard sand with a scraper, measure the diameters of the two vertical directions of the circle with a ruler, then brush the standard sand on the cement board with a clean brush to weigh the quality. The *TD* of the cement board surface can be calculated by Equation (2). The determination of the *TD* of the cement slab is shown in Figure 5. The *TD* measurement results for untreated, grooved and aggregate-exposed interfaces are 0.59 mm, 1.67 mm and 4.43 mm respectively.

$$TD = 4V/\pi d^2. \quad (2)$$

In which, V is the sand volume to filling the uneven part under the measuring circle (mm^3), d is the diameter of the measuring circle (mm).

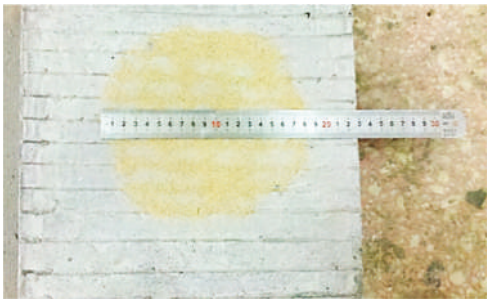

Figure 5. Method to measure the texture depth.

2.3. Experimental Schematic

In order to evaluate the impact of PS as a substitute of asphalt mixture aggregate, waterproof and cohesive layer material type, bridge deck interface treatment, normal pressure, test temperature and loading rate on the interlaminar bonding behavior of bridge deck pavement, the following tests were conducted:

(1) **Impact of PS as a substitute of asphalt mixture aggregate.** The asphalt mixture of AC-16C was used to compare the interlaminar bonding of PS as a substitute of asphalt mixture aggregate: one is named as limestone asphalt mixture in which the asphalt mixture aggregate was limestone and filler and the other was named as PS asphalt mixture in which the fine limestone aggregate of 0.075 mm to 4.75 mm and fillers were replaced by PS and PS powder in equal amounts.

(2) **Impact of waterproof and cohesive layer material type.** In order to compare the interlaminar bonding behavior of different bonding layer materials, SBS modified asphalt, SBS modified asphalt mixed with PS micro-powder and SBS modified asphalt mixed with an anti-stripping agent were selected for comparison.

(3) **Impact of bridge deck interface treatment.** In order to analyze the impact of different interface conditions on the shear resistance of interlayer, the bonding characteristics of untreated, grooved, and aggregate-exposed interfaces were evaluated.

(4) **Impact of normal pressure.** In order to study the influence of normal pressure on interlaminar shear strength, the test with normal pressures of 0 MPa, 0.3 MPa, 0.5 MPa and 0.7 MPa were conducted and compared respectively.

(5) **Impact of temperature.** The test temperature has a significant effect on the interlaminar shear strength. In order to obtain the impact of the test temperature on the interlaminar shear strength, five test temperatures of 25 °C, 40 °C, 50 °C, 60 °C and 70 °C were selected to conduct comparison tests.

(6) **Impact of shear rate.** In order to simulate the effect of different driving speeds on the interlaminar shear performance, five different shear loading rates of 1 mm/min, 5 mm/min, 10 mm/min, 20 mm/min and 50 mm/min were selected to conduct comparison tests.

3. Results and Discussions

3.1. Impact of PS as Asphalt Mixture Aggregate Substitute

The direct shear strength between concrete deck and asphalt pavement was measured to evaluate the impact of PS as limestone substitute on the interlaminar bonding performance. The SBS modified asphalt was used in the interlaminar bonding layer, and the test temperature was 60 °C. In order to ensure the specimen had a constant test temperature, the specimens were put into the environmental chamber for 4 h before the test, the shear rate was 10 mm/min, the vertical pressure was 0.5 Mpa. The three different interface types of untreated, grooved and aggregate-exposed were selected for comparative study. The test results are shown in Table 3. The comparison figure is shown in Figure 6.

Table 3. Impact of aggregate and interlayer treatment on the interlaminar bonding.

Aggregate Type	Interface Type	Max Shear Force (kN)	Shear Strength (MPa)
Limestone Asphalt Mixture	Untreated	2.061	0.322
	Grooved	2.784	0.435
	Aggregate-exposed	3.725	0.582
PS Asphalt Mixture	Untreated	2.266	0.354
	Grooved	3.072	0.480
	Aggregate-exposed	4.089	0.639

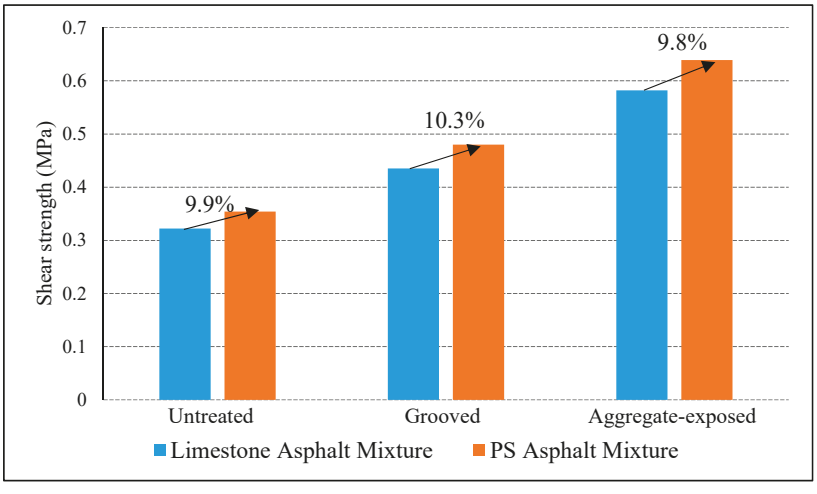

Figure 6. Impact of aggregate and interlayer treatment on the interlaminar bonding.

As shown in Table 3 and Figure 6, the interlaminar shear strength corresponding to the PS asphalt mixture is higher than that of limestone asphalt mixture for all three kinds of interface types, and the increasement corresponding to untreated, grooved and aggregate-exposed interfaces were 9.9%, 10.3% and 9.8% respectively. The main reason is that PS is alkaline and have a larger specific surface area, so it shows better adhesion to asphalt binder compared with limestone powder. As a result, the bonding effect between PS asphalt mixture and SBS modified asphalt material is improved, the shear strength and interlaminar stability of the bridge deck and asphalt pavement are improved.

3.2. Impact of Interfacial Surface on the Interlaminar Bonding

In order to study the influence of surface treatment on the shear resistance of the bridge deck, three kinds of interface types were evaluated in this paper, which including untreated interface, the grooved interface, and aggregate-exposed interface. Indoor direct shear tests were carried out on bridge deck pavement composed of two kinds of pavement materials: PS asphalt mixture and limestone asphalt mixture. The interlaminar bond coating materials were SBS modified asphalt, the test temperature was 60 °C, the shear rate was 10 mm/min, and the normal pressure was 0.5 MPa. The test results were also shown in Table 3 and Figure 6.

From Figure 6, it can be seen that both the shear strength of PS asphalt mixture and the limestone asphalt mixture shows the same relation for all three interface types: aggregate-exposed interface > grooved interface > untreated interface. When the paving layer is a limestone asphalt mixture, the shear strength of the grooved interface and the aggregate-exposed interface were increased by 35.1% and 80.7% respectively compared with the original untreated interface. In addition, for the PS asphalt mixture, the shear strength of the grooved interface and the aggregate-exposed interface were increased by 44.1% and 80.5% respectively compared with the original interface.

As mentioned earlier, the *TD* size of the three interface types is sorted as aggregate-exposed interface > grooved interface > untreated interface. The relation of *TD* on the shear strength of the composite structure is shown in Figure 7. The results showed that the shear strength closely related to the surface textural of the bridge deck, the rougher the texture of the deck surface and the greater the value of *TD*, the greater the shear strength of the corresponding deck pavement structure.

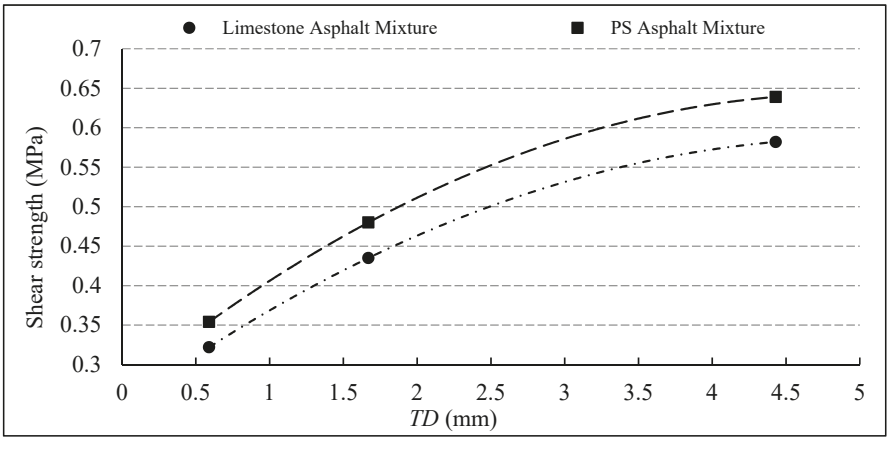

Figure 7. Impact of texture depth on the interlaminar bonding.

3.3. Impact of Waterproof and Cohesive Layer Material Type

In order to compare and study the influence of waterproof and cohesive coating material on the interlaminar shear resistance and to improve the interlaminar stability of bridge deck pavement, the interlaminar shear tests of SBS modified asphalt, SBS modified asphalt with PS micro-powder, and SBS modified asphalt with surfactant (anti-stripping agent) were carried out. The interlaminar shear test was conducted with three interface types mentioned above respectively. The PS asphalt mixture was used as a pavement layer. The test temperature was 60 °C, the shear rate was 10 mm/min, and the vertical pressure was 0.5 MPa. The test results are as shown in Table 4 and the comparative figure is shown in Figure 8.

Table 4. Interlaminar shear strength of different waterproof and cohesive materials.

Bonding Material	Interface Type	Max Shear Force (kN)	Shear Strength (MPa)
SBS asphalt	Untreated	2.266	0.354
	Grooved	3.027	0.480
	Aggregate-exposed	4.089	0.639
SBS asphalt with PS Micro-powder	Untreated	2.406	0.376
	Grooved	3.347	0.523
	Aggregate-exposed	4.224	0.660
SBS asphalt with anti-stripping agent	Untreated	2.323	0.363
	Grooved	3.226	0.504
	Aggregate-exposed	4.333	0.677

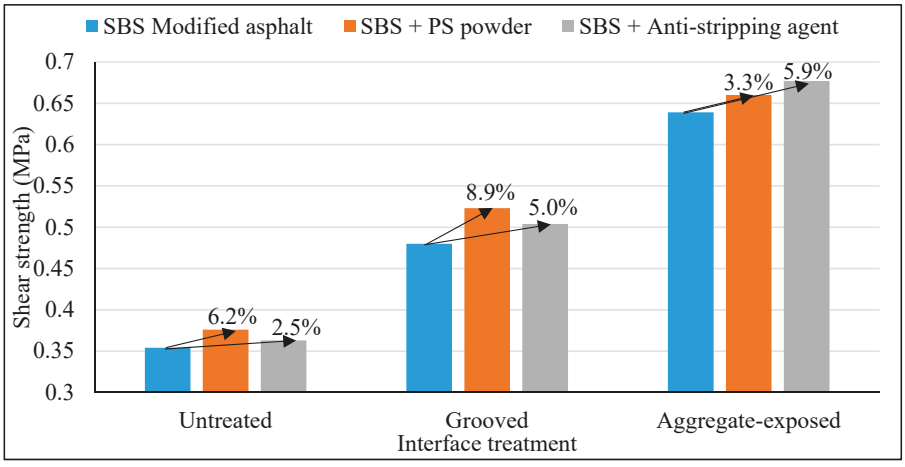

Figure 8. Interlaminar shear strength of different waterproof and cohesive materials.

As can be seen from Table 4 and Figure 8, For the original untreated interface, the shear strength increase by 6.2% and 2.5%, the grooved interface increased by 8.9% and 5.0% and the aggregate-exposed interface increased by 3.3% and 5.9%, respectively. The results show that the interlaminar shear strength of SBS asphalt with PS powder and SBS asphalt with anti-stripping agent were higher than that of SBS asphalt. The reason is that the surface of the grooves and exposed coarse aggregate increased the adhesion ability between the bridge deck and asphalt pavement, therefore, the contribution of the PS powder or anti-stripping agent on the interlayer shear stress of treated interface is greater than that of the untreated interface.

3.4. Impact of Normal Pressure

The mechanical properties of bridge deck pavement are greatly influenced by the grade of vehicle load. As the normal pressure at the interface of pavement and bridge deck is below 0.7 MPa at most cases, therefore, the tested normal pressure for the interlaminar bonding properties was in the range of 0 MPa to 0.7 MPa. In order to better study the impact of different vehicle loads on the shear stability of deck pavement, different normal pressures of 0 MPa, 0.3 MPa, 0.5 MPa and 0.7 MPa were selected respectively to conduct the direct shear test. SBS modified asphalt was used as a waterproof and cohesive layer and PS asphalt mixture was used as a bridge deck surface layer. The experimental temperature was 60 °C and the shear rate was 10 mm/min. The results of shear tests were shown in Table 5 and Figure 9.

Table 5. Test results of interlaminar shear strength under different normal pressures.

Pavement Mixture	Normal Pressure (MPa)	Max Shear Force (kN)	Shear Strength (MPa)
PS asphalt mixture	0	0.352	0.055
	0.3	2.169	0.339
	0.5	3.072	0.480
	0.7	4.166	0.651

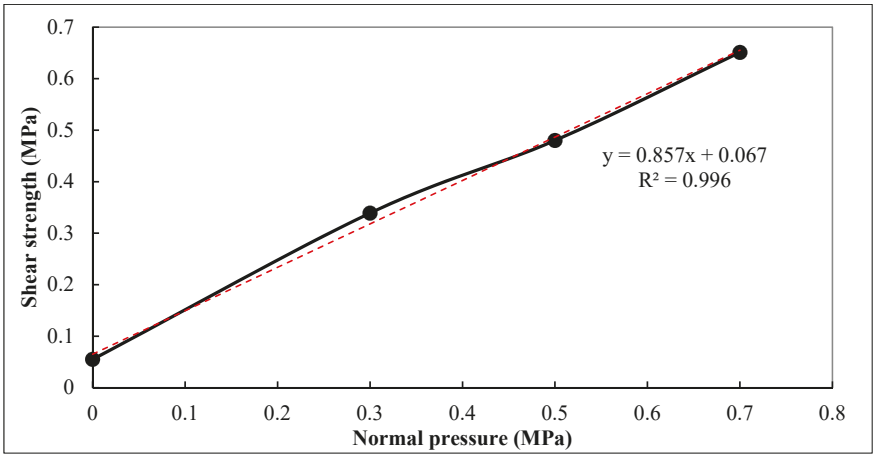

Figure 9. Relationship between normal pressure and interlaminar shear strength.

Although the factors affecting the interlaminar bonding properties are very complicated, as it can be seen from Figure 9, it is reasonable to assume it satisfied the Mohr-Coulomb strength theory when the normal pressure was below 0.7 MPa, in which the interlaminar shear strength has a linear relation with the normal pressure. In addition, based on the Mohr-Coulomb strength theory, the interlaminar shear failure will not occur if the interlaminar shear stress caused by vehicle load satisfied the following equation:

$$\tau < c + \sigma_z tg\varphi \quad (3)$$

where c is the cohesion between asphalt pavement and cement deck, σ_z is the normal compressive stress on the shear surface, and $\sigma_z tg\varphi$ is the friction between the rough surface texture structure of bridge deck and the asphalt mixture of pavement. The linear regression equation of the interlaminar shear strength and the corresponding cohesive force c and internal friction angle φ of the grooved interface under different normal pressures are shown below.

$$\tau = 0.067 + 0.857\sigma \left(R^2 = 0.996\right). \quad (4)$$

In which, the cohesive strength of c = 0.067 MPa, and the internal friction angle φ = 40.6°.

3.5. Impact of Temperature on Interlaminar Shear Strength

As the interlayer bonding material of bridge deck pavement is usually viscoelastic material, the bonding properties are sensitive to temperature change, therefore, the bridge deck pavement tended to occur interlaminar shear deformation due to the decrease of bond performance at summer high-temperature conditions.

In order to study the influence of temperature on interlaminar shear strength of PS asphalt mixture, the interlaminar shear tests were carried out at 25 °C, 40 °C, 50 °C, 60 °C and 70 °C respectively. In order to ensure the temperature field of the specimen was uniform, the specimens were placed

in the environmental chamber for 4 h before the test. The interlaminar bonding material was SBS modified asphalt, and the interface was grooves treated. The experimental interlaminar shear rate was 10mm/min and the normal pressure was 0.5 MPa. The test results are shown in Table 6.

Table 6. Results of interlaminar shear tests at different temperatures.

Mixture Type	Temperature (°C)	Maximum Shear (kN)	Shear Strength (MPa)
PS asphalt mixture	25	5.318	0.831
	40	3.757	0.587
	50	3.347	0.523
	60	3.027	0.480
	70	2.835	0.443

As it can be seen from Figure 10, the influence of temperature on the interlaminar shear stress of PS asphalt pavement is very obvious, the interlaminar shear strength decreases gradually with the increase of temperature, and the influence slope varies in a different temperature range. It can be calculated from the diagram that the interlaminar shear strength decreased by 29.4% when the temperature increased from 25 °C to 40 °C, the shear strength decreased by 10.9% when the temperature raised from 40 °C to 50 °C, the interlaminar shear strength decreased by 8.9% when the temperature raised from 50 °C to 60 °C, and the interlaminar shear strength decreased by 7.7% when the temperature raised from 60 °C to 70 °C. From the experimental data, it can be seen that the interlaminar shear strength at 60 °C is only 57.7% of that at 25 °C, this would explain the reason why the interlaminar shear failure of bridge deck pavement occurs mostly in the high-temperature season.

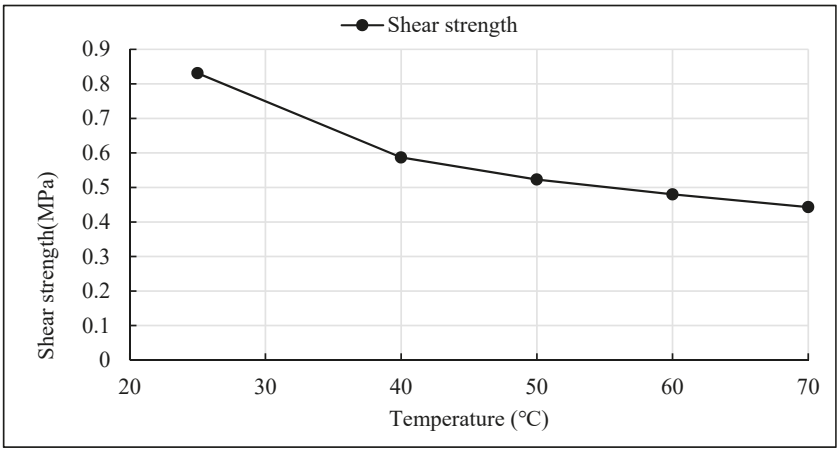

Figure 10. Relation of interlaminar shear strength with temperature.

3.6. Impact of Shear Rate on Interlaminar Shear Strength

In order to study the influence of different driving speed on the shear stress of PS asphalt pavement, various shear rates of 1 mm/min, 5 mm/min, 10 mm/min, 20 mm/min and 50 mm/min were used to simulate the different driving speeds. The grooved interface was used in these tests, the waterproof and cohesive material was SBS modified asphalt. The test temperature was 60 °C and the normal pressure was 0.5 Mpa. The test results are shown in Table 7 and Figure 10.

Table 7. Results of interlaminar shear strength tests at different shear rates.

Pavement Mixture	Shear Rate (mm/min)	Max Shear Force (kN)	Shear Strength (MPa)
PS asphalt mixture	1	2.425	0.379
	5	2.765	0.432
	10	3.072	0.480
	20	3.149	0.492
	50	2.976	0.465

As shown in Figure 11, the shear rate had a significant effect on the shear strength between layers, and the shear strength increased with the increase of shear rate when the shear rate was below 10mm/min, and when the shear rate increased from 1 mm/min to 10 mm/min, the effect of loading rate on shear strength was especially significant. As it can see from that test data that the shear strength of 10 mm/min was 26.6% higher than that of 1 mm/min. As the loading rate continues to increase, the test curve gradually tends to smooth and stable, that is, when the loading rate was large, the influence of loading rate on the interlaminar shear strength became smaller. This also shows that the vehicle's damage to the pavement of the bridge deck at high speed was less than at lower speed.

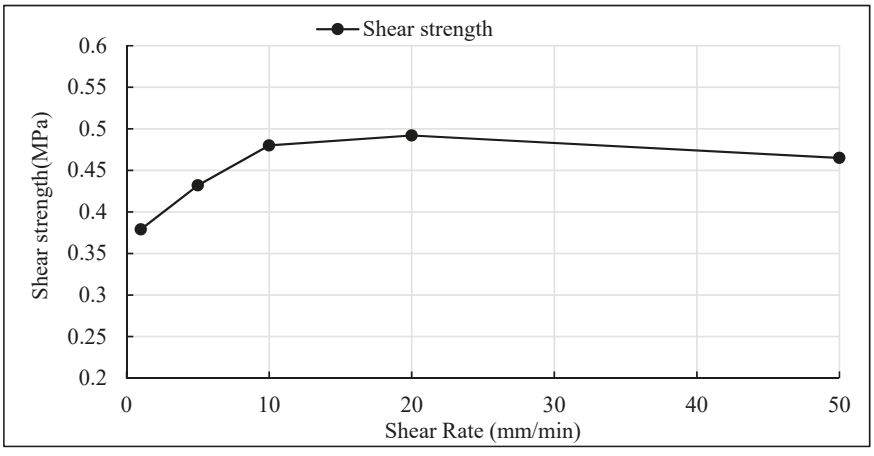

Figure 11. Relationship between shear rate and interlaminar shear strength.

4. Conclusions

This research evaluated the factors impacting the interlayer bonding and shear resistance of cement concrete bridge asphalt pavement, the comparatively tests including PS as a substitute of fine aggregate for asphalt mixture, interface characteristics, normal pressure, waterproof and cohesive layer types, temperature and shear rate. The following conclusions can be drawn:

(1) After the substitution of limestone aggregate between the size of 0.075 mm and 4.75 mm in the asphalt mixture with an equal amount of PS and PS powder, the bonding characteristics between surface asphalt mixture and bridge deck were improved, the interlaminar shear resistance and interlaminar stability were increased.

(2) The interfacial treatment of the bridge deck had a significant effect on the shear resistance of the deck. The rougher the surface texture and the greater the TD of the surface, the greater the shear resistance of the deck. The result indicated the aggregate-exposed treatment could increase the shear strength up to 80% compared with the untreated interface. It was an effective way to improve the shear resistance of bridge deck pavement by grooved or aggregate-exposed treatment.

(3) The impact of the test conditions on the interlaminar shear strength is significant. The interlaminar shear resistance increases with the increase of normal pressure, and the shear strength decreases gradually with the increase of test temperature. The interlaminar shear strength increases with the increase of shear rate in a certain range and tends to be stable when the shear rate is getting higher than 10 mm/min.

Overall, the bonding performance of bridge deck pavement can be improved by replacing the limestone aggregate and filler of 0.075–4.75 mm in asphalt mixture with PS and PS powder respectively. The rougher the deck surface is, the better the bonding strength between layers will be. Deck surfaces treated with the grooved or aggregate-exposed method can significantly improve the interlaminar bonding performance. Both PS powder and anti-stripping agent can improve the adhesion performance of SBS modified asphalt as a bonding layer.

Author Contributions: Conceptualization, G.Q.; Data curation, S.L. and H.Y.; Formal analysis, H.Y.; Funding acquisition, G.Q.; Investigation, S.L. and X.G.; Methodology, H.Y.; Project administration, G.Q.; Resources, G.Q.; Software, X.G.; Supervision, H.Y.; Visualization, X.G.; Writing—Original Draft, S.L.; Writing—Review & Editing, H.Y.

Funding: The research was funded by the National Key R and D Program of China (SQ2018YFB160027); National Natural Science Foundation of China (51778071 and 51808058); open fund (kfj180103) of National Engineering Laboratory of Highway Maintenance Technology (Changsha University of Science and Technology).

Conflicts of Interest: The authors declare no conflict of interest.

References

1. Zhang, Z.; Hu, C.; Wang, B. Research on the design method of asphalt concrete pavement for concrete bridge deck structure. *China J. Highw. Transp.* **2001**, *14*, 58–61. [CrossRef]
2. European Asphalt Pavement Association. *Asphalt Pavements on Bridge Decks*; EAPA Position Paper; European Asphalt Pavement Association: Brussels, Belgium, 2013.
3. Jiang, M.; Wang, Z.; Huang, X.; He, Y.; Zhang, L.; Ning, P.; Fu, J.; Liu, H. Secondary pollution prediction of recycling process of yellow phosphorus slag by moulding under thermal state. *J. Cent. South Univ. (Sci. Technol.)* **2016**, *47*, 1078–1084. [CrossRef]
4. Quan, J.; Zhang, K.; Ma, B. Effect of Pore Solution pH Value and Hydration Process on Phosphorous Slag Replacing of Slag. *Bull. Chin. Ceram. Soc.* **2016**, *35*, 2513–2517, 2523. [CrossRef]
5. Allahverdi, A.; Mahinroosta, M. Mechanical activation of chemically activated high phosphorous slag content cement. *Powder Technol.* **2013**, *245*, 182–188. [CrossRef]
6. Zhao, G.; Gao, Y.; Li, Y.; Zheng, A.; Kang, X. Research and experiment on the mechanical property of sleeper concrete adding phosphorus slag. *Concrete* **2011**, *9*, 84–86. [CrossRef]
7. Chen, X.; Zeng, L.; Fang, K. Anti-crack performance of phosphorus slag concrete. *Wuhan Univ. J. Sci.* **2009**, *14*, 80–86. [CrossRef]
8. He, X.; Ye, Q.; Yang, J.; Dai, F.; Su, Y.; Wang, Y.; Bohumir, S. Physico-chemical Characteristics of Wet-milled Ultrafine-granulated Phosphorus Slag as a Supplementary Cementitious Material. *J. Wuhan Univ. Technol. Sci. Ed.* **2018**, *33*, 625–633. [CrossRef]
9. Hu, J. Comparison between the effects of superfine steel slag and superfine phosphorus slag on the long-term performances and durability of concrete. *J. Anal. Calorim.* **2017**, *128*, 1251–1263. [CrossRef]
10. Mehdizadeh, H.; Kani, E.N. Modeling the influence of chemical composition on compressive strength behavior of alkali-activated phosphorus slag cement using statistical design. *Can. J. Civ. Eng.* **2018**, *45*, 1073–1083. [CrossRef]
11. Qian, G.; Bai, S.; Ju, S.; Huang, T. Laboratory Evaluation on Recycling Waste Phosphorus Slag as the Mineral Filler in Hot-Mix Asphalt. *J. Mater. Civ. Eng.* **2013**, *25*, 846–850. [CrossRef]
12. Qian, G.; Wang, K.; Bai, X.; Xiao, T.; Jin, D.; Huang, Q. Effects of surface modified phosphate slag powder on performance of asphalt and asphalt mixture. *Constr. Mater.* **2018**, *158*, 1081–1089. [CrossRef]
13. Sheng, Y.; Zhang, B.; Yan, Y.; Chen, H.; Xiong, R.; Geng, J. Effects of phosphorus slag powder and polyester fiber on performance characteristics of asphalt binders and resultant mixtures. *Constr. Mater.* **2017**, *141*, 289–295. [CrossRef]

14. Bazzaz, M. Experimental and Analytical Procedures to Characterize Mechanical Properties of Asphalt Concrete Materials for Airfield Pavement Applications. Ph.D. Thesis, University of Kansas, Lawrence, KS, USA, 2018.
15. Bazzaz, M.; Darabi, M.K.; Little, D.N.; Garg, N. A Straightforward Procedure to Characterize Nonlinear Viscoelastic Response of Asphalt Concrete at High Temperatures. *Transp. Res. Rec.* **2018**, *2672*, 481–492. [CrossRef]
16. Wang, W.; Liu, S.; Wang, Q.; Yuan, W.; Chen, M.; Hao, X.; Ma, S.; Liang, X. The Impact of Traffic-Induced Bridge Vibration on Rapid Repairing High-Performance Concrete for Bridge Deck Pavement Repairs. *Adv. Mater. Sci. Eng.* **2014**, *2672*, 481–492. [CrossRef]
17. Li, Y.; Li, S.; Lv, R.; Zhang, P.; Xu, Y.; Hou, G.; Cui, C. Research on failure mode and mechanism of different types of waterproof adhesive materials for bridge deck. *Int. J. Pavement Eng.* **2015**, *16*, 602–608. [CrossRef]
18. Liu, Y.; Wu, J.; Chen, J. Mechanical properties of a waterproofing adhesive layer used on concrete bridges under heavy traffic and temperature loading. *Int. J. Adhes. Adhes.* **2014**, *48*, 102–109. [CrossRef]
19. Sheng, Y.; Wang, Q.; Li, H. Theoretical Analysis of Extreme Temperatures and Thermal Stresses in Bridge Deck Pavements. *Int. J. Pavement Res. Technol.* **2011**, *4*, 238–243.
20. He, D.; Xiong, X.; Dong, Q. Typical Structure of Bridge Deck Asphalt Pavement of Cement Concrete Bridge. *J. Chongqing Jiaotong Univ. (Nat. Sci.)* **2011**, *30*, 27–30, 73.
21. Jia, J. Research on Shearing Resistance of Asphalt Pavement and Bridge Deck Pavement. Ph.D. Thesis, Chang'an University, Chang'an, China, 2011.
22. Ren, W.; Han, S.; Li, J.; Chen, D. Application of Chip-Springkling Technology to Concrete Bridge Asphalt Pavement Structure. *J. Build. Mater.* **2017**, *20*, 222–228. [CrossRef]
23. Xu, O.; Han, S.; Yu, J. Research on Improvement of Structural Stability for Concrete Bridge Deck Pavement. *J. Wuhan Univ. Technol.* **2010**, *32*, 22–24, 69.
24. Liu, H.; Li, Y.; Zhang, Q.; Hao, P. Deformation characteristic and mechanism of blisters in cement concrete bridge deck pavement. *Constr. Mater.* **2018**, *172*, 358–369. [CrossRef]
25. Lee, B.J.; Kim, Y.Y. Durability of Latex Modified Concrete Mixed with a Shrinkage Reducing Agent for Bridge Deck Pavement. *Int. J. Struct. Mater.* **2018**, *12*, 23. [CrossRef]
26. Ministry of Transport of the People's Republic of China. *Standard Test Methods of Bitumen and Bituminous Mixtures for Highway Engineering: JTG E20-2011*; Ministry of Transport of the People's Republic of China: Beijing, China, 2011.
27. Ministry of Transport of the People's Republic of China. *Technical Specification for Construction of Highway Asphalt Pavement: JTG F40-2017*; Ministry of Transport of the People's Republic of China: Beijing, China, 2017.
28. Ministry of Transport of the People's Republic of China. *Technique Guidelines for Construction of Highway Cement Concrete Pavement: JTG/T F30-2014*; Ministry of Transport of the People's Republic of China: Beijing, China, 2014.
29. Ministry of Transport of the People's Republic of China. *Field Test Methods of Subgrade and Pavement for Highway Engineering: JTG E60-2008*; Ministry of Transport of the People's Republic of China: Beijing, China, 2008.

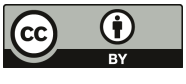

materials

MDPI

Article

Assessment for Sustainable Use of Quarry Fines as Pavement Construction Materials: Part I—Description of Basic Quarry Fine Properties

Yinning Zhang *, Leena Katariina Korkiala-Tanttu, Henry Gustavsson and Amandine Miksic

Department of Civil Engineering, Aalto University, 00076 Aalto, Finland; leena.korkiala-tanttu@aalto.fi (L.K-T.); henry.gustavsson@aalto.fi (H.G.); amandine.miksic@aalto.fi (A.M.)
* Correspondence: yinning.zhang@aalto.fi

Received: 5 March 2019; Accepted: 10 April 2019; Published: 12 April 2019

Abstract: As a secondary material, quarry fines are a valuable material to be reused for many purposes in civil engineering projects. The aggregate source depletion, especially the lack of high quality aggregates as expected in the future, as well as the demand for a carbon-neutral society and circular economy, also promotes the high-volume utilization of secondary materials such as quarry fines. The aim of this study is to do a feasibility assessment including a series of laboratory tests and analyses to evaluate the properties of quarry fine materials to determine if this type of material could be qualified as pavement construction material in high volume. The gradation information obtained from both sieving and hydrometer tests indicates the frost susceptibility of unstabilized quarry fines, therefore frost heave tests were performed and which further suggest the necessity of stabilization to improve its properties for pavement applications, especially in structural layers such as base, subbase, or filter layers. Some other general information and properties of unbound quarry fines, especially regarding their validity for application in pavement engineering are also investigated and discussed.

Keywords: sustainable; secondary materials; quarry waste; frost susceptibility

1. Introduction

One big challenge in road engineering is the economic and ecological use of soil and aggregate materials. The design of pavement layers in Finland is mainly based on empirical methods, which are presented as tabulated model structures [1]. This has led to a situation where high quality virgin aggregates have been used in excess and the use of secondary materials has been challenging [2]. Finland, in proportion to its population, is one of biggest user of aggregates inside the European Union. Annually, 80–100 million tons of aggregates are used in Finland [3]. The conditions of cold climate and long distances caused by the relatively low density of population both increase the need to use a lot of aggregates [4]. Road and street construction consumes about 50 million tons of non-renewable aggregates and the amount of CO_2 emissions caused is 0.8 million tons annually [5]. Besides, in Europe the built environment is responsible for 40% of greenhouse gases emission, 50% of resource extraction, and 30%–45% of waste production [6]. According to Ehrukainen, the application of secondary or recycled materials was only 1% of the total use of aggregates [7]. Of the total consumption of aggregates, around 10% is used to produce concrete and 10% to produce asphalt concrete [4]. Therefore, it is of vital importance to significantly increase the utilization of "waste" materials.

Finland has a good source of natural rock for aggregate production, thus the motivation to use recycled material has been low in the past. Now, with the increase in the price of natural aggregates as well as the increased level of consciousness regarding environmental preservation and the promotion of a circular economy, strategies and targets have been proposed and are now enforced. The European Commission set four waste directives in 2018 [8]. The focus of the directives is to decrease the amount

of waste, to increase recycling, and to diminish the need for landfills. A more solid aim is to increase the recycling, reuse, and other utilization of building and demolition waste up to 70% in weight by 2020 [9]. The United Nations Agenda for Sustainable Development, called Agenda 2030, also sets targets towards carbon-neutral societies by 2030 [10]. Finland has committed itself to taking action in regards to this agenda, including the aim to promote carbon-neutrality and the wise use of resources [11]. Many big cities, e.g., Helsinki, Espoo, Vantaa, Tampere, and Turku have defined their own targets for carbon neutrality and a circular economy. For example, the city of Helsinki has set a target to be carbon-neutral by 2035 [12]. These targets also require a much higher level of circular economy and promote the use of secondary materials. In summary, the reduction in natural resources and increasing consciousness regarding environment preservation have led to the established trend of utilizing secondary materials at higher levels in the near future, which is also the motivation of this study.

2. Literature Review

According to United States Environmental Protection Agency (EPA), non-hazardous secondary materials refers to any materials that are not the primary product of manufacturing or commercial processes but are the byproducts of such processes, including post-consumer material, post-industrial material, and scrap [13]. The European Commission also defines the waste that can be recycled and injected back into the economy as secondary raw materials [14]. On one hand, these materials may be considered as waste which needs to be treated and disposed of. On the other hand, many of them can have material or British Thermal Unit (BTU) value, with the possibility of being reused and managed for other industrial purposes with little or no harm to the environment.

Quarry waste is one such type of secondary material that unavoidably comes from the overburden, interburden, and extraction and processing of aggregates and includes quarry fines from processing activities [15]. As a general concept, quarry waste actually consists of different material types known as “quarry fines”, “quarry dust”, “stone byproducts”, “recycled aggregates”, “quarry powder wastes”, and so forth [16]. Quarry fines have become a real problem in the quarry industry because of two main reasons. Firstly, the higher the fraction of fines contained in the material, the more easily the material can be dislocated by gravity, wind, and water, and the more difficult the material is to handle, store, and dispose of. Very fine crusher dust can be generated during crushing and screening processes and is easily dispersed into the atmosphere, contaminating the air. Secondly, the recent tax policy has promoted the possible utilization or management of large stockpiles of quarry fines to minimize the adverse social and environmental effects caused by this material, but effective high-volume applications are underdeveloped. Moreover, many places around the world will be facing problems of reduced rock resources in the future, which will result in an inadequate production of aggregates and an increase in high quality aggregate prices. Quarry fines could provide alternatives to alleviate the problem of aggregate shortages in the civil engineering industry. Consequently, methods of utilization of quarry fines are in demand, regardless of the quarry sources.

Table 1 presents a substantial amount of under-utilized quarry fines produced and accumulated at Lemminkäinen Infra Oy in Finland over the recent years. Besides Lemminkäinen Infra Oy, there are some other aggregate producers. For example, Destia Oy had a total of 194 000 tons of quarry fines around Finland in 2015 [17]. These numbers indicate a clear potential for economic and environmental benefits from the appropriate utilization and application of this material.

Table 1. The amount of quarry fines at Lemminkäinen Infra Oy [18].

Grain Size (mm)	2016 (tons)	2017 (tons)	Accumulation/Year (tons)	Accumulation since 2017 (%)
0/3	824,300	875,800	51,500	5.9
0/6	118,000	127,300	9,300	7.3
In total	942,300	1,003,100	60,800	6.1

Similarly to other granular unbound materials, one possible way of utilizing this type of quarry waste material is for landfill or pavement constructions. In Europe, the project "Alternative materials in road construction (ALT-MAT)" undertaken from 1998 to 1999 has been focused on utilizing different types of secondary/alternative materials for pavement base/subbase layers [19]. Many of the investigated secondary materials, including municipal solid waste incinerator (MSWI) bottom ashes and all types of slags, are fine-grained unbound materials that have shown positive results (both mechanically and environmentally) as pavement base/subbase materials. However, even though previous research has proven that there is a promising future for applications using many of the secondary materials in road construction, the research into quarry fines, and especially Finnish quarry fines, is still inadequate and many detailed aspects require further study. These aspects include physical and mechanical properties, durability evaluation, leaching properties, quarry fine applications in high volume, and so forth.

Since 2007, there has been an increase in research focusing on utilizing quarry waste as a construction material in the field of civil engineering. It has been implemented to fabricate artificial aggregates [20], hemp concrete [21], and mortars. In general, quarry fine materials have been found to be effective in improving the properties of conventional civil engineering materials, which has also been the most common application of this material in previous research. Quarry fines have been proven to be effective in mitigating the early decreasing of strength due to fly ash application [22]. It was also found that the partial replacement of cement by granite quarry dust is beneficial in several aspects including good durable behavior, less drying shrinkage and expansion, lower possibility of early-age cracking, while keeping strength properties comparable [23]. When used as stabilizer, quarry waste could improve the properties of soils in terms of better workability, a decrease in optimal water content and an increase in maximum dry unit weight [24,25], better swell and shrinkage properties for expansive soil [26], and satisfactory durability under freeze-thaw cycles [27]. Quarry fines were also employed as an addition to natural soils to improve properties such as grading and compaction characteristics, strength, and to reduce swelling and plasticity [24]. For flexible pavements, quarry fines have been utilized to improve physical, mechanical, and swelling properties of soil subgrade and subbase [28].

Extended research attempts have been made to utilize quarry waste in constructions for both non-bearing [21,29] and structural purposes [20,22,23,29–31]. Non-bearing blocks made of quarry waste and other additives are common for wall partitions and decorations. In addition, the most common application area of quarry fines in Finland today is as the uppermost unbound layer of yards, fields, and low-volume streets [17]. For structural purposes, there are mainly three types of effective applications utilizing quarry waste. One is to use quarry waste as a substitute for sands/filler in different percentages in concrete [22,30,32,33], and the other is to replace part of cement by the quarry waste to produce concrete [22], or even employ quarry waste as an additive to improve soil properties [23–27]. In other words, it is common to employ quarry waste as an alternative material to reduce the dosage of other materials (more expensive, more in demand, or less environmentally friendly) or as an additive, rather than using quarry waste as a major construction material. In fact, most of the previous research applies less than 50% quarry waste [19–21,23–27], and the majority applies 5% to 30% as aggregates/fillers to develop different types of concrete. This might be related to the high requirements for quality and the mechanical properties of concrete materials for adequate structural performance. Especially

when applied to asphalt concrete for pavement constructions, quarry waste is only recommended by researchers for low-to-moderate volume traffic [32,34]. Another key point that can be summarized from current research is the inadequate durability evaluation of quarry-waste-based construction materials. There is only limited research conducted into durability evaluations of quarry-waste-based materials, and some of these have shown a reduction in durability with the incorporation of quarry waste [30]. However, a qualified pavement construction material should have enough durability in moist environments and also adequate frost-resistance for its application in cold regions. It should also be noted that the applications of the secondary quarry fine materials in ground water area would need permissions from the environment agencies in Finland, especially where active use of ground water is needed.

In this study, a comprehensive assessment including a series of laboratory tests and analyses was conducted to evaluate the properties of quarry fine materials, which have not been well-established in the past. Even though quarry fines have shown very promising results as an alternative or additive material in previous research, its properties as a pavement construction material are not clear. Unlike most previous studies, which apply quarry wastes only in a limited amount, the main purpose of this study was to determine if this type of byproduct could be qualified as a pavement base, subbase, or any other construction material, and explore a way to utilize it in high volumes. The benefits of utilizing this byproduct in high volumes include reducing the carbon footprint and promoting a circular economy, considering it can be easily found and obtained at most quarry sites. In addition, another inadequate aspect of previous research, the evaluation of the durability of quarry fines, was investigated here in term of a frost-susceptibility test to verify the suitability of this material for applications in cold regions. Some basic information and properties of unbound quarry fines, especially regarding their validity for application in pavement engineering were investigated and discussed here as a preliminary study and foundation to further research.

3. Material Sampling and Preparation

In general, adopting a proper sampling method using a specified apparatus helps avoid biased sampling and provides reliable test results. To obtain representative samples of the average properties of a batch at plants, the European standard SFS-EN 932-1 "Tests for general properties of aggregates. Part 1: Methods for sampling" has been followed for material sampling [35]. It should be noted that even though sampling from the stationary conveyor belt or from the stream of material is recommended, in practice, the quarry fines were only available from stockpiles at the plants when the authors collected them. However, to avoid segregation-caused biased results, sampling increments were randomly selected from as many parts of the batch as possible, and an adequate number of sampling increments was used to reduce the influence of the heterogeneity of the batch.

In total, around 100 kg of quarry fines with a 0–4 mm particle size were collected from the Koskenkylä quarry of Destia Oy, packaged into 10-kg capacity buckets, and directly transferred back to the laboratory for storage. The collected quarry fines are from high quality granite host rock according to CE marking, with major mineral compositions of plagioclase (50.4%) and quartz (39.6%). Reduction of a bulk sample by a riffle box or by the quartering method, as recommended in the standard, was conducted to obtain the amount of materials required for further research purposes. The reduced batches were heated in oven at (110 ± 5) °C to remove excess moisture and obtain a constant mass following the European standard SFS-EN 1097-5 "Tests for mechanical and physical properties of aggregates. Part 5: Determination of the mater content by drying in a ventilated oven" [36]. This was important to maintain the identical status of all of the batches so that water content can be accurately controlled for any further specimen preparation and testing.

4. Description of Basic Quarry Fine Properties

4.1. Gradation of the Quarry Fines

The particle size distribution of the quarry fines with a 0–4mm grain size was obtained according to European standard SFS-EN 933-1 "Tests for geometrical properties of aggregates. Part 1: Determination of particle size distribution. Sieving method" [37]. The wet sieving method is necessary for naturally agglomerated materials or materials containing a large amount of fine fractions because fine fractions with static charges are more prone to clumping. Washing breaks down the agglomerations and also helps the separation of fines from coarse fractions [38], which improves the results of particle distribution from the successive sieving process.

4.1.1. Wet Sieving Method

A trial test using the wet sieving method was conducted to determine the fine contents of the quarry fines. It showed that the fine content of quarry fines reaches as high as 12.5%. According to the trial test results, it was decided that the wet sieving method and a hydrometer test are necessary for the quarry fines in order to get reliable results due to the large amount of fine fractions (<0.063 mm). Figure 1 presents the gradation curve of quarry fines with a 0–4 mm particle size obtained from both the wet and dry sieving methods, together with the limits for pavement base, subbase, and filter layers required by Finnish and European standards (Tables S1 and S2). The gradation curve of quarry fine materials as obtained from wet and dry sieving methods shows differences in finer grains but the difference appears to have no significant effects regarding the qualification for base/subbase/filter layer requirements. It was found that the quarry fines are not qualified for pavement base materials according to the gradation information only, whereas around half of the gradation curve stay inside the limits for subbase [39]. However, because of the gradation curve that sits on the lower limit of subbase requirements, it is hard to validate quarry fines for either base or subbase from the gradation information only, and thus a mechanical test to determine the strength of quarry fines will be planned and performed in the future. As a filter layer, the material can be qualified completely since the gradation curve sits inside the limits, stays only at one side of the c limit, and also satisfies the requirement $D_{15}/\ d_{85} < 5$ [39].

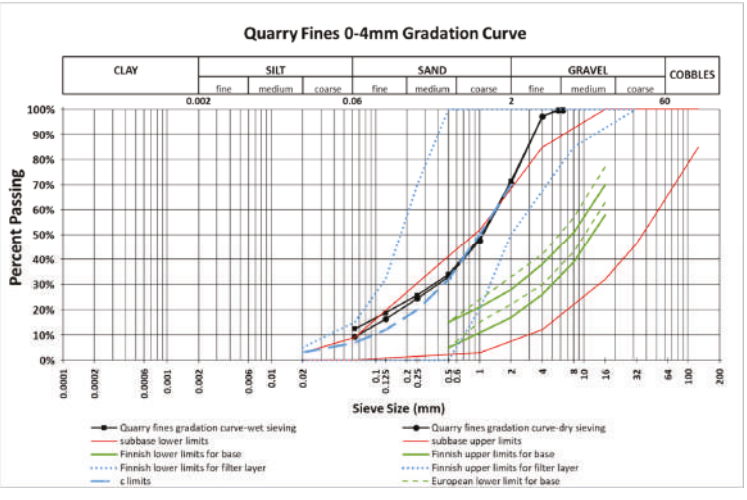

Figure 1. Gradation curves of quarry fines with a 0–4 mm particle size and the limits for pavement base, subbase, and filter layers according to Finnish and European requirements.

D_{15} is a grain size equivalent to 15 percent of the permeation of granular material (insulating layer material); d_{85} is the grain size of the finer material (bottom), having a permeation percentage of 85.

The coefficient of uniformity (C_u) and the coefficient of gradation (C_c) are calculated by Equations (1) and (2) to evaluate the grade of quarry fines. The classifications as listed in the European standard SFS-EN ISO 14688-2:2018 "Geotechnical investigation and testing" [40]. Identification and classification of soil. Part 2: Principles for a classification" were followed to categorize the grading of quarry fines used in this study.

$$C_u = \frac{D_{60}}{D_{10}} \quad (1)$$

$$C_c = \frac{(D_{30})^2}{D_{10} \times D_{60}} \quad (2)$$

For well-graded sand, $C_u > 15$ and $1 \leq C_c \leq 3$.

The coefficient of uniformity (C_u) and the coefficient of gradation (C_c) were determined to be 28.8 and 2.2, respectively. Therefore, the quarry fines can be classified as well-graded materials. The same classification is also valid according to the Unified Soil Classification System. From the 0.45 power maximum density graph shown in Figure 2, it can be observed that the quarry fines have the gradation characteristics of both fine- and dense-graded material, with the fine-graded characteristic being dominant. This characteristic is better captured when a wet sieving method is applied.

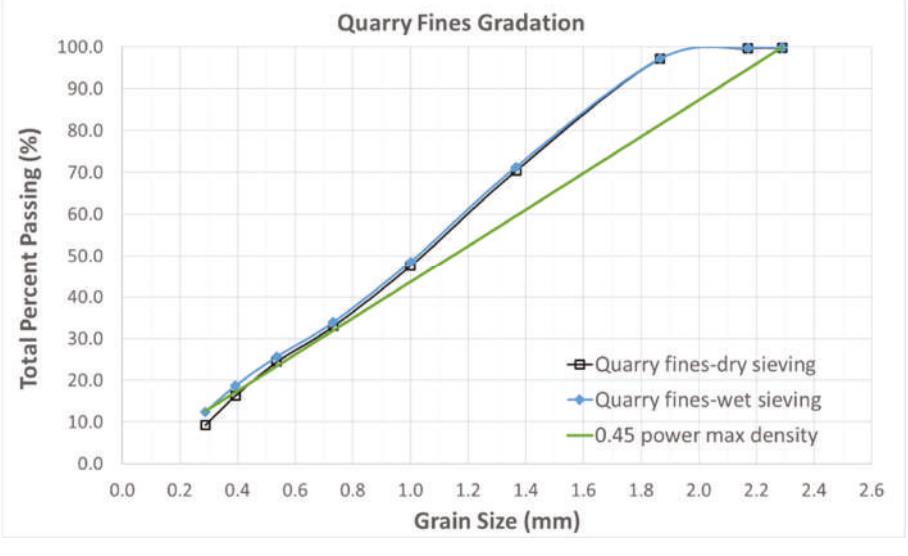

Figure 2. 0.45 power maximum density graph for quarry fines.

4.1.2. Hydrometer Method

The particle size distribution of the fine fraction significantly influences the frost susceptibility of granular materials, which can be determined by hydrometer test. A quarry fine sample containing only fine fraction (finer than 0.063 mm) was obtained by sieving the 0–4 mm quarry fine material mechanically and was tested for gradation with the hydrometer test. This method is based on the phenomenon of particles of different sizes settling by gravitation in a liquid at different rates, as well as Strokes' law, which establishes a relationship between the terminal velocity of a particle and other parameters of the fluid and material properties. The European standard SFS-EN ISO 17892-4: 2016 "Geotechnical investigation and testing" [41]. Laboratory testing of soil. Part 4: Determination of

particle size distribution" was followed to perform the hydrometer test on quarry fine samples. Two samples were tested and the average was used for data analysis (Table S3).

Figure 3 shows the gradation curve of quarry fines provided by the quarry plant, the gradation curve obtained from combining the results from wet sieving and the hydrometer tests, as well as the four regions defining different potentials of frost susceptibility for different granular materials. This chart is typically used to estimate the frost susceptibility of materials according to their gradation curves, based on the criterion proposed by the ISSMGE Technical Committee on Frost, which is also the guide for the Finnish Road Administration [42]. If the gradation curve stays within region 1 only, this material can be seen as frost susceptible, but in region 1L the susceptibility is low. Gradation curves falling completely in regions 2, 3, or 4 indicate non-frost-susceptibility. However, any curves spanning one region to another in the finer part (left), similar to the gradation curve of quarry fines shown in Figure 3, can be seen as frost susceptible. The highly consistent part of the gradation curves obtained from laboratory tests and provided by the quarry plant Destia, although only available for particles coarser than 0.063mm, have shown the reliability of the gradation information. The completed gradation curve a containing finer particle distribution (<0.063mm) indicates that frost susceptibility tests are greatly necessary for quarry fine materials since untreated frost susceptible material is not appropriate to be applied in base, subbase, or filter layers in pavements. Consequently, an improvement in the quarry fine materials to validate their application in pavement constructions, such as stabilization techniques, are highly recommended.

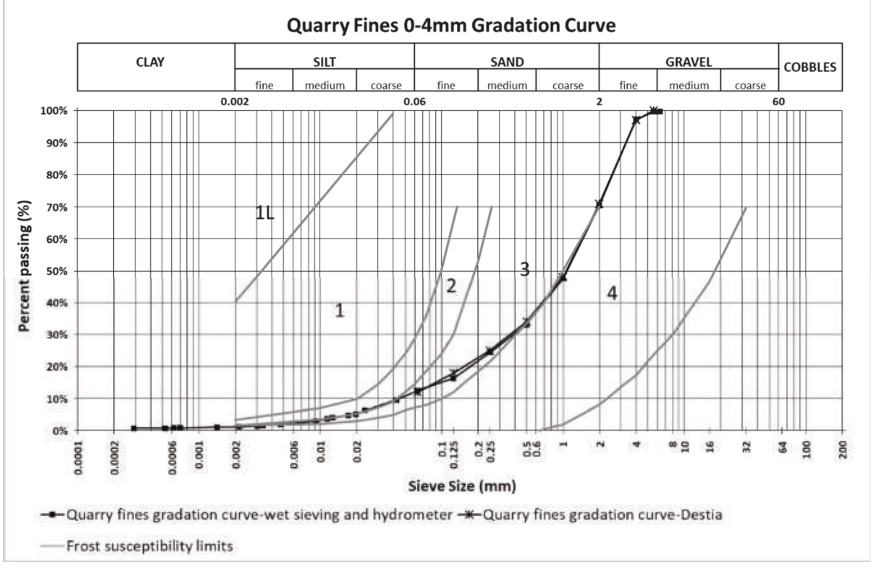

Figure 3. Estimation of frost susceptibility from the gradation curves of quarry fines according to ISSMGE [42]. Adapted with permission from [42]; 2005, Slunga, E., Saarelainen, S.

4.2. Density and Water Content

Granular material properties are closely related to moisture content. When compacted, the particles come together more closely and the dry density increases. The maximum dry density that can be achieved mainly depends on not only the effective compaction work but also the water content of the mixture. For a given degree of compaction work, there is typically an optimum water content at which the dry density reaches a maximum value for the non-free-draining materials. However, for a self-draining mixture, which is defined by the difference in water content before and after

compaction being larger than 0.3%, may not have a well-defined water-density relationship. Therefore, a preliminary evaluation of the quarry fines to determine if they are a self-draining material is the first step to adoption.

The European standard EN 13286-2: 2010 "Unbound and hydraulically bound mixtures. Part 2: Test methods for laboratory reference density and water content—Proctor compaction" [43] was followed to characterize the water-density relationship of quarry fines, as shown in Figure 4. According to the difference between initial and final water content before and after compaction, quarry fines can be categorized as a self-draining material with a maximum difference in water content of 1.6%. It is also interesting to note that such variations in water content due to compaction are also related to the initial water content of the quarry fines. If more water is added to achieve a higher initial water content, the mixture is more prone to draining the excess water during compaction and thus the water content difference is larger.

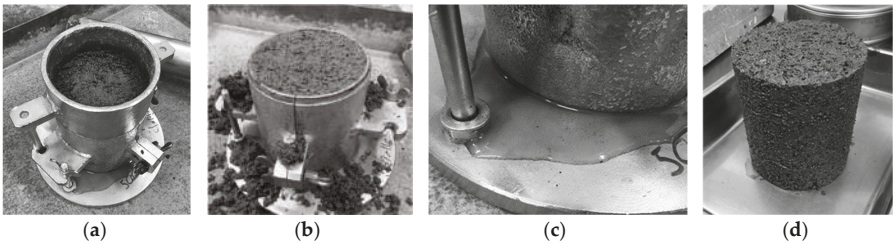

Figure 4. Laboratory reference density and water content by Proctor compaction method: (**a**) Specimen with mold during compactions; (**b**) Compacted quarry fine specimen in mold; (**c**) Self-draining water during the compaction; (**d**) Compacted quarry fine specimen for water content determination.

Figure 5 and Table S4 present the relationship between the final water content and the dry density of the quarry fines. It is found that even though the quarry fines have self-draining properties, a maximum dry density still exists at the optimal water content of 9.3%. The maximum dry density of quarry fines that can be achieved from the Proctor test is 2.04 Mg/m^3, as shown in Figure 5. However, in comparison to the zero air void curve, it can be seen that water content has limited influence on the dry density of quarry fines. All of these findings have shown combined characteristics of both self-draining and fine-graded granular materials and have also indicated the complicated properties of this material.

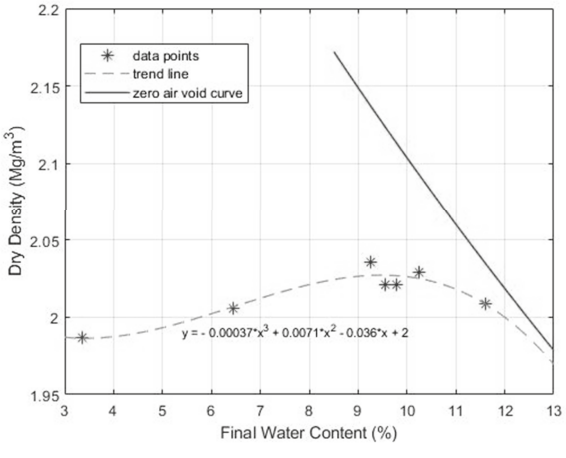

Figure 5. Variation of compacted dry density versus final water content.

4.3. Permeability

Permeability is another dominant property of pavement base and subbase materials in pavement design since excessive moisture inside the pavement structure would bring adverse effects to the performance of the system. Water-related deteriorations in highway pavements have been commonly and widely observed in the past decades, and the inadequate drainage of base and subbase layers is one of the contributors. The permeability of quarry fine material, however, has not been well established in the past. The determination of the permeability of the quarry fine specimens is very necessary and could be used as a baseline to validate the application of this material as pavement base, subbase, or even other applications.

Laboratory tests were conducted on unbound quarry fine specimens compacted at the optimum water content as determined by Proctor method. The falling head method provided by the Finnish Road and Water Engineering Board, which is suitable for fine-grained materials with intermediate-to-low permeability, was followed [44]. Whether the flow behavior of quarry fine specimens during the falling head test complies with Darcy's Law based on laminar flow is the first key question that needed to be answered, considering that Darcy's Law is adopted for permeability calculations in this method. To do so, a graph of change of head versus time was plotted to determine the linear part of the curve (if any) indicating the validity of Darcy's law (Table S5 and Figure 6).

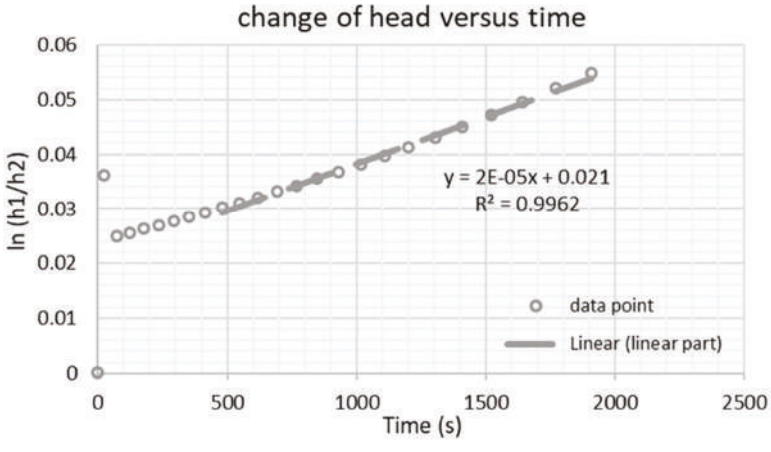

Figure 6. Change of head versus time during falling head permeability test.

As indicated in Figure 6, not all the data points obtained from the falling head permeability test are appropriate to be used for calculating permeability based on Darcy's law. The non-linear hydraulic gradient–velocity relationship at the beginning of the test shows that during this period, Darcy's law is not applicable. Therefore, only data from the successive time period (around 500 s from the beginning till the end) was adopted for data analysis. Figure 7 shows the permeability results of the unbound quarry fine specimen from a series of successive repeated tests. The coefficient of permeability of the quarry fine specimen increases slightly and then levels off in the sixth repeated test, at 5.75×10^{-5} m/s. According to Federal Highway Administration (FHWA) guidelines, this coefficient of permeability for quarry fines with a 0–4 mm particle size is still far below the requirements for a drainage aggregate base, which should have a minimum permeability of 500 ft/day (1.75×10^{-3} m/s). Instead, it is comparable to the typical coefficient of permeability of fine gravel, coarse and medium sand, and dense-graded aggregate base (4.2×10^{-5} to 1.43×10^{-4} m/s) [45] and is slightly higher than many of the reported situations from experiments or in the field nowadays [46,47]. Generally, based on the laboratory-determined permeability properties of quarry fines and the literature data, it was found that the permeability of quarry fine specimens falls within the typical permeability ranges of commonly

adopted conventional pavement base and subbase materials, thus it can be validated for associated applications from the view of permeability. Since there are hardly any permeability requirements for the filter layer, the validity of quarry fines as filter layer material from permeability aspect is not possible. However, considering the major function of filter layers is to prevent fines immigration and frost actions in cold regions, lower permeability is desirable and a higher degree of compaction is consequently recommended for this purpose.

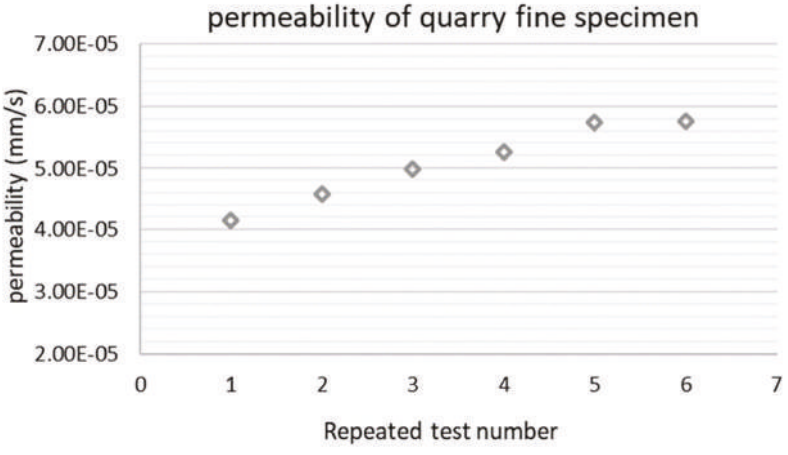

Figure 7. Permeability results of the unbound quarry fine specimen.

4.4. Capillary Rise

In capillary theory, frost heave is closely related to the rate of temperature decrease, pore sizes between particles, and the hydraulic conductivity of the unfrozen part of the material [48]. If the material can easily draw water up to the frozen zone by capillary actions and also has a high hydraulic conductivity which facilitates the delivery of a large quantity of water, large ice lenses are able to form and it is possible that the material is frost-susceptible. Therefore, to better understand the frost susceptibility of quarry fine material, capillary rise test according to Finnish test method provided by the Road and Water Engineering Board was performed [44]. It was found that the capillary rise values for virgin quarry fine samples are in range of 0.70 to 0.85 m, with an average of 0.804 m, based on four repeated laboratory tests. This capillary rise value is just in accordance with the limitation set by the Finnish railway department regarding frost susceptibility, indicating that the virgin quarry fines is possibly frost-susceptible and improvements are necessary. The capillary rise test results are consistent with the gradation information and further verified the necessity for stabilization.

4.5. Frost Heave

According to the lab-determined gradation information as well as existing information on frost susceptibility (Figure 3), the quarry fines with a 0–4 mm particle size might be frost-susceptible. It was therefore necessary to investigate frost susceptibility with a frost heave test.

The frost heave test method description TPPT-R07 by VTT communities and infrastructure [49] was followed to test unbound quarry fines. Specimens of 100 mm diameter and 100 mm height were compacted at the optimal water content using the Proctor method to reach maximum dry density. The specimen, together with its mold, is then kept frozen overnight for conditioning. The extruded frozen specimen was then placed with filter paper and a stone on the bottom of the test cell (Figure 8), covered with a rubber membrane and the top cap. The rubber membrane was fixed to the cap and the bottom of the test cell with O-rings, similar to the procedures in a triaxial test. After applying a thin layer of

silicone to the surface of the membrane, the insulated split barrels were greased to the specimen and membrane. External support rings were then tightened to ensure the supporting of insulated barrels. Finally, the displacement transducers and the loading frame were attached to the cap of the test cell.

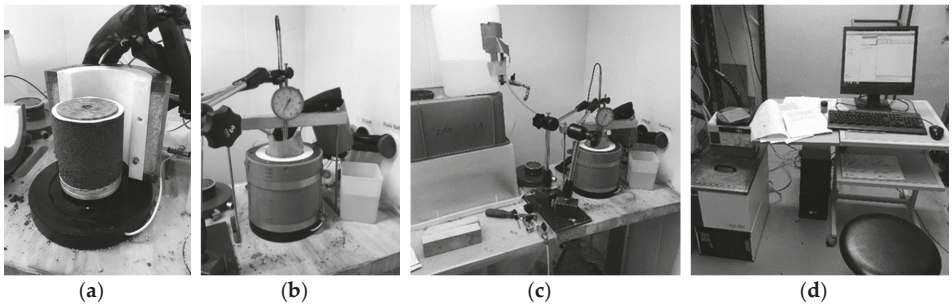

(**a**) (**b**) (**c**) (**d**)

Figure 8. Frost heave test on quarry fine specimen: (**a**) Frozen quarry fine specimen mounted on the test apparatus; (**b**) Assembled specimen; (**c**) Assembled specimen with water supply; (**d**) Computer and temperature control system).

A series of frost heave tests, including three individual frost heave tests and intermediate thawing processes of different surfacing loading conditions, were performed on the specimen. The conditions adopted in the frost heave and thawing processes are listed in Table 2. Since there are six temperature sensors embedded in the insulated barrels at different depths and two on each of the top cap and the bottom of the test cell, the temperature profile throughout the specimen could be recorded during the test, and the 0 °C isotherm (assumed as the freezing front) could be calculated by interpolation. Water intake from the bottom filter stone was allowed during the entire frost heave test to simulate the moisture transfer from ground water in practice.

Table 2. Frost heave and thawing conditions adopted in the test.

Step	Loading Condition	Temperature		Time Period	Water Level of External Water Reservoir
		Top	Bottom		
Preliminary freezing	Unloaded *	−3 °C	+1 °C	24 h	N/A
Thawing and preloading	20 kPa	+3 °C	+3 °C	24 h, or until constant height **	Top level of specimen
Frost heave	unloaded	−3 °C	+1 °C	until zero net frost penetration *** (at least 24 h)	At the middle of specimen height
Intermediate thawing	20 kPa	−0.5 °C	+15 °C	until constant height	At the middle of specimen height
1st frost heave	20 kPa	−3 °C	+1 °C	until zero net frost penetration (at least 24 h)	At the middle of specimen height
Intermediate thawing	40 kPa	−0.5 °C	+15 °C	until constant height	At the middle of specimen height
2nd frost heave	40 kPa	−3 °C	+1 °C	until zero net frost penetration (at least 24 h)	At the middle of specimen height

Notes: Unloaded * means the specimen is loaded by the frame only (3.5 kPa); Constant height ** means the height of the specimen is unchanged for more than four hours; Net frost penetration *** is the frost penetration minus frost heave, for more than four hours.

Figure 8 shows the quarry fine specimen and frost heave test apparatus as applied in this study. Figure 9 presents the total heave, depth of frost front during the test, and some frost susceptibility

parameters and indicators of quarry fines as obtained from the test. All these data and results are derived from the first frost heave test with a surface loading of 3.5 kPa (Table S6).

There are several parameters and frost susceptibility indicators that can be derived from the frost heave test, as shown in Figure 9:

- h is the frost heave, or the change in height of the specimen during the test, in mm;
- z is the depth of frost penetration, which is the sum of the initial height and the frost heave minus the height of the unfrozen part of the specimen, in mm;
- h/z is the frost heave ratio, which is an indicator of the relative percentage of frost heaving from the depth of frost penetration, in %;
- SP is the segregation potential, or frost heave coefficient, which is the ratio between the frost heave rate and the actual temperature gradient over the frozen part of the specimen, in mm^2/Kh.

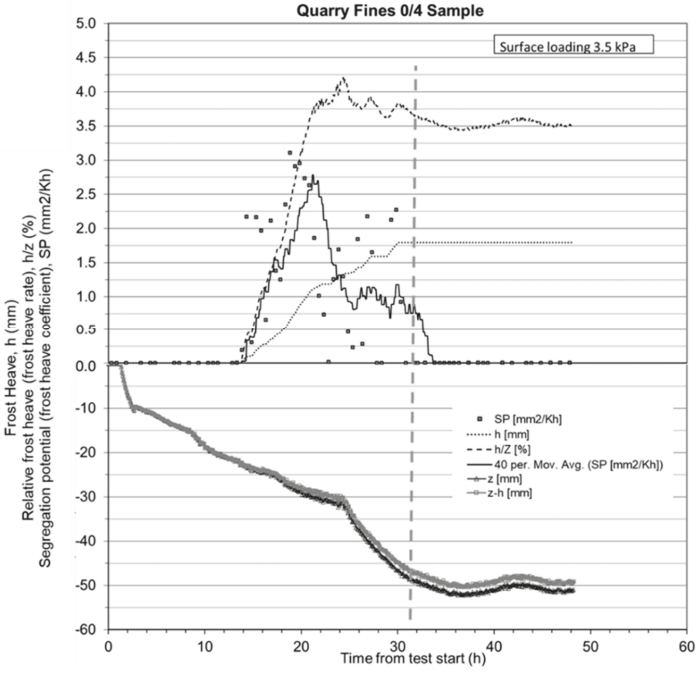

Figure 9. Frost heave parameters of a quarry fines (0–4mm) sample.

As shown in Figure 9, the total frost heave (h) of the quarry fine specimen in the unloaded frost heave period can be divided into three stages. In the very first stage, from the beginning of the test to 13.67 h, there is no obvious frost heave observed, even though the temperature inside the specimen decreased significantly. In the second stage, when the temperature at the very top of specimen dropped to around zero, total heave started to increase strongly with time. During this stage, water inside the specimen froze and expanded against the particles, which resulted in a total height increase in the specimen. Finally, in the last stage when the temperature throughout the specimen reached equilibrium status, the total frost heave leveled off at around 1.79 mm. Accordingly, the depth of frost front (height of the unfrozen part) decreased with the origin at the very bottom of the specimen, or the depth of frost part of the specimen increased as the top plate of the specimen was kept cool by the circulation of cryomat-cooled liquid. The depth of frost penetration remained stable at about 50.0mm from the time when the temperature throughout the whole specimen was stable. The frost heave ratio is also plotted

as *h*/*z* in Figure 9, showing that it increased and finally leveled off at 3.5% during the unloaded frost heave test.

The net depth of frost penetration (*z*–*h*), which is the depth of frost penetration minus frost heave, has the same changing tendency with time as for the depth of frost penetration. This curve is critical in finding out the segregation potential (*SP*) value for this quarry fine material and is used as a reference. The *SP*, however, was found to be a much more scattered data series than the other parameters, but the trend can still be approximated by moving average techniques. The *SP* value can be read from Figure 9 on the predictive moving average curve of the SP data, at the very first point where the net depth of frost penetration becomes stable. In this case, it was found that there was a transition period 30 h after the beginning of test, when the *SP* values suddenly decreased, becoming negligibly small. The *SP* value of quarry fine material in this study, was found to be just within this area. The exact point was obtained by looking for the point on the *z*–*h* curve that has the same *z*–*h* value as the average *z*–*h* value from this point and afterwards. This point was found to be at 32.09 h from the beginning of test, and the corresponding *SP* value at this point is 0.75 on the moving average curve. It should be noted that this SP value is conservative because afterwards the frost heave is stable and the SP value becomes negligible.

The segregation potential of the unbound quarry fines with 0–4 mm particle sizes is then determined to be 0.75. When compared to the frost susceptibility classification in the literature, as listed in Table 3, it appears that the segregation potential values indicats a frost class of low susceptibility. The results from the laboratory capillary test further verify this low potential for frost susceptibility, showing that the capillary rise of the quarry fines with a 0–4 mm particle size is around 70 to 85 mm (Officially the limit is 1.0 meter but nowadays the Finnish agencies are more prone to use stricter requirements). Even though the unbound quarry fine materials is not very frost susceptible, it is still to some extent susceptible to frost actions and thus not safe to be used for pavements as it is, especially in cold regions. In this regard, stabilization techniques are necessary to improve the frost susceptibility of quarry fines and enable its applications in pavement base, subbase, or filter layers.

Table 3. Determination of the frost susceptibility of a soil type [42,50].

Frost Class	Segregation Potential SP (mm^2/Kh)
Negligible	<0.5
Low	0.5–1.5
Medium	1.5–3.0
Strong	>3.0

5. Discussion and Conclusions

The aggregate source depletion, as well as the demand for a carbon-neutral society and circular economy, all promote the high-volume utilization of secondary materials such as quarry fines. In this research, a feasibility assessment including a series of laboratory tests and analyses were conducted to evaluate the properties of quarry fine materials to determine if this type of material could be qualified for pavement base, subbase, or filter layers, especially in high volume applications, as well as to evaluate the durability of quarry fines in term of frost susceptibility. The main conclusions are listed as follows:

- The wet sieving method is more appropriate for determining the gradation curve of quarry fines with a 0–4 mm grain size. Based on gradation information obtained from laboratory sieving and hydrometer tests, the quarry fines used in this study can be classified as well-graded with the gradation characteristics of both fine- and dense-graded material. It also shows that virgin quarry fines can satisfy the requirements for a filter layer but not for a base or subbase, and indicates that quarry fines might be frost susceptible.

- The virgin quarry fines showed self-draining properties. Nevertheless, a maximum dry density exists at the optimal water content of 9.3%, even though only a very limited influence of water content can be observed on the dry density.
- The coefficient of permeability of unstabilized quarry fine specimen was around 5.75×10-5 m/s as determined by the falling head method. This value falls within the typical permeability ranges of commonly adopted conventional pavement base and subbase materials and can be validated for application in base, subbase, and other layers from the view of permeability. To be validated for filter layers, a higher degree of compaction is desirable to prevent fines immigration and frost actions in cold regions.
- According to the frost heave test results, it was found that the changing of total frost heave is closely related to the temperature and depth of frost penetration throughout the specimen.
- The quarry fine specimen in the unloaded frost heave test can be classified into the low frost-susceptibility class according to the segregation potential values. In addition, gradation information and capillary rise test results have all verified this finding. As a result, it is concluded that the unstabilized quarry fines should be classified as frost-susceptible to ensure sound and reliable design and good performance in the long-run. To improve the frost-susceptible properties of quarry fines, stabilization techniques are necessary to qualify their application as pavement construction materials. Further research is undergoing and will be presented in the future.

Supplementary Materials: The following are available online at http://www.mdpi.com/1996-1944/12/8/1209/s1, supplementary materials.docx. Table S1: Particle size distribution of quarry fines by sieving method, Table S2: Gradation limits for different layers, Table S3: Hydrometer test results of particle size distribution (0–0.063 mm), Table S4: Dry density versus final water content from Proctor test, Table S5: Permeability test results, Table S6: Frost heave test results.

Author Contributions: Conceptualization, L.K-T.; Methodology, Y.Z., H.G., and A.M.; Software, Y.Z.; Validation, Y.Z., H.G. and L.K-T.; Formal Analysis, Y.Z., H.G.; Investigation, Y.Z.; Resources, L.K-T.; Data Curation, Y.Z., L.K-T.; Writing—Original Draft Preparation, Y.Z.; Writing—Review and Editing, L.K-T., H.G. and A.M.; Visualization, Y.Z., L.K-T.; Supervision, L.K-T.; Project Administration, L.K-T.; Funding Acquisition, L.K-T.

Funding: This research received no external funding.

Acknowledgments: This research was supported by the School of Engineering, Aalto University, for financing the researchers, and Destia Ltd. for providing the raw materials. We would like to present our gratitude to our colleagues Hakala Veli-Antti, Peltonen Petri, Nikiforow Heli, Makowska Michalina, Eloranta Pekka, and Borén Mari from Destia Oy, who provided expertise that greatly assisted the research.

Conflicts of Interest: The authors declare no conflict of interest. The funders had no role in the design of the study, the collection, analysis, or interpretation of data, the writing of the manuscript, or in the decision to publish the results.

References

1. Finnish Road Administration. *Tierakenteen Suunnittelu*; Edita Prima Oy: Helsinki, Finland, 2004; p. 69. ISBN 951-803-403-6.
2. Kolisoja, P. Resilient Deformation Characteristics of Granular Materials. Ph.D. Thesis, Tampere University of Technology, Tampere, Finland, 1997.
3. Betoni. Kiviaines. Available online: https://betoni.com/tietoa-betonista/perustietopaketti/betoni-rakennusmateriaalina/kiviaines/ (accessed on 7 December 2018).
4. Hernesniemi, H.; Berg-Andersson, B.; Rantala, O. *Kalliosta Kullaksi—Kummusta Klusteriksi*; Elinkeinoelämän tutkimuslaitos. ETLA, Taloustieto: Helsinki, Finland, 2011; p. 241. ISBN 978-951-628-527-9.
5. Korkiala-Tanttu, L.; Tenhunen, J.; Eskola, P.; Häkkinen, T.; Hiltunen, M.-R.; Tuominen, A. *Environmental Values and Ecoindicators of the Infra Construction*; Finnra Reports; Finnish Road Administration: Helsinki, Finland, 2006; p. 53. ISBN 951-803-713-2.
6. Henrotay, C. Buildings as Materials Bank. In Proceedings of the Rakentamisen kiertotalouden ajankohtaispäivät, Helsinki, Finland, 7–8 November 2018.

7. Ehrukainen, E. Kiviainesten kestävä kierrätys ja käyttö. Available online: http://www.uusiomaarakentaminen.fi/sites/default/files/Kiviainesten%20kest%C3%A4v%C3%A4%20kierr%C3%A4tys%20ja%20k%C3%A4ytt%C3%B6%20%E2%80%93%20Eija%20Ehrukainen_0.pdf (accessed on 7 December 2018).
8. Levinen, R. Jätedirectiivin rakennusalaa koskevat muutokset, The changes for building industry caused by the waste directive. In Proceedings of the Rakentamisen kiertotalouden ajankohtaispäivät, Helsinki, Finland, 7–8 November 2018.
9. European Commission. Directive (EU) 2018/851 of the European Parliament and of the Council of 30 May 2018 Amending Directive 2008/98/EC on Waste (Text with EEA Relevance). 2018. Available online: https://eur-lex.europa.eu/eli/dir/2018/851/oj (accessed on 6 February 2019).
10. United Nations. The Sustainable Development Agenda. 2018. Available online: https://www.un.org/sustainabledevelopment/development-agenda/ (accessed on 7 December 2018).
11. Prime Minister's Office. *Government Report on the 2030 Agenda for Sustainable Development. Sustainable Development in Finland—Long-Term, Coherent and Inclusive Action*; Prime Minister's Office: Helsinki, Finland, 2017; p. 57. ISBN 978-952-287-392-7.
12. Major of Helsinki. Hiilineutraali Helsinki 2035- Toimenpideohjelma. Available online: https://www.hel.fi/static/liitteet/kaupunkiymparisto/julkaisut/julkaisut/HNH-2035-toimenpideohjelma.pdf (accessed on 7 December 2018).
13. EPA. Identification of Non-Hazardous Secondary Materials That Are Solid Waste. Available online: https://www.epa.gov/rcra/identification-non-hazardous-secondary-materials-are-solid-waste (accessed on 8 July 2018).
14. European Commission. Raw Materials. Available online: http://ec.europa.eu/environment/green-growth/raw-materials/index_en.htm (accessed on 8 July 2018).
15. Mitchell, C. Quarry Fines and Waste. Available online: https://www.bgs.ac.uk/downloads/start.cfm?id=1449 (accessed on 8 July 2018).
16. Galetakis, M.; Soultana, A. A review on the utilisation of quarry and ornamental stone industry fine by-products in the construction sector. *Constr. Build. Mater.* **2016**, *102*, 769–781. [CrossRef]
17. Pitkänen, I.-J. Selvitys Destia Oy:n kivituhkamääristä ja kivituhkan nykyisistä ja uusista käyttömahdollisuuksista. Bachelor's Thesis, Savonia University of Applied Science, Kuopio, Finland, 2015.
18. Melander, M. Kivituhkan soveltuminen sidotun kantavan kerroksen runkoaineeksi. Master's Thesis, Aalto University, Espoo, Finland, 2018.
19. Reid, J.M.; Evans, R.D.; Holnsteiner, R.; Wimmer, B.; Gaggl, W.; Berg, F.; Pihl, K.A.; Milvang-Jensen, O.; Hjelmar, O.; Rathmeyer, H.; et al. *ALT-MAT: Alternative Materials in Road Construction*. The European Commission under the Transport RTD Programme of the 4th Framework Programme. 2001, p. 190. Available online: https://trimis.ec.europa.eu/sites/default/files/project/documents/20040909_172706_52558_alt-mat.pdf. (accessed on 7 December 2018).
20. Thomas, J.; Harilal, B. Mechanical properties of cold bonded quarry dust aggregate concrete subjected to elevated temperature. *Constr. Build. Mater.* **2016**, *125*, 724–730. [CrossRef]
21. Dubois, V.; Wirquin, E.; Flament, C.; Sloma, P. Fresh and hardened state properties of hemp concrete made up of a large proportion of quarry fines for the production of blocks. *Constr. Build. Mater.* **2016**, *102*, 84–93. [CrossRef]
22. Rai, B.; Kumar, S.; Satish, K. Effect of Fly Ash on Mortar Mixes with Quarry Dust as Fine Aggregate. *Adv. Mater. Sci. Eng.* **2014**, *2014*, 1–7. [CrossRef]
23. Medina, G.; Sáez del Bosque, I.F.; Frías, M.; Sánchez de Rojas, M.I.; Medina, C. Durability of new recycled granite quarry dust-bearing cements. *Constr. Build. Mater.* **2018**, *187*, 414–425. [CrossRef]
24. Amadi, A.A. Enhancing durability of quarry fines modified black cotton soil subgrade with cement kiln dust stabilization. *Transp. Geotech.* **2014**, *1*, 55–61. [CrossRef]
25. Sivrikaya, O.; Kıyıldı, K.R.; Karaca, Z. Recycling waste from natural stone processing plants to stabilize clayey soil. *Environ. Earth Sci.* **2014**, *71*, 4397–4407. [CrossRef]
26. Oncu, S.; Bilsel, H. Ageing effect on swell, shrinkage and flexural strength of sand and waste marble powder stabilized expansive soil. *E3S Web Conf.* **2016**, *9*, 1–6. [CrossRef]
27. Gurbuz, A. Marble powder to stabilise clayey soils in subbases for road construction. *Road Mater. Pavement Des.* **2015**, *16*, 481–492. [CrossRef]

28. Gautam, P.K.; Kalla, P.; Jethoo, A.S.; Agrawal, R.; Singh, H. Sustainable use of waste in flexible pavement: A review. *Constr. Build. Mater.* **2018**, *180*, 239–253. [CrossRef]
29. Galetakis, M.; Piperidi, C.; Vasiliou, A.; Alevizos, G.; Steiakakis, E. Experimental investigation of the utilization of quarry dust for the production of microcement-based building elements by self-flowing molding casting. *Constr. Build. Mater.* **2016**, *107*, 247–254. [CrossRef]
30. Vijayalakshmi, M.; Sekar, A.S.S.; Prabhu, G.G. Strength and durability properties of concrete made with granite industry waste. *Constr. Build. Mater.* **2013**, *46*, 1–7. [CrossRef]
31. Galetakis, M.; Alevizos, G.; Leventakis, K. Evaluation of fine limestone quarry by-products, for the production of building elements—An experimental approach. *Constr. Build. Mater.* **2012**, *26*, 122–130. [CrossRef]
32. Karasahin, M.; Terzi, S. Evaluation of marble waste dust in the mixture of asphaltic concrete. *Constr. Build. Mater.* **2007**, *21*, 616–620. [CrossRef]
33. Karakus, A. Investigating on possible use of Diyarbakir basalt waste in Stone Mastic Asphalt. *Constr. Build. Mater.* **2011**, *25*, 3502–3507. [CrossRef]
34. Akbulut, H.; Gurer, C. Use of aggregates produced from marble quarry waste in asphalt pavements. *Build. Environ.* **2007**, *42*, 1921–1930. [CrossRef]
35. Finnish Standard Association. *SFS-EN 932-1 Tests for General Properties of Aggregates. Part 1: Methods for Sampling*; CENELEC Management Centre: Brussels, Belgium, 1997; p. 27.
36. Finnish Standard Association. *SFS-EN 1097-5 Tests for Mechanical and Physical Properties of Aggregates. Part 5: Determination of the Mater Content by Drying in a Ventilated Oven*; CENELEC Management Centre: Brussels, Belgium, 2008; p. 11.
37. Finnish Standard Association. *SFS-EN 933-1 Tests for Geometrical Properties of Aggregates. Part 1: Determination of Particle Size Distribution. Sieving Method*; CENELEC Management Centre: Brussels, Belgium, 2012; p. 18.
38. Test Sieving: Principles and Procedures. A Discussion of the Uses, Capabilities, and Limitations of Testing Sieves as Analytical Tools. Available online: http://www.advantechmfg.com/pdf/Principles%20and%20Procedures%2002_21_2013.pdf (accessed on 8 July 2018).
39. *InfraRYL 2010 Code of Building Practice, Infrastructure, Part 1: Roads and Areas*; 21300 Kantavat kerrokset; Rakennustieto Oy: Helsinki, Finland, 2010; pp. 318–320. ISBN 978-951-682-958-9.
40. Finnish Standard Association. *SFS-EN ISO 14688-2:2018 Geotechnical Investigation and Testing. Identification and Classification of Soil. Part 2: Principles for a Classification (ISO 14688-2:2017)*; CENELEC Management Centre: Brussels, Belgium, 2018; p. 18.
41. Finnish Standard Association. *SFS-EN ISO 17892-4:2016 Geotechnical Investigation and Testing. Laboratory Testing of Soil. Part 4: Determination of Particle Size Distribution*; CENELEC Management Centre: Brussels, Belgium, 2016; p. 37.
42. Slunga, E.; Saarelainen, S. Determination of frost-susceptibility of soils. In Proceedings of the 16th International Conference on Soil Mechanics and Geotechnical Engineering, Osaka, Japan, 12–16 September 2005; Millpress: Rotterdam, The Netherlands, 2005; pp. 3577–3578.
43. Finnish Standard Association. *EN 13286-2: 2010 Unbound and Hydraulically Bound Mixtures- Part 2: Test Methods for Laboratory Reference Density and Water Content- Proctor Compaction*; CENELEC Management Centre: Brussels, Belgium, 2010; p. 29.
44. Road and Water Engineering Board. *Construction Research and Design Part II Laboratory Tests*; Government of Road and Water Construction: Helsinki, Finland, 1970. (In Finnish)
45. Tangpithakkul, R. Study of Permeability of Pavement Base Materials. Master's Thesis, Ohio University, Athens, OH, USA, 1997.
46. Vermont Agency of Transportation. Permeability of Highway Base and Subbase Material. Available online: https://vtrans.vermont.gov/sites/aot/files/highway/documents/materialsandresearch/completedprojects/AOT_PermeabilityofHighwayBaseandSub-baseMaterial.pdf (accessed on 8 July 2018).
47. Khoury, N.N.; Zaman, M.M.; Ghabchi, R.; Kazmee, H. *Stability and Permeability of Proposed Aggregate Bases in Oklahoma. Report No.FHWA-OK-09-05*; Oklahoma Department of Transportation Planning and Research Division: Oklahoma City, OK, USA, 2010; p. 243.
48. Chamberlain, E.J. *Frost Susceptibility of Soil Review of Index Tests. Report No. Monograph 81-2*; Federal Aviation Administration (Systems Research and Development Service) and Federal Highway Administration (Office of Research): Washington, DC, USA, 1981; p. 121.

49. Onninen, H. *Method Description TPPT-R07 Frost Heave Test Thaw Compression Test*; VTT Communities and Infrastructure: Espoo, Finland, 1999; p. 10.
50. Slunga, E.; Saarelainen, S. Determination of Frost-Susceptibility of Soil. Available online: https://www.issmge.org/uploads/publications/1/33/1989_02_0171.pdf (accessed on 8 July 2018).

materials

MDPI

Article

Assessment for Sustainable Use of Quarry Fines as Pavement Construction Materials: Part II-Stabilization and Characterization of Quarry Fine Materials

Yinning Zhang [1,*], Leena Katariina Korkiala-Tanttu [1] and Mari Borén [2]

[1] Department of Civil Engineering, Aalto University, 00076 Aalto, Finland
[2] Destia Oy, Neilikkatie 17, 01301 Vantaa, Finland
* Correspondence: yinning.zhang@aalto.fi

Received: 1 July 2019; Accepted: 24 July 2019; Published: 1 August 2019

Abstract: A secondary by-product, quarry fines, has previously been investigated for applications in high volume as pavement construction materials. Results from a series of laboratory tests suggest qualified basic properties except for the possibility of frost susceptibility for the virgin quarry fines. In Part II of the research, stabilized quarry fine specimens were prepared and investigated in view of the mechanical behavior, and the durability represented by susceptibility to freezing and thawing cycles. The unconfined compressive strength, which is also the commonly used strength indicator, was adopted to evaluate the validity of the stabilized quarry fines as pavement construction materials. The laboratory-determined parameters were then compared among specimens treated with different stabilizers and with the typical requirements for pavement base/subbase layers. The stabilized quarry fines can be qualified for applications in pavement base, subbase and filter layer depending on the types of stabilizers used and degrees of compaction achieved.

Keywords: sustainable; secondary materials; quarry fines; freezing-thawing

1. Background

Quarry fine is a secondary by-product produced from the processing of rocks or aggregates yet of great material value for many civil engineering purposes. A huge amount of quarry fine materials is produced every year as a by-product of processing aggregates. Being an under-utilized material, the majority of it is just stored. At present, the most common application area of quarry fines in Finland is to use it as the uppermost unbound layer of yards, fields and low-volume streets [1]. Some research has also found that quarry fines could be used as an alternative to Portland cement for concrete [2], a stabilizer/additive to improve soil properties [2–6], and a substitute to sands/filler in concrete [7–10]. However, compared with the under-utilized portion, the quarry fine that has found its application in practice is still far from adequate. Unfortunately, these "leftover" quarry fine materials, if not appropriately treated, will lead to environmental and economic problems in society since the fine fraction of quarry fines will be easily dispersed by gravity, water and wind. Moreover, in the light of resource depletion and the promotion of a carbon-neutral society, wise utilization of existing resources is of vital importance. Under this circumstance, an effective way to utilize the quarry fine material in large volume is needed, and research activities regarding the characterization of this material to validate the promising applications are necessary.

As verified and stated in the previous research published earlier [11], basic properties of the unbound quarry fine materials have been investigated by a series of laboratory tests and analysis. Based on the particle distribution information obtained from both sieving and hydrometer methods,

as well as the frost heave test results, it was found that the unbound quarry fines of 0–4 mm are prone to be frost-susceptible. The mechanical properties of quarry fine materials alone do not satisfy most of the requirements for a base or subbase as provided by many agencies. Thus, the stabilization of quarry fines to improve its properties for pavement base/subbase applications is potentially an effective way of utilizing it in higher volumes. The main motivations of the design, improvement and application of stabilized quarry fines as base/subbase material are listed as follows.

(1) Conventional road construction materials of good quality, the majority as natural resources, are becoming scare due to the booming population, urbanization and industrial developments in the past few decades. Demanding sustainability and environmentally-friendly construction activities has become essential to all the countries encountering this problem. Numerous environmental constrains have been implemented by many countries, such as the EU Landfill Directive.

(2) An increasing amount of industrial by-products have so far been stored, leading to environmental problems and waste of resources. As this problem has become more widely recognized, there have been increasing efforts to reuse industrial by-products in infrastructure constructions. Often these by-products have been used as stabilizers for treating weak soils. Several existing researches have demonstrated very promising results from utilizing industrial by-products to stabilize and improve the properties of various soil types. Results have shown that not only material strength, but also freeze-thaw performance, and compaction can be enhanced by applications of by-product binders. [12–14].

(3) There is a need for improving the long-term performance and increasing the lifespan of current infrastructure systems to achieve sustainable development. Therefore, higher requirements for material strength, stability and durability are necessary, and the application of stabilized base/subbase to achieve better performance is welcomed. Numerous types of recycled materials have been investigated for their effectiveness in cementation and ground improvement in previous research, including but not limited to Portland cement (PC), ground granulated blast furnace slag (GGBS), fly ash, recycled gypsum, cement kiln dust (CKD), bentonite and so forth [15]. All the existing experience in different types of stabilizers has been used as instructive information for stabilizing quarry fines as a pavement construction material in this study.

The aim of this follow-up study is to compare different binder materials to widen the usability of quarry fines, to define the mechanical properties of the stabilized samples, to assess their durability in laboratory, and to access their suitability as a pavement construction material. The tested mechanical property of the stabilized quarry fines was Unconfined Compressive Strength (UCS), whereas the durability of the stabilized quarry fines was further verified by a freeze-thaw test and capillary rise test. Last but not least, the feasibility of the quarry fine materials for pavement construction in the base, subbase or filter layer has been discussed. This study concentrates mainly on the mechanical and durability properties, not on the environmental (leaching or emission) issues.

2. Virgin Quarry Fine Materials

In the previous study [11], virgin quarry fine materials of 0 to 4 mm grain size, produced at the quarry in Koskenkylä by Destia Oy, were collected and investigated through a series of laboratory tests. The host rock of quarry is very high quality rock with extremely good abrasion value [16], which is only about 1% of what Finnish host rock material fulfills. Based on the results of previous research, the unbound quarry fine materials are shown to be good-quality and well-graded aggregates with both fine- and dense-graded characteristics. It has shown self-draining properties, but still a maximum dry density can be achieved, even though the influence of water content on dry density is low. The coefficient of permeability also complies with the conventional values in pavement base and subbase layers. In general, it is a promising material to be utilized for pavement constructions with regard to gradation, compactability and permeability. However, both the gradation information and frost heave test results have shown frost-susceptibility of the virgin quarry fines.

To improve the performances of quarry fines, several types of stabilizers were used in this study. Further laboratory tests were performed to characterize the stabilized quarry fine materials and to access its feasibility in pavement constructions. Comparison analysis between cement-stabilized quarry fines (as a reference material) and quarry fines stabilized with other binders gives good evidence to show how effective different types of stabilizers are and to which part of the pavement the stabilized materials can be applied.

3. Characterization of Stabilized Quarry Fines As Construction Material for Pavements

The main issue in the stabilization is to determine what type of stabilizer would be effective for better performance, cost-effectiveness and environmental friendliness. In this regard, the cement, which is one of the most commonly used and well established stabilizers for granular materials around the world, was selected as a reference material. It provided a baseline for comparisons with other types of by-product stabilizers: Ecolan and fly-ash stabilizers. These two types of potential stabilizers were proven to be effective as stabilizers, and their detailed components as well as the adopted ratios to quarry fines are introduced in the following sections.

3.1. Specimen Preparation

The appropriate dosage or proportion of each ingredient of stabilized material is the key factor to obtain better performance. The determination of mixture proportions requires a large amount of laboratory testing including aggregate gradation tests, reference density tests to determine the relationship between water content and dry density, selection of the relevant water content, and possibly activator content for each stabilizer. Moreover, the situation is even more complicated when it comes to the stabilized materials due to potential hydraulic reactions between the stabilizer and water. In this study, the mix proportions were selected either based on earlier laboratory and field test results, empirical knowledge, or suggestions from experienced agencies. The following section describes how the mixture design was determined for laboratory experiments.

- Cement type and content: For cement-stabilized quarry fines, quick cement by Finnsementti (pikasementti, Finnsementti Oy, Parainen, Finland) [17] was chosen because it is the purest calcium carbonate of current cement types, and many older researches have been made with relatively pure cement. Cement content was selected based on Finnish guidelines of overlay structures [18]. According to the guidelines, the typical cement content for stabilized soil is 2.5% to 5.0%. Considering the general experience that lower cement content is beneficial to the long-term performance of a stabilized base [19], as well as that for weather resistance the cement content should be more than 4.5% [18], the final two levels of cement content are determined to be 2.5% and 4.5% for quarry fine stabilization.
- Ecolan stabilizer contents: Ecolan stabilizer (Kolliantal och-slag, Renotech Oy, Turku, Finland) composed of coal ash, wood biomass, lime and cement, was also selected. The contents adopted for this stabilizer were selected to be 4.5% and 6.5% with suggestions from the earlier tests [20].
- Fly ash-based stabilizer content: Fly ash-based stabilizer is composed of 100% coal combustion residuals (CCRs) with a major component of fly ash. The stabilizer content was selected based on existing experience of the typical fly ash content as suggested for a stabilized base course by FHWA (federal highway administration) [21,22]. It suggests that a content of 12% to 30% of fly ash, with an activator of lime or cement adopted together, should be added to stabilize the pavement base course. Therefore, considering economy and environmental efficiency, two levels of low fly ash-based stabilizer content, 12% and 15%, were selected. Cement was also used as an activator in the fly ash-based mixture because the further pozzolanic reactions require an alkali condition to form cementitious Calcium-Silicate-Hydrate (C-S-H) gels and to stabilize the quarry fines. A cement content of 1% was adopted as an activator in the fly ash-stabilized quarry fines according to the FHWA recommended activator content of 0.5% to 1.5% for Portland cement [21].

- Optimal water content: The optimal water content of the unbound quarry fines was determined according to European standard in previous research [11]. The as-determined optimal water content of 9.26% was used as reference to select water content for adequate compaction.
- Water to cement ratio: Water-to-cement ratio was selected for effective hydraulic reactions when the quarry fines were stabilized with different stabilizers. According to recommendations by American Concrete Institute (ACI) [21] for the fly ash concrete, two levels within the typical range of 0.4 and 0.6 were adopted for stabilized quarry fines.

Following the designed ingredient proportions, raw materials of designed dosages were mixed in an electrical mixer thoroughly to get a batch for triplicated specimens. Each stabilized quarry fine specimen was fabricated by compacting a certain mass of material into a 50-mm-diameter mold in three layers until a final height of 100 mm and a degree of compaction of 85%, was reached. The compaction energy was kept the same for the three layers of triplicated specimens by keeping the same blow number and dropping from the same height, which also ensures a homogeneous specimen as much as possible.

Since the 85% degree of compaction is the highest level that can be achieved by manual compaction, the specimens of 50 mm diameter were only used to determine the best mixture design. To achieve a higher degree of compaction, more specimens were prepared using the gyratory compactor with the best mixture design to evaluate performances of stabilized quarry fines.

3.2. Capillary Rise

Capillary actions driven by matric suction will pull water upwards to the frozen zone, whereas hydraulic conductivity will allow quantities of water to be transferred to the frozen zone. As a result, ice lenses are able to form continuously in the material and problems related with frost heave, and freezing-thawing can occur. In Part 1 [11], virgin quarry fines of grain size 0–4 mm have been proven to be frost susceptible based on laboratory-determined indicators: segregation potential. The effectiveness of applying stabilization techniques were evaluated by capillary rise test according to the European standard SFS-EN 13057: Products and systems for the protection and repair of concrete structures. Test methods. Determination of resistance of capillary absorption [23].

There are different analyzing methods to obtain the absorption coefficient, including a 30 min method, one tangent method, and two tangent method [24]. The main difference of these methods is the way of selecting effective data points for the coefficient calculation. In this study, it was found that different methods have very limited influence on the final results, and one tangent method was used to determine the indicator "absorption coefficient" by following the European standard. The absorption coefficient was defined as the gradient of the prediction line between water uptake per unit area and square root of time (Figure 1). All the groups showed flat end portions, which indicated full saturation before the end of test, thus only the initial linear part of the graph has been used for gradient determination in this study.

The results show that the capillary sorption coefficients of stabilized quarry fine specimens are comparable to but still higher than the coefficients of concrete in the literature, if the same test method (EN 13057) is adopted. The average rate of water absorption for concrete cross-beam with silane of 20-year service life is from 0.247 to 1.033 mg/cm^2 s$^{1/2}$ [25]. The reported coefficients for hardened concrete containing recycled aggregate, air-entraining agent, cement, fly ash, and superplasticizer of varied proportions were from 0.746 to 1.549 mg/cm^2 s$^{1/2}$ (5.56 to 24.0 cm^2/s) [26]. Similar ranges can be found in other studies where the coefficient is from 0.68 to 2.21 mg/cm^2 s$^{1/2}$ [27]. On the other hand, the coefficients for quick cement-stabilized quarry fine specimens were 1.24 to 3.56 mg/cm^2 s$^{1/2}$, and for quarry fine specimens stabilized with Ecolan or fly ash-based stabilizer, higher values from 5.85 to 11.36 mg/cm^2 s$^{1/2}$, and 9.27 to 14.41 mg/cm^2 s$^{1/2}$ were obtained. If compared with mixtures of river sand and natural hydraulic lime, similar water absorption coefficients between 7.9 and 19.2 mg/cm^2 s$^{1/2}$ have been published [24]. This coefficient for the building material was determined by European standard EN 1925 where a similar test method was used [28].

It can also be seen from Figure 1 that cement-stabilized quarry fines need a longer time to reach the status of full saturation compared with Ecolan-stabilized and fly ash-stabilized quarry fines, indicating that the Ecolan-stabilized and fly ash-stabilized quarry fines are more prone to absorb water and subject to freeze–thaw cycles. This finding can be further verified by the results of the freeze–thaw test presented in the following sections.

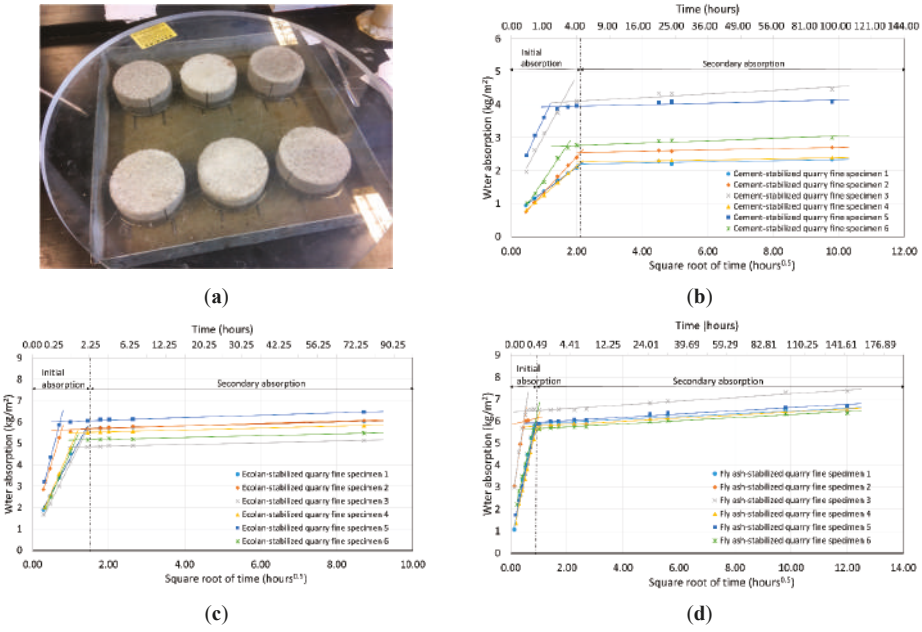

Figure 1. Capillary rise test: (**a**) specimens in one group; (**b**) water absorption of cement-stabilized quarry fines; (**c**) water absorption of Ecolan-stabilized quarry fines; (**d**) water absorption of fly ash-stabilized quarry fines.

3.3. Unconfined Compressive Strength

3.3.1. Determination of the Mix Design

Unconfined compressive test is one of the methods that is normally adopted to determine the strength of bound materials. Unconfined Compressive Strength (UCS) is a typical strength parameter used by not only researchers but also industries in civil engineering to verify if the mixture is suitable for applications with satisfactory performance. There are also empirical relationships developed to predict other material properties such as resilient modulus from the unconfined compressive strength. In pavement engineering, many research reports, specifications and standards have suggested the minimum UCS of stabilized material for base and subbase layers of pavement. In this consideration, the UCS has been selected in this study as the indicator to determine the best mix design for stabilizing quarry fines. Table 1 lists some of the requirements as provided by different agencies.

The standard test method Geotechnical investigation and testing. Laboratory testing of soil. Part 7: Unconfined compression test (ISO 17892-7:2017) was followed to determine the unconfined compressive strength. Stabilized quarry fine specimens of 50 mm diameter and 100 mm height were compressed at a strain rate of 1.0 mm per minute (between 1% and 2% of the specimen height per minute) while the load, displacement and elapsed time were recorded for further data processing. At a given mix design, triplicated quarry fine specimens were tested successively and the average

was adopted in data analysis. Table 2 lists all the mixture designs of the specimens and the highest compressive strength together with the best mixture option that has been achieved.

Table 1. Unconfined compressive strength requirements for base/subbase/subgrade of pavements.

References	Minimum or Typical UCS Ranges (MPa)	Curing Period	Applications
Portland Cement Association [29]	2.068–5.516 (300–800 psi)	7 days	Medium- to high-volume roads for subbase/base
Mechanistic-Empirical Pavement Design Guide (MEPDG) [30]	1.72 (250 psi) 5.17 (750 psi)	7 days for cement and 28 days for lime-fly ash or cement fly ash	for subbase, subgrade for base
Austroads [31]	2.0 1.0–2.0	28 days curing and 4 h soaking prior to testing	bound pavement materials (stabilizer > 3%) subgrade, lightly-bound pavement materials (stabilizer < 3%)
Federal Highway Administration (FHWA) [32,33]	4.1 0.7 1.0 1.4	N/A 7-day cure at 105 °F (40 °C) 7-day cure at 105 °F (40 °C) 7-day cure	for stabilized drainable base in cold regions to resist frost deterioration subgrade lime/soil subgrade lime/fly ash/soil subgrade cement/soil, cement/fly ash/soil, or fly ash/soil
InfraRYL [34]	3.0–8.0 5.0–13.0 1.0–2.0	7-day cure 28-day cure 28-day cure	cement-stabilized cement-stabilized blast furnace slag stabilized

The maximum compressive strength of quarry fine specimens stabilized with quick cement at 85% degree of compaction reached around 2.5 MPa for a 28-day curing period in this study, compared to a lowest strength of 0.703 MPa that is only 28.1% of the maximum strength. This result indicates the profound influences of mixture design, or the stabilizer and water content, and associated compaction energy on the final strength of stabilized quarry fine materials. It is found in this study that a lower water-to-binder ratio and higher cement content added to the quarry fine specimen brings higher compressive strength of cement-stabilized quarry fine mixture. The same trends can be found for quarry fines stabilized with fly ash and an activator of cement. Nevertheless, different situations can be observed for other types of stabilizers. When the Ecolan stabilizer is applied, a higher water-to-stabilizer ratio and stabilizer content are needed to get higher compressive strength. It is also found that the fly ash itself has shown little improvement to the strength of quarry fines, but with a small amount of activator (e.g., cement) added, higher strength can be achieved. Generally, quarry fine specimens stabilized with quick cement have the highest UCS, whereas those stabilized with other binders consisting of coal ash with the same or even higher stabilizer content are less strong.

The undrained shear strength predicted from the UCS, as well as the secant modulus or modulus of deformation E_{50}, which was obtained from the data corresponding to half the maximum UCS [35,36], are also listed in Table 2. Figure 2 presents the relationship between the UCS and modulus of deformation from the laboratory test data for stabilized quarry fine specimens of different stabilizer content, water content and compaction energy. It is found that the modulus of deformation E_{50} of cement-stabilized quarry fines can be predicted as having an approximate value of 5 to 125 × UCS, even though the strength and modulus of cemented quarry fines are much higher than that of the cemented clay. For quarry fines stabilized with Ecolan and fly ash-based stabilizers (with activator), the coefficients are of 72 to 468 × UCS and of 35 to 179 × UCS respectively. The multiplier coefficients of Ecolan-stabilized quarry fines are higher than the typical coefficients of undisturbed cemented clays from 50 to 300 [37], while the fly ash-stabilized quarry fines have similar coefficients to undisturbed cemented clays.

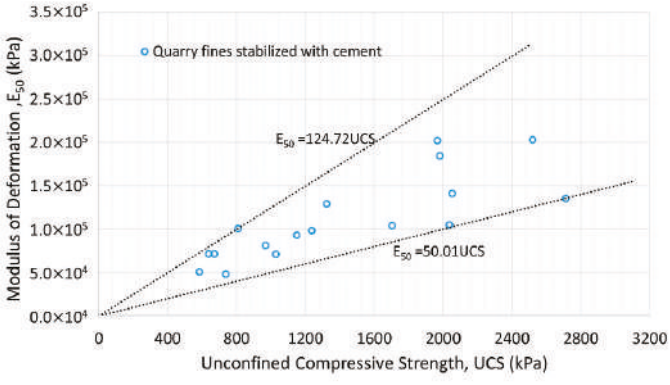

(**a**)

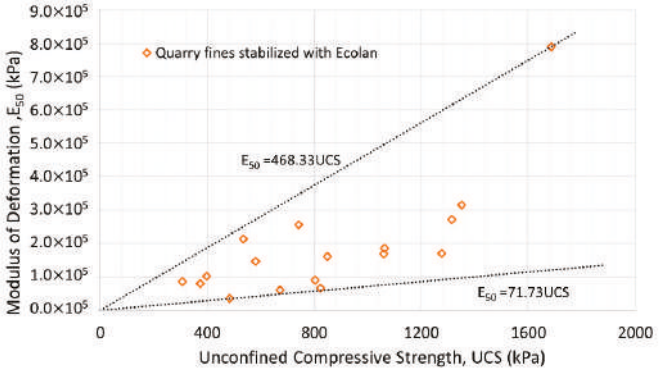

(**b**)

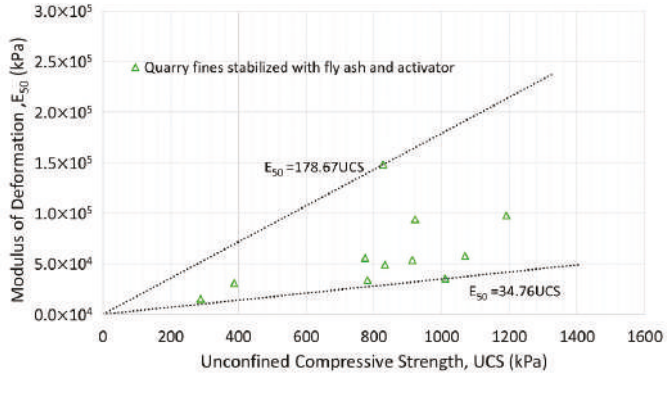

(**c**)

Figure 2. Modulus of deformation versus unconfined compressive strength of stabilized quarry fines: (**a**) Quarry fines stabilized with cement; (**b**) Quarry fines stabilized with Ecolan; (**c**) Quarry fines stabilized with fly ash and activator.

Table 2. Types of stabilized quarry fine specimens and their strengths.

Quick Cement Stabilized Quarry Fine Specimen #	Stabilizer Content	Water to Binder Ratio	** Unconfined Compressive Strength, kPa	Undrained Shear Strength, kPa	Secant Modulus/Deformation Modulus E50, MPa
A1–A3	4.5%	0.4	1741.2	870.59	172.08
A4–A6	4.5%	0.6	1924.4	962.22	115.10
B1–B3	2.5%	0.4	758.8	379.41	60.68
B4–B6	2.5%	0.6	703.5	351.77	82.63
C1–C3*	4.5%	0.0	2483.2	1241.59	196.64
C4–C6	2.5%	0.0	1128.0	563.98	87.92
Ecolan Stabilized Quarry Fine Specimen #	**Binder Content**	**Water to Binder Ratio**	**** Unconfined Compressive Strength, kPa**	**Undrained Shear Strength, kPa**	**Secant Modulus/Deformation Modulus E50, MPa**
E1–E3	4.5%	0.4	632.9	316.44	142.16
E4–E6	4.5%	0.6	713.2	356.59	95.85
F1–F3	6.5%	0.4	993.6	496.82	167.09
F4–F6*	6.5%	0.6	1316.7	658.35	225.64
G1–G3	4.5%	0.0	365.0	182.51	90.38
G4–G6	6.5%	0.0	981.7	490.83	273.83
Fly ash + Cement Stabilized Quarry Fine Specimen #	**Binder Content + Activator Content**	**Water to Binder Ratio**	**** Unconfined Compressive Strength, kPa**	**Undrained Shear Strength, kPa**	**Secant Modulus/Deformation Modulus E50, MPa**
H1–H3 *	12.0% + 1%	0.0	846.1	423.08	105.85
H4–H6	15.0% + 1%	0.0	571.3	285.67	42.44
H7–H9	12.0% + 1%	0.6	795.1	397.54	43.41
H10–H12	15.0% + 1%	0.6	734.8	367.40	34.56

* highest unconfined compressive strength, the best mixture; ** Curing conditions: 100% humidity, 25 °C, 28-day.

On the other hand, it can be seen from Table 2 that part of the compressive strength satisfies the requirements provided by several agencies as listed in Table 1. However, it is not convincing to qualify the best mixture for applications in pavement subbase and even base layers, considering that the quarry fines stabilized by Ecolan and fly ash-based stabilizers are around or below the lowest requirement, and much higher thresholds are required by the other agencies. Moreover, to resist frost deteriorations in cold regions, a higher compressive strength should be satisfied. Therefore, the test results as presented previously are only utilized to determine the best mixture design and the appropriate curing conditions. Considering that the degree of compaction of these specimens is 85% but most of the agencies require a higher degree (e.g., >90% in Finnish guidelines) especially for pavement base/subbase layer, higher strength is necessary and achievable for the same mix design at a higher compaction energy.

3.3.2. Influence of Degree of Compaction and Curing Days

Figure 3 shows that the degree of compaction has significant effects on the unconfined compressive strength for the cement-stabilized quarry fine specimens. The 100% degree of compaction does not imply a practical status of zero air voids, but is the highest degree of compaction that can be achieved by a gyratory compactor after 512 gyrations. It can be seen from the figure that the value of UCS has increased exponentially as the degree of compaction increased from 85% to 100% and that the UCS of stabilized quarry fine specimens of 96% degree compaction can adequately satisfy the requirements of pavement base/subbase provided by different agencies. It is therefore concluded that stabilized quarry fine materials can be qualified for pavement base/subbase applications in term of unconfined compressive strength, as long as appropriately designed and constructed. A least degree of compaction of 93% is recommended for cement-stabilized quarry fines with 0–4 mm grain size and 4.5% cement content for such purposes. For quarry fines stabilized by Ecolan, or fly ash and activator, at least a 93% or higher degree of compaction is necessary to validate their applications in base or subbase. Therefore, more stabilized quarry fine specimens with the best mixture design were prepared by

gyratory compactor to achieve at least a 93% degree of compaction, and the following characterization of stabilized quarry fines is only based on these denser specimens.

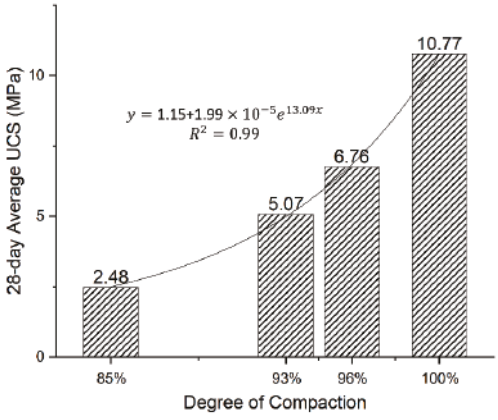

Figure 3. Effects of degree of compaction on the unconfined compressive strength.

Other than degree of compaction, the duration of curing time also influences the strength of stabilized quarry fines. In this study, the curing condition of 100% humidity was applied for all the stabilized quarry fine specimens of all the types of stabilizers. Figure 4 displays the influence of curing time on the UCS of stabilized quarry fines.

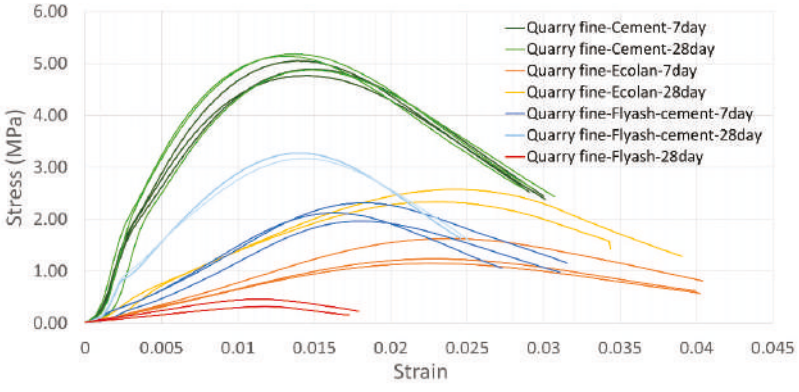

Figure 4. Effects of curing time on the unconfined compressive strength of stabilized quarry fines.

From the relationships between stress and strain in Figure 4, it can be seen that the type of stabilizer and mix design have influenced the way of deformation and failure under the same loading conditions. Quarry fines stabilized with Ecolan stabilizer have higher strains at failure whereas the cement-stabilized quarry fines demonstrate the most similar stress–strain relationship/shape of curve for different curing times. To better present the effects of curing time, an indicator based on "deformation-ductility ratio", which is originally developed for reinforced concrete, was developed and adopted. As shown in Figure 5, the strain–ductility ratio (SDR) is capable of considering the strains between the first yield point and the point where the strength is reduced to a certain percentage, serving as a good indicator for evaluating the ductility of the material. Table 3 lists the strain–ductility ratio (Equation (1)) of different stabilized quarry fines of 7-day and 28-day age, showing that cement-stabilized quarry fine is the most stable mixture regarding curing time. Ecolan-stabilized and fly ash-stabilized quarry fines all

became more ductile and easier to yield, whereas the fly ash-stabilized quarry fines show considerable increase in ductility within curing time.

$$Strain - ductility\ ratio = \frac{\varepsilon_{50}}{\varepsilon_y} \quad (1)$$

where ε_{50} is the strain corresponding to 50% of the compressive strength after failure, and ε_y is the strain at first yield point.

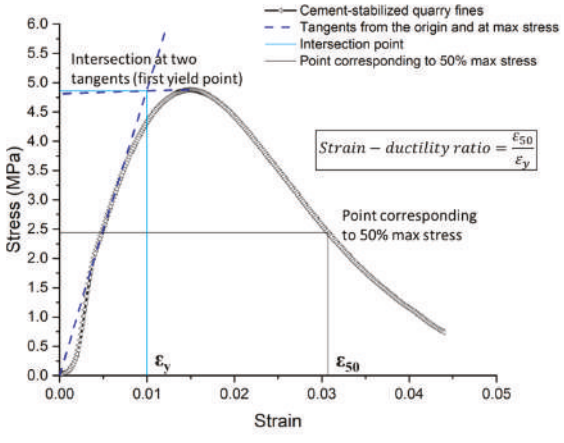

Figure 5. Strain–ductility ratio from stress–strain relationship.

Table 3. Strain–ductility ratio of stabilized quarry fines at 7-day and 28-day ages.

Type of Specimen	Cement-Stabilized Quarry Fines		Ecolan-Stabilized Quarry Fines		Fly Ash-Stabilized Quarry Fines	
Curing Days	7-day	28-day	7-day	28-day	7-day	28-day
Average SDR	3.64	3.63	2.14	2.24	1.95	2.45
* $\varepsilon_{y,ave}$	0.00817	0.00829	0.0188	0.0164	0.0153	0.0108
** $\varepsilon_{f,ave}$	0.0144	0.0139	0.0234	0.0237	0.0175	0.0148

* Average first yield strain; ** Average strain at failure.

The change in strength and ductility is linked to the continuous reaction between water and the binders during the curing period. The changes in strength due to curing time also vary among different mixtures. It is interesting to see that a longer curing time with the presence of water does not necessarily have positive effects on the development of unconfined compressive strength for stabilized quarry fine materials. In fact, the compressive strengths of cement-stabilized quarry fines are hardly changed even undergoing a longer period of curing time from 7 days to 28 days, with an average of 4.91 MPa and 5.07 MPa respectively. It is possibly related with the fast strength development of quick cement as a stabilizer for quarry fines, so that a longer period of exposure to moisture can be harmful to the strength of cement-stabilized quarry fines. However, when Ecolan or fly ash plus cement was used as a stabilizer, the strength increased by 78.6% and 42.5% from 7 days to 28 days.

3.3.3. Comparison with Requirements

To validate the stabilized quarry fine materials for pavement constructions in terms of unconfined compressive strength, unconfined compressive strength tests were conducted only on stabilized specimens of a higher degree of compaction (93% and 96%). These specimens were prepared using the gyratory compaction method, following the most promising mixture design as obtained from the previously mentioned investigation. Typical strength limits for pavement base, subbase and

subgrade as listed in Table 1 were used to assess the potential applications of the stabilized quarry fine materials. Figure 6 shows the average unconfined compressive strength of each mix based on triplicated specimens.

It should be noted that only 7- and 28-day ages were used in this research so that the stabilizations mainly based on hydraulic reactions are considered, rather than the slow-setting pozzolanic and carbonation reactions.

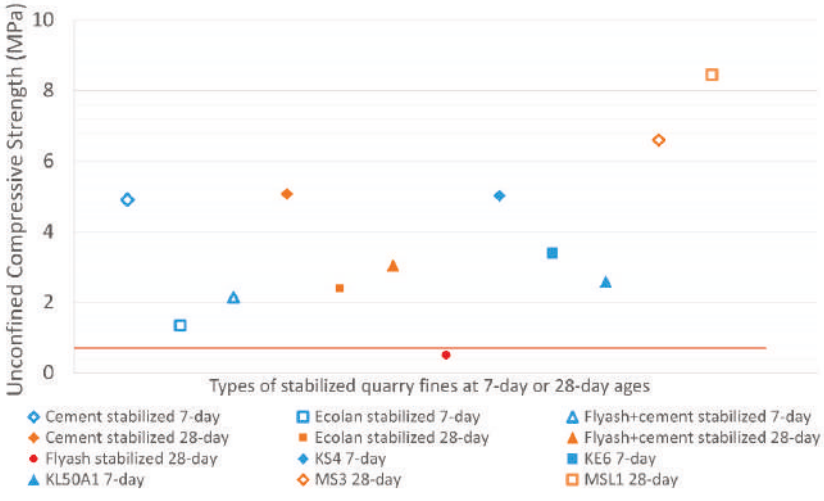

Figure 6. Average unconfined compressive strength of stabilized quarry fine specimens.

In fact, the lower limit of 0.7 MPa as plotted in Figure 6 is the minimum requirement of all the recommended lower limits by different agencies as listed in Table 1. It can be seen as the lowest limit that should be satisfied to qualify high-volume applications of stabilized quarry fine materials for pavement construction, in either base, subbase or subgrade. Fly ash itself has been proven to be not suitable to stabilize quarry fines because of its low strength. However, when a small amount of cement is used as an activator, the strength can be improved significantly and the stabilized quarry fines would have adequate strength (28-day, about 3 MPa) even for the base layer in medium to high volume roads according to Portland Cement Association. The other agency's requirements also suggest its adequate strength for applications in subbase and subgrade. However, the quarry fines stabilized with Ecolan are more suitable for subbase and subgrade according to the agencies listed in Table 1. When quick cement is used as a stabilizer, stabilized quarry fines can be satisfactorily qualified by most of the agencies as base material in medium to high volume roads, in terms of unconfined compressive strength.

Results from previous research are also plotted in Figure 6 for comparison [20,38]. The specimens KS4, KE6 and KL50A1 are quarry fines (0–3 mm) stabilized with plus cement, Ecolan stabilizer and 50% fly ash with 1% cement as activator. The 7-day unconfined compressive strength of cement-stabilized specimens is quite similar, while for the other two types of stabilizers, the previous research obtained higher strengths mainly due to higher degree of compaction (DOC, 96%). If the gradation of aggregates was improved by adding more coarse fractions such as crushed rock of 0–20mm, the strength will be improved significantly as shown for specimens MS3 (5% plus cement) and MSL1 (2% plus cement + 6% fly ash).

3.3.4. Failure Modes

The major cracking types developed in the stabilized quarry fine specimens after unconfined compressive test are shown in Figure 7, where two types of cracks caused by extension and shear

have been observed. However, in this study, the combinations of tensile splitting and inclined shear cracks are the main failure modes, and the barrel-shaped specimen after testing with cracks indicates semi-plastic characteristics of the stabilized quarry fine materials. Among all 18 quarry fine specimens stabilized with quick cement, 16 of them are observed to have combined extension and shear cracks as the failure mode, while the other two are found to have only extension cracks after compression. Therefore, combined extension and shear failures can be recognized as the main failure mode of cement-stabilized quarry fines under unconfined compression conditions.

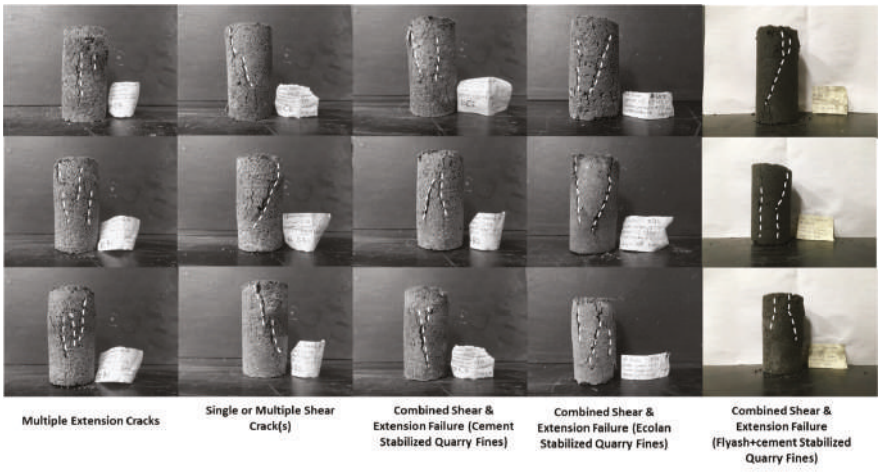

Figure 7. Cracking types (first two columns) and major failure mode (column three to five) of the stabilized quarry fine specimens in unconfined compressive test.

The same main failure mode of combined extension and shear can also be observed for the Ecolan-stabilized and fly ash plus cement-stabilized quarry fine specimens. Two out of the total 18 Ecolan-stabilized specimens were found to have multiple extension cracks while the others all have combined extension and shear failures. For quarry fines stabilized with fly ash plus cement, two out of the total 12 specimens only have failure mode of multiple extension cracks and the rest all have combined cracks. There seems to be no significant difference in failure mode for the quarry fines stabilized by the three types of stabilizers as adopted in this study.

3.4. Freeze–Thawing Properties

Ground freezing and thawing is a result of the annual cycle of temperatures, which is also a common situation encountered in Nordic countries. A recent study found that with global climate changes, the intensity of thaw weakening will be more serious [39], and the annual number of freeze–thaw cycles is increasing. As a candidate construction material, stabilized quarry fines should be capable to sustain in such severe environmental conditions. The resistance of the stabilized quarry fines to the cyclic action of freezing and thawing is critical to the performances of buildings and infrastructures in cold regions, and thus is estimated by freeze–thaw testing. The technical specification CEN/TS 13286-54 Test method for the determination of frost susceptibility. Resistance to freezing and thawing of hydraulically bound mixtures was followed to conduct the test on stabilized quarry fines [40].

In the first stage, cylindrical stabilized quarry fine specimens of 100 mm diameter and height were prepared using gyratory compactor ICT to achieve 96% degree of compaction. The specimens for freeze-thaw testing were fabricated according to the most promising mix designs to achieve the highest UCS as obtained from previous tests. For each type of stabilizer, six specimens were fabricated,

kept in mould, and cured in a humidity room for 28 days. Then they were removed from the mould and divided into Set A and B with three specimens in each. As a result, the first stage was finished to allow adequate strength development for the specimens. The second stage consists of the application of freeze-thaw cycles and the strength test. Both of the two sets were placed in a humidity room to prevent the loss of moisture, and Set A was removed from the humidity room after 2 days and wrapped and placed in a low temperature cabinet for 10 freeze-thaw cycles, whereas Set B was kept in a humidity room until the conditioning of Set A was finished. Then all the specimens were used in an unconfined compressive strength test and the freeze–thaw retained strength ratio was calculated.

As shown in Figure 8, one freeze-thaw cycle takes 24 hours to finish, and the controlled temperature inside the low temperature cabinet was within the limits as suggested by the specifications. The monitored temperature was measured inside a cubic cement concrete specimen placed inside the cabinet.

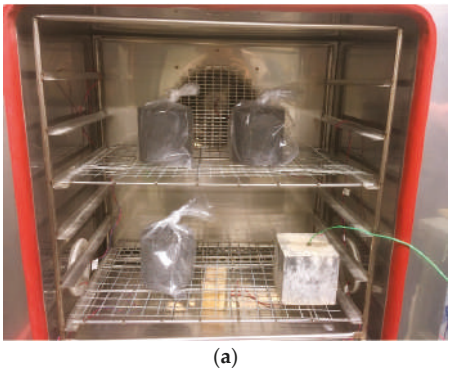

(**a**)

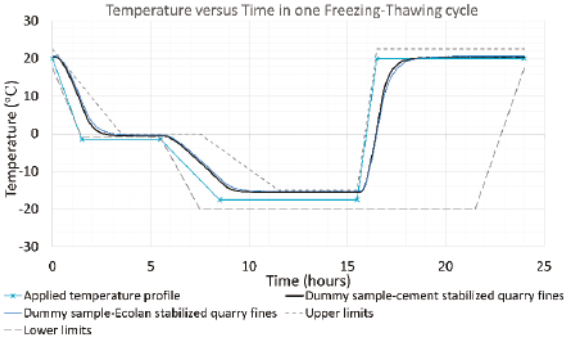

(**b**)

Figure 8. Freeze–thaw test: (**a**) Stabilized quarry fine specimens inside the chamber; (**b**) Temperature profile applied in freeze–thaw cycles.

Based on the unconfined compressive strength of both Set A and B quarry fine specimens subjected to none or 10 freeze-thaw cycles, no distinguished differences were found between the two sets. However, still the average UCS of regular specimens is higher than that of conditioned specimens, and the strain corresponding to the UCS at failure has increased. Based on calculations, some indicators including the previously mentioned strain-ductility ratio, the freeze-thaw retained strength ratio is presented in Table 4.

Table 4. Indicators to evaluate effects of freeze-thaw cycles.

Type of Specimen	Cement-Stabilized Quarry Fines		Ecolan-Stabilized Quarry Fines		Fly Ash-Stabilized Quarry Fines	
Freezing-Thawing Conditions	No Freezing-Thawing Cycles	10 Freezing-Thawing Cycles	No Freezing-Thawing Cycles	10 Freezing-Thawing Cycles	No Freezing-Thawing Cycles	10 Freezing-Thawing Cycles
Average SDR	1.81	1.50	1.76	1.23	1.41	1.36
$\varepsilon_{y,ave}$	0.0149	0.0201	0.0231	0.0332	0.0169	0.0190
$\varepsilon_{f,ave}$	0.0204	0.0240	0.0308	0.0379	0.0193	0.0211
FTR	0.946		0.808		0.662	

Where FTR is the freeze–thaw retained strength ratio $\frac{R_A}{R_B}$, and R_A and R_B are the mean value of strength for Set A and Set B, respectively.

Subjected to 10 freeze-thawing cycles, the specimens have been deteriorated in terms of reduced UCS and strain-ductility ratios. As shown in Table 4, given the same external loading conditions, the specimens have become less ductile after the cyclic freeze-thawing conditions, whereas the strains at first yield point and at failure all increase. This can be further interpreted as the materials subject to freeze-thawing cycles were deformed more before failure but became more brittle and easy to break after the peak stress. From the curves of cement-stabilized quarry fines, there are obvious relaxation stages after the beginning of the load for the conditioned specimens, contributing to the total strains at failure. On the other hand, based on the freeze-thaw retained strength ratio, it can be seen that the deteriorations caused by 10 freezing and thawing cycles for the cement-stabilized quarry fine specimens were not significant. This qualifies the cement-stabilized quarry fines as a pavement construction material for different layers. The deteriorations caused by freeze-thawing cycles for Ecolan-stabilized quarry fines were more serious, which resulted in a decrease in the UCS by about 20%. Yet, this amount of deterioration in the UCS is normal for stabilized granular materials such as lime-treated kaolinite [41,42] and fiber-reinforced clay [43,44]. However, improvement is still necessary to enhance the freeze-thawing resistance for quarry fines stabilized with fly ash, even though the ratio is right on the limit set by Finnish guidelines of 6.7 [18]. The fundamental mechanism behind such a difference in freeze-thawing resistance of quarry fines stabilized with different stabilizers stills need to be investigated from a finer-scale point of view. Related research and results will be introduced in the future.

4. Discussion on Potential Applications of Quarry Fine Materials

Existing research has already presented several applications of virgin quarry fine materials, including as a partial substitute to cement and as an additive to improve the properties of soils, whereas these applications are only in limited volumes. The virgin quarry fines of 0–4mm as adopted in this study have a similar particle size distribution to well-graded sand, and a coefficient of permeability around 5.75×10^{-5} m/s [11] indicates its potential material value in construction for civil engineering purposes. However, considering that the previous test results have also suggested possible frost-susceptive properties, stabilizers were applied to improve the properties of virgin quarry fines as a construction material. Unconfined compressive strengths of the stabilized quarry fine materials were investigated by laboratory tests, which further verified the potential of the stabilized quarry fines for civil engineering applications from the strength point of view.

Based on the typical strength and durability requirements for materials used in pavement structural layers, the stabilized quarry fine materials can qualify for high-volume civil engineering applications, as long as they are well designed and compacted to enough degrees. One of the most possible applications is in road construction. The stabilized quarry fines can be qualified for base, subbase, filter layers, and subgrade depending on the different stabilizers used and degrees of compaction achieved. Nevertheless, applications for pavement subbases are much more suggested. This is because higher quality material is better for base layers to ensure pavement performances in the long run, and unbound material is more favorable for the filter layers considering cost efficiency. The other

possible applications include but are not limited to embankment building, landfill construction, and construction site leveling, where strength requirements are not high.

However, when the strength requirements are high, it is still possible to utilize the stabilized quarry fine materials. It is well-established that particle size distribution of the aggregate has shown important effects on the unconfined compressive strength of mixtures. This has also been seen when comparing the results of this research with the previous ones. When coarse particles are added to quarry fines to obtain a good gradation curve and compaction, the strength can be improved significantly. Therefore, in situations where higher strength is required, either modifying the gradation of quarry fines by adding more coarse fractions or increasing the DOC level (if achievable in field) would be options.

On the other hand, even though the resistance to freeze-thawing cycles of the stabilized quarry fines is acceptable based on laboratory results in this study, the detrimental effects of salt have been found somewhere else. In situations where freeze-thawing cycles are presented and deicing agent is applied, the resistance would be impaired especially for the cement-stabilized quarry fines. It is therefore suggested that for pavements where deicing agent is needed, a waterproof asphalt concrete surface layer would be helpful to reduce the salt infiltration and maintain the resistance of the underlying stabilized quarry fine layers to freeze-thawing cycles.

It should be noted that all these potential high-volume applications are based on the assumption that the quarry fine materials can satisfy all the environmental requirements set by the government. Also, there are still some uncertainties of the conclusions made in this study, mainly due to the limited number of specimens that has been tested and the possible variations of the material quality over different quarries.

5. Conclusions

- It is found that the modulus of deformation E_{50} of cement or fly ash (with activator) stabilized quarry fines can be predicted with a similar multiplier coefficient to cemented clays. For quarry fines treated with Ecolan stabilizer, the multiplier coefficients are higher than the typical coefficients of undisturbed cemented clays. The differences in multiplier coefficients among mixtures are mainly due to different virgin material properties, water content and the type of stabilizer applied.
- The UCS of stabilized quarry fine specimens of 96% degree of compaction can adequately satisfy the requirements of pavement base/subbase provided by different agencies in terms of strength, as long as appropriately designed and constructed. A least 93% degree of compaction is recommended for cement-stabilized quarry fines with the proposed mixture design, to be qualified for applications in base layers. When Ecolan or flyash with cement is used as the stabilizer, a higher degree of compaction would work better.
- Higher cement content and a lower water-to-cement ratio will result in stiffer cement-stabilized quarry fine materials. A similar situation was also observed on quarry fine specimens stabilized by the fly ash and activator. The opposite situation was found for the Ecolan stabilizer where a higher stabilizer content and water-to-stabilizer ratio will lead to higher strength.
- Combined extension and shear failures can be recognized as the main failure mode of stabilized quarry fines under unconfined compression conditions.
- The specimens subjected to freeze-thawing cycles have been deteriorated in terms of reduced bearing capacity and the increased deformation given the same external loading conditions. The freeze-thaw retained strength ratio indicates that the deteriorations caused by 10 freeze-thaw cycles were very limited for cement-stabilized quarry fines which can be qualified as a pavement construction material. For the Ecolan or fly ash-stabilized (with activator) quarry fines, higher susceptibilities, yet within the requirements, were observed, indicating a need for improvements. The results of the capillary rise test also support this finding.
- When the strength requirements are high (such as for base layer), it is still possible to utilize the stabilized quarry fine materials by modifying the gradation or increasing the DOC level (if achievable in field).

- For pavements where a deicing agent is needed, a waterproof asphalt concrete surface layer is suggested to maintain the resistance of the underlying stabilized quarry fine layers to freeze-thawing cycles.

6. Future Research

In this research, varied stress-strain relationships under the same loading conditions for the quarry fine specimens stabilized with different stabilizers have been observed. In the future research, another mechanical test, such as Repeated Load Triaxle (RLT) test, may be conducted to further investigate its mechanical properties. Fundamental mechanisms lying behind this, as well as the different UCS values caused by different binding effects of various stabilizers, still need to be investigated. A future study based on more fundamental, fine-scaled investigation with Scanning Electron Microscopy (SEM) and Energy Dispersive Spectroscopy (EDS) techniques will be conducted to compare mineral compositions of quarry fines and host rock, and to explain the binding and freeze-thawing effects on quarry fines.

Author Contributions: Ceptualization, L.K.K.-T.; Methodology, Y.Z. and L.K.K.-T.; Software, Y.Z.; Validation, Y.Z., and L.K.K.-T.; Formal Analysis, Y.Z. and L.K.K.-T.; Investigation, Y.Z., L.K.K.-T. and M.B.; Resources, L.K.K.-T. and M.B.; Data Curation, Y.Z. and L.K.K.-T.; Writing—Original Draft Preparation, Y.Z. and L.K.K.-T.; Writing—Review and Editing, L.K.K.-T. and M.B.; Visualization, Y.Z. and L.K.K.-T.; Supervision, L.K.K.-T. and M.B.; Project Administration, L.K.K.-T. and M.B.; Funding Acquisition, L.K.K.-T. and M.B.

Funding: This research received no external funding.

Acknowledgments: This research was supported by the School of Engineering, Aalto University, for financing the researchers, and Destia Ltd. for providing the raw materials. We would like to present our gratitude to our colleagues Amandine Miksic, Hakala Veli-Antti, Eloranta Pekka, and Henry Gustavsson, who provided expertise that greatly assisted the research.

Conflicts of Interest: The authors declare no conflict of interest. The funders had no role in the design of the study, the collection, analysis, or interpretation of data, the writing of the manuscript, or in the decision to publish the results.

References and Notes

1. Pitkänen, I.J. Selvitys Destia Oy: n kivituhkamääristä ja kivituhkan nykyisistä ja uusista käyttömahdollisuuksista. Bachelor's Thesis, Savonia University of Applied Science, Kuopio, Finland, November 2015.
2. Medina, G.; Sáez del Bosque, I.F.; Frías, M.; Sánchez de Rojas, M.I.; Medina, C. Durability of new recycled granite quarry dust-bearing cements. *Constr. Build. Mater.* **2018**, *187*, 414–425. [CrossRef]
3. Amadi, A.A. Enhancing durability of quarry fines modified black cotton soil subgrade with cement kiln dust stabilization. *Transp. Geotech.* **2014**, *1*, 55–61. [CrossRef]
4. Sivrikaya, O.; Kıyıldı, K.R.; Karaca, Z. Recycling waste from natural stone processing plants to stabilize clayey soil. *Environ. Earth Sci.* **2014**, *71*, 4397–4407. [CrossRef]
5. Oncu, S.; Bilsel, H. Ageing effect on swell, shrinkage and flexural strength of sand and waste marble powder stabilized expansive soil. *E3S Web Conf.* **2016**, *9*, 1–6. [CrossRef]
6. Gurbuz, A. Marble powder to stabilise clayey soils in subbases for road construction. *Road. Mater. Pavement Des.* **2015**, *16*, 481–492. [CrossRef]
7. Rai, B.; Kumar, S.; Satish, K. Eect of Fly Ash on Mortar Mixes with Quarry Dust as Fine Aggregate. *Adv. Mater. Sci. Eng.* **2014**, *2014*, 1–7. [CrossRef]
8. Vijayalakshmi, M.; Sekar, A.S.S.; Prabhu, G.G. Strength and durability properties of concrete made with granite industry waste. *Constr. Build. Mater.* **2013**, *46*, 1–7. [CrossRef]
9. Karasahin, M.; Terzi, S. Evaluation of marble waste dust in the mixture of asphaltic concrete. *Constr. Build. Mater.* **2007**, *21*, 616–620. [CrossRef]
10. Karakus, A. Investigating on possible use of Diyarbakir basalt waste in Stone Mastic Asphalt. *Constr. Build. Mater.* **2011**, *25*, 3502–3507. [CrossRef]
11. Zhang, Y.; Korkiala-Tanttu, L.; Gustavsson, H.; Miksic, A. Assessment for sustainable use of quarry fines as pavement construction materials: Part I description of basic quarry fine properties. *Materials* **2019**, *12*, 1209. [CrossRef] [PubMed]

12. Sargent, P.; Rouainia, M.; Hughes, P.N.; Glendinning, S. Alkali Activation of Industrial By-Products for use in Soil Stabilisation. In Proceedings of the ISSMGE Technical Committee TC 211 International Symposium on Ground Improvement (IS-GI BRUSSELS 2012): Recent Research, Advances & Execution Aspects of Ground Improvement Works, Proceedings of the International Symposium, Brussels, Belgium, 31 May–1 June 2012; Denies, N., Huybrechts, N., Eds.; ISSMGE TC211 and BBRI: Brussels, Belgium, 2012; Volume II, pp. 467–477.
13. Mirzaeifar, H.; Abdi, M.R. Stabilizing clays using basic oxygen steel slag (BOS). In Proceedings of the Recent Research, Advances & Execution Aspects of Ground Improvement Works, Proceedings of the International Symposium, Brussels, Belgium, 31 May–1 June 2012; Denies, N., Huybrechts, N., Eds.; ISSMGE TC211 and BBRI: Brussels, Belgium, 2012; Volume II, pp. 403–410.
14. Blanck, G.; Cuisinier, O.; Masrouri, F. A non-traditional treatment for the compaction of fine-grained soils. In Proceedings of the Recent Research, Advances & Execution Aspects of Ground Improvement Works, Proceedings of the International Symposium, Brussels, Belgium, 31 May–1 June 2012; Denies, N., Huybrechts, N., Eds.; ISSMGE TC211 and BBRI: Brussels, Belgium, 2012; Volume II, pp. 281–287.
15. Kamei, T.; Ahmed, A.; Shibi, T. Recycled basanite in conjunction with coal ash for stabilization of soft clay soil. In Proceedings of the Recent Research, Advances & Execution Aspects of Ground Improvement Works, Proceedings of the International Symposium, Brussels, Belgium, 31 May–1 June 2012; Denies, N., Huybrechts, N., Eds.; ISSMGE TC211 and BBRI: Brussels, Belgium, 2012; Volume II, pp. 373–384.
16. CE marking of quarry fines. Delivered by Destia Oy. Neilikkatie 17, 01301 Vantaa.
17. CE marking of pikacement. Delivered by Finnsementti Oy. 21600 Parainen.
18. Tiehallinto. Päällysrakenteen Stabilointi. Available online: https://julkaisut.vayla.fi/thohje/pdf/2100055-v-07paallysrakenteen_stabilointi.pdf (accessed on 24 September 2018).
19. Guthrie, W.S.; Sebesta, S.; Scullion, T. *Selecting Optimum Cement Contents for Stabilizing Aggregate Base Materials*; Report No. FHWA/TX-05/7-4920-2; Texas Department of Transportation: Austin, TX, USA, February 2002.
20. Melander, M. Suitability of by-product fines for stabilized base course. Master's Thesis, Aalto University, Helsinki, Finland, May 2018.
21. American Coal Ash Association. Fly Ash Facts for Highway Engineers. Available online: https://www.fhwa.dot.gov/pavement/recycling/fafacts.pdf (accessed on 24 September 2018).
22. Federal Highway Administration Research and Technology. User Guidelines for Waste and Byproduct Materials in Pavement Construction. Available online: https://www.fhwa.dot.gov/publications/research/infrastructure/structures/97148/cfa55.cfm (accessed on 24 September 2018).
23. Finnish Standard Association. *SFS-EN 13057 Products and Systems for the Protection and Repair of Concrete Structures. Test Methods. Determination of Resistance of Capillary Absorption*; CENELEC Management Centre: Brussels, Belgium, 1997.
24. Karagiannis, N.; Karoglou, M.; Bakolas, A.; Moropoulou, A. *Building Materials Capillary Rise Coefficient: Concepts, Determination and Parameters Involved*; Delgado, J., Ed.; New Approaches to Building Pathology and Durability. Building Pathology and Rehabilitation; Springer: Singapore, 2016; Volume 6.
25. Christodoulou, C.; Goodier, C.I.; Austin, S.A.; Webb, J.; Glass, G.K. Long-term performance of surface impregnation of reinforced concrete structures with silane. *Constr. Build. Mater.* **2013**, *48*, 708–716. [CrossRef]
26. Yeşim, T.; Remzi, Ş. Compressive Strength and Capillary Water Absorption of Concrete Containing Recycled Aggregate. *Int. Sch. Sci. Res. Innov.* **2015**, *9*, 995–999.
27. Mors, R.; Jonkers, H. Effect on Concrete Surface Water Absorption upon Addition of Lactate Derived Agent. *Constr. Build. Mater.* **2017**, *7*, 51. [CrossRef]
28. Finnish Standard Association. *SFS-EN 1925 Natural Stone Test Methods. Determination of Water Absorption Coefficient by Capillarity*; CENELEC Management Centre: Brussels, Belgium, 1999.
29. *Portland Cement Association: Soil-Cement Laboratory Handbook 1992*; Portland Cement Association: Skokie, IL, USA, 1992; p. 59.
30. American Association of State Highway and Transportation Officials. *Mechanistic Empirical Pavement Design Guide A Manual of Practice*; Interim Edition; AASHTO: Washington, DC, USA, 2008; ISBN 978-1-56051-423-7.
31. Jameson, G. *Guide to Pavement Technology Part 4D: Stabilised Materials Edition 2.1*; Austroads Ltd.: Sydney, NSW, Australia, 2019; ISBN 978-1-925854-17-6.
32. Geotechnical Aspects of Pavements - Reference Manual/Participant Workbook (Publication No. FHWA NHI-05-037). U.S. Department of Transportation. Available online: https://www.fhwa.dot.gov/engineering/geotech/pubs/05037/05037.pdf (accessed on 24 September 2018).

33. Federal Highway Administration. Standard Specifications for Construction of Roads and Bridges on Federal Highway ProjectsFP-14. Available online: https://flh.fhwa.dot.gov/resources/specs/fp-14/fp14.pdf (accessed on 24 September 2018).
34. *InfraRYL 2010 Code of Building Practice, Infrastructure, Part 1: Roads and Areas*; Rakennustieto Oy: Helsinki, Finland; ISBN 978-951-682-958-9.
35. Bieniawski, Z.T.; Bernede, M.J. Suggested Methods for Determining the Uniaxial Compressive Strength and Deformability of Rock Materials. *Int. J. Rock Mech. Min. Sci. Geomech. Abstr.* **1979**, *16*, 137–140.
36. Strozyk, J.; Tankiewicz, M. The elastic undrained modulus Eu50 for stiff consolidated clays related to the concept of stress history and normalized soil properties. *Stud. Geotechnica. Mech.* **2016**, *38*, 67–72. [CrossRef]
37. Ayeldeen, M.; Hara, Y.; Kitazume, M.; Negm, A. Unconfined Compressive Strength of Compacted Disturbed Cement-Stabilized Soft Clay. *Int. J. Geosynth. Ground. Eng.* **2016**, *2*, 10. [CrossRef]
38. Kortelainen, L. The frost resistance of stabilized base course. Master's Thesis, Aalto University, Helsinki, Finland, June 2019.
39. Saarelainen, S.; Gustavsson, H.; Korkiala-Tanttu, L. Climate change and freezing conditions in Finland. In Proceedings of the 19th International Conference on Soil Mechanics and Geotechnical Engineering, ISSMGE, Seoul, Korea, 17–21 September 2017; pp. 1411–1414.
40. Finnish Standard Association. *CEN/TS 13286-54:2014 Unbound and Hydraulically Bound Mixtures. Part 54: Test Method for the Determination of Frost Susceptibility. Resistance to Freezing and Thawing of Hydraulically Bound Mixtures*; CENELEC Management Centre: Brussels, Belgium, 2014.
41. Ismeik, M.; Shaqour, F. Effectiveness of lime in stabilising subgrade soils subjected to freeze–thaw cycles. *Road. Mater. Pavement. Design.* **2018**, 1–19. [CrossRef]
42. Firoozi, A.A.; Taha, M.R.; Firoozi, A.A.; Khan, T.A. The influence of freeze-thaw cycles on unconfined compressive strength of clay soils treated with lime. *Jurnal. Teknol. (Sci. Eng.)* **2015**, *76*, 107–113.
43. Ghazavi, M.; Roustaie, M. The influence of freeze–thaw cycles on the unconfined compressive strength offiber-reinforced clay. *Cold. Regions. Sci. Technol.* **2010**, *61*, 125–131. [CrossRef]
44. Orakoglu Firat, M.; Liu, J. Effect of freeze-thaw cycles on triaxial strength properties of fiber-reinforced clayey soil. KSCE. *J. Civil. Eng.* **2017**, *21*, 2128–2140.